DESIGN, FABRICATION, TESTING, AND DATA ANALYSIS OF ADAM II CONCEPT (PROPULSIVE WING)

PART III TESTING IN 17-FOOT TEST SECTION OF 7-FT X 10-FT WIND TUNNEL, NASA LANGLEY RESEARCH CENTER

R. D. Meyer
W. E. Brownrigg, Jr.
R. B. English
et al

FOREWORD

The work reported upon herein was performed by the Vought Aeronautics Division (VAD) of the LTV Aerospace Corporation of Dallas, Texas, under Contract Nr. AF33(615)-3293, Project Nr. 1366, Task Nr. 136617, supported jointly by the United States Air Force and the United States Army. Air Force support for this effort was made possible through the use of Air Force Flight Dynamics Laboratory Director's Funds. After shakedown testing by the Contractor, the major tests were conducted by the NASA Langley Research Center, Hampton, Virginia, in the 17-foot test section of the LRC 7-foot x 10-foot wind tunnel and in the LRC 16-foot transonic wind tunnel.

The actual wind tunnel testing was started on 2 December 1966 and was completed on 7 July 1967. This report was submitted by the authors in December, 1967.

Acknowledgements are due to many individuals in the Air Force, the Army, and the Langley Research Center. Particular reference is made to Mr. P. P. Antonatos of the Air Force Flight Dynamics Laboratory, who suggested the use of a single model for high and low speed testing in the Langley Research Center wind tunnels; to Messrs. F. M. Rogallo, R. E. Kuhn, A. D. Hammond, K.E. Spreeman, and Garl C. Gentry of the LRC Low Speed Vehicle Branch, who conducted the low speed testing; to Messrs. B. W. Corson, Jr., J. F. Runckel, J. Schmeer, L. B. Salters, Jr., E. M. Brummal, C. F. Whitcomb, and E. E. Lee, Jr., of the LRC 16-foot Transonic Wind Tunnels Branch, who conducted the high speed testing; and to Messrs. J. Gaurino and Carl Roberts of the LRC Instrumentation Research Department, and Mr. John Wilson of the Air Force Flight Dynamics Laboratory, who assisted in resolving problems in the internal strain gage balance used for high speed testing.

The use of photographs of the model in the Langley Research Center Wind Tunnels, furnished by LRC, is gratefully acknowledged.

The program monitor for the Air Force was Major Edward P. Miller, FDMM, Air Force Flight Dynamics Laboratory, Wright-Patterson Air Force Base, Ohio, assisted by Mr. Robert R. Jeffries of the same organization. The program monitor for the Army was Mr. LeRoy T. Burrows, SAVFE-TP, U. S. Army Aviation Materiel Laboratories, Fort Eustis, Virginia. The principal investigator for the Contractor was Mr. B. R. Winborn. Coauthor of this report for the Contractor was Mr. Jim K. Davidson.

This report is presented in four parts, as follows:

Design, Fabrication Testing, and Data Analysis of ADAM II Concept (Propulsive Wing), Part I General and Summary Information

Design, Fabrication Testing, and Data Analysis of ADAM II Concept (Propulsive Wing), Part II Shakedown Testing in the VAD 7-foot by 10-foot Low Speed Wind Tunnel

Design, Fabrication Testing, and Data Analysis of ADAM II Concept (Propulsive Wing), Part III Hover and Transition Mode Testing in the 17-foot Test Section of the Langley Research Center 7-foot by 10-foot Low Speed Wind Tunnel

Design, Fabrication Testing, and Data Analysis of ADAM II Concept (Propulsive Wing), Part IV Cruise Mode and High Speed Testing in the Langley Research Center 16-foot Transonic Wind Tunnel

This technical report has been reviewed and is approved.

Philip P. Antonatos

PHILIP P. ANTONATOS
Chief, Flight Mechanics Division
Air Force Flight Dynamics Laboratory

ABSTRACT

An analysis of selected data obtained from a low speed wind tunnel test of a straight, low aspect ratio propulsive wing V/STOL aircraft concept is presented. Essential features of the model are four compressed air tip driven fans in the wing with vectorable exhaust, fixed exhausts blowing over the top of the flap simulating hot gas turbine exhaust, a forward-facing nose fan for pitch control with a vectorable exhaust, and tail surfaces mounted on booms extending aft as part of the wing tips. The model was tested in the V/STOL mode where the propulsive flows were deflected symmetrically downward by internal vanes at 30, 60, and 90 degrees and by flap deflections from 30 to 90 degrees. Stability, control, and a limited amount of pressure data were obtained for various flow deflections, momentum coefficients, configuration changes, and ground board heights. Because of the proximity of the tails to the wing tip vortex, the horizontal tail contribution to longitudinal stability is increased due to favorable upwash, and the directional stability contribution of the vertical tail is reduced due to high angles of sidewash. Removing the vertical tails from the booms and adding a centerline vertical tail to the fuselage improved directional stability and the linearity of the pitching moment curves. At high momentum coefficients, the high velocity propulsive flow induces additional dynamic pressure at the horizontal tails, and control effectiveness is improved. At low momentum coefficients the horizontal tail effectiveness is low. Control by deflection of the propulsive flow with wing vanes and flaps is adequate. In general, the effect of the ground board is to increase thrust-included lift by increasing bottom surface pressures and to reduce the effective exhaust flow deflection angle. Drag increments due to ground effects vary with vane and flap deflections.

vi is blank

TABLE OF CONTENTS

LIST OF ILLUSTRATIONS

LIST OF ILLUSTRATIONS (continued)

LIST OF TABLE

SECTION I

INTRODUCTION

This report concerns the results of the LRC low speed wind tunnel tests conducted to obtain the transition and hover mode characteristics, both in and out of ground effects. A run log of the test is presented in Appendix I.

All of the data presented include thrust in the force and moment coefficiencts. The level of thrust is indicated by net thrust coefficient. Momentum coefficient based on wing fan plus primary gross thrust is used for comparison with previous test results. Momentum coefficient (or gross thrust coefficient) defined by $C_\mu = \Sigma F_G/qS$ is the accepted correlating parameter for jet flap work and was adopted for the ADAM propulsive wing. For the special case of the jet flap, $C_\mu = \dot{M}_j V_j/qS$. For this model, $C_\mu = \Sigma\left|(\dot{m}_f + \dot{m}_c)V_J/g\right|/qS$, since the compressed air used to drive the tip turbine fans and simulate the primary flow is added to the system. The momentum coefficients in this report include the nose fan and its drive air gross thrust. Net thrust is gross thrust less ram drag; therefore, the net thrust coefficient for the model is: $C_T = \Sigma\left|(\dot{m}_f + \dot{m}_c)V_J/g - \dot{m}_f V_o/g\right|/qS$. The net thrust coefficients in this report include nose fan gross thrust, drive air, and ram drag. An additional ram drag corresponding to the compressed air mass flow, $\dot{m}_f V_o/g$, would be present on the airplane. For ADAM II tests, gross thrust and subsequently momentum coefficient was computed from pressure distributions at the primary, secondary, and nose fan flow exits. The distribution of gross thrust among the propulsive flows on the model was, in general, approximately 17% for each of the five fans, and 7.5% for each of the left- and right-wing primary exits. VAD has done some private development of thrust removal techniques. However, additional work is required before the external aerodynamic forces can be separated. Since the measured aerodynamic coefficients include thrust, large lift coefficients, large pitching moment coefficients, and large negative drag coefficients are to be expected. It was found that the inclusion of thrust in the data did not particularly detract from the analysis. Since the definition of C_μ has freestream dynamic pressure in the denominator, the actual airplane operating range of C_μ extends from about 0.03 at high speed flight to infinity at hover.

For the runs with the model in the hover configuration at tunnel $q = 0$, the coefficient denominator was set equal to 1.0 for data reduction purposes; therefore, the thrust included force and moment coefficients represent pounds and inch-pounds acting on the model. The hover configuration (90° vane box) was also tested wind-on to provide data at finite C_μ's. In this case, high lift coefficients are generated that consist mainly of the thrust coefficients with very little external aerodynamics involved. This corresponds to very slow forward speeds in the hover configuration. Aerodynamic stability or instability is now less significant in the usual sense, and the data are more useful in determining other phenomena such as gust response.

A rework of the nose fan exit and installation of screens in the primary exhaust for this test eliminated the separated nose fan flow found in the shakedown tests and reported in Part II, and improved the flow distribution over the flaps. Variations in C_μ were obtained by varying either fan rpm or changing tunnel q. Although cooling of the model structure due to expansion of the drive air was expected, high atmospheric humidity created icing that interfered with obtaining surface pressure data. It is felt that stability data were not adversely affected. Model variations included vane box, flap and horizontal tail deflections, tail buildup, and variations in fan rpm. Also differential settings of vane box angle, flap angle, and fan rpm were tested for control authority. Tests included pitch runs at zero yaw angle, yaw runs at constant angles of pitch, and variations in tunnel q and fan rpm at zero pitch and yaw. There were also pitch and yaw runs in the presence of a moving ground plane and model height variations above the ground plane with the model held at zero pitch and yaw. When using the 30-degree vane box, the nose fan exit was swiveled to direct the flow along the bottom of the fuselage. For the 60- and 90-degree vane box settings, the nose fan exit was set to direct the flow 90 degrees downward. The nose fan was normally open and operative for the tests of the basic configuration.

The analysis of the selected data presented in this report points out the general transition and hover mode characteristics of the configuration. Since the model was not built to develop the configuration and most of the pressure data were unobtainable because of ice, there is much that is unknown about the flow conditions responsible for the observed stability characteristics.

SECTION II

ANALYSIS

1. LONGITUDINAL STABILITY AND CONTROL

ADAM II aerodynamic characteristics are strongly influenced by high-velocity vectorable propulsive flows and vortex interferences. In analyzing the wind tunnel results, it is convenient to consider configurations with zero- and 30-degree vane box deflections as related aerodynamic vehicles, as opposed to the 60- and 90-degree vane box configurations being primarily propulsive vehicles. For this series of tests, the flap was normally deflected an amount to produce a primary flow deflection along its upper surface equal to the vane box setting.

a. 30-Degree Vane Box

Tests of the 30° vane box configuration with 11° flap show quite different stability characteristics than that obtained from tests of the cruise configuration. A sketch, comparing typical pitching moment data for the two configurations, is presented in Figure 1.

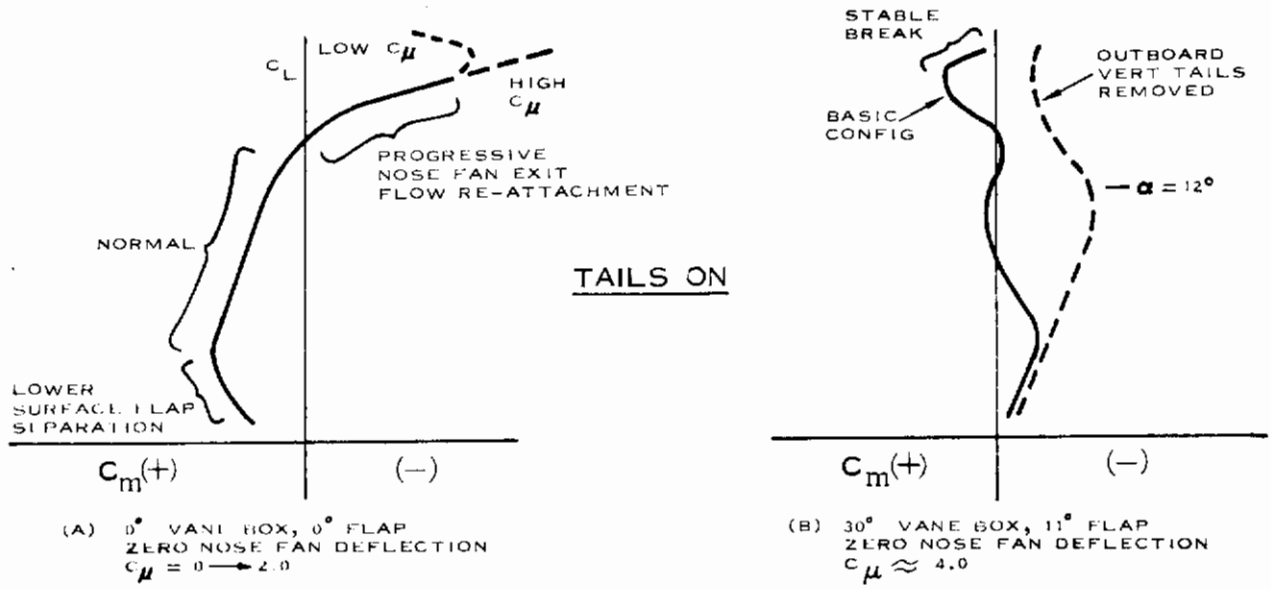

(A) 0° VANE BOX, 0° FLAP
ZERO NOSE FAN DEFLECTION
$C_\mu = 0 \longrightarrow 2.0$

(B) 30° VANE BOX, 11° FLAP
ZERO NOSE FAN DEFLECTION
$C_\mu \approx 4.0$

Figure 1. Comparison of Stability Characteristics, Zero and 30° Vane Box Deflection

Figure 1(a) shows the characteristics attributed to the cruise configuration as obtained from LTV low speed test 229 and reported in Part II. The unstable change in slope at low lift coefficients is thought to be separation from the flap lower surface (or possible aft fuselage and/or boom); and the stable change in slope at high lift coefficients is believed to be progressive reattachment of a separated nose fan exit flow. For the LRC 17-foot low speed tests, a rework of the nose fan exhaust ducts and changing to the 30° vane box and 11° flap configuration resulted in the shape presented in Figure 1(b). The lower end of the curve does not show the unstable break of Figure 1(a), which is believed to be due to the downward flap deflection changing the flow characteristics to eliminate suspected flap separation, and there is no evidence of a separated nose fan exit flow. Also illustrated in Figure 1(b) is the significant effect of the outboard vertical tails on longitudinal stability. Removing the vertical tails from the vicinity of the wing tip vortices results in a marked improvement in linearity up to 12 degrees angle of attack, and reduces the magnitude of the stable break at high lift coefficients. Curve nonlinearities such as those of Figure 1 are useful to deduce flow conditions and lead to improvements in the configuration. Some nonlinearities are apparently due to vortex patterns changing with angle of attack and altering the forces induced on adjacent surfaces. Other nonlinearities are a result of flow separation on various parts of the model. Complete assessment of ADAM II flying qualities can come after the configuration is optimized and moment curves are more nearly linear.

Examples of lift and pitching moment data obtained for various levels of momentum coefficient and tail combinations are presented in Figures 2, 3, and 4. For the windmilling case, runs 190 and 220 of Figures 2(a) and 2(b) indicate a C_{m_o} shift due to adding the outboard vertical tails. A reasonable value of ΔC_{m_o} due to vertical tail drag is +0.01 to +0.02, less than half that observed. Some additional C_{m_o} shift may be expected as a result of the wing tip vortex inducing pressures on the vertical tail which carry down onto horizontal surfaces; however, a stability change would also be expected as the vortex changes strength and position with angle of attack. Other C_{m_o} shifts are also observed. Appendix II discusses these shifts and questions the validity of certain runs, including run 220. As shown in Figure 2(c), the loss of C_{L_α} occurs in proceeding upward from -6 degrees angle of attack that is regained at +6 degrees, with corresponding changes in C_{m_α} shown in Figure 2(b). The symmetry of these changes suggests the passage of the wing tip vortex over the horizontal tail. At +9 to +15 degrees, a large loss in C_{L_α} accompanies a positive change in C_{m_α}. The magnitude of the C_{L_α} change suggests wing stall. Above 15 degrees some additional stalling is evident with a further increase in positive C_{m_α}. In this region the tail-on data of Figure 2(b) exhibits a slightly reduced but constant value of tail effectiveness and shows that the horizontal tails do not contribute to longitudinal stability. These data imply that the local angle of attack at the horizontal tail is invariant with increasing model angle of attack; i.e., $d\epsilon/d\alpha = 1.0$.

Figure 3 presents longitudinal data when the momentum coefficient is increased to approximately 4.0 and again shows a strong effect due to the outboard vertical tails. At -3 degrees of angle of attack, Figure 3(b)

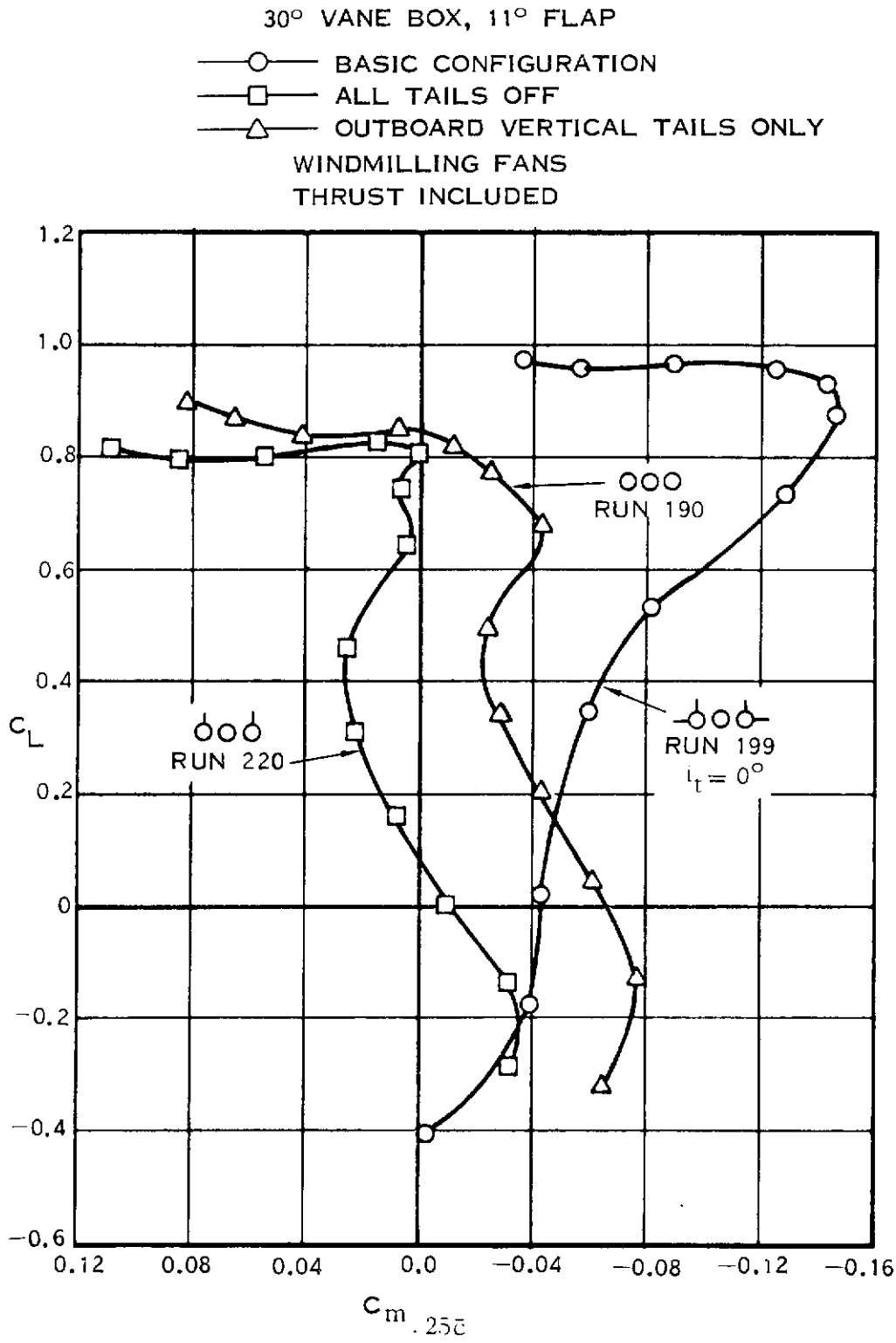

(a) C_L VS C_m

Figure 2. Effect of Tail Buildup on Longitudinal Characteristics - Windmilling

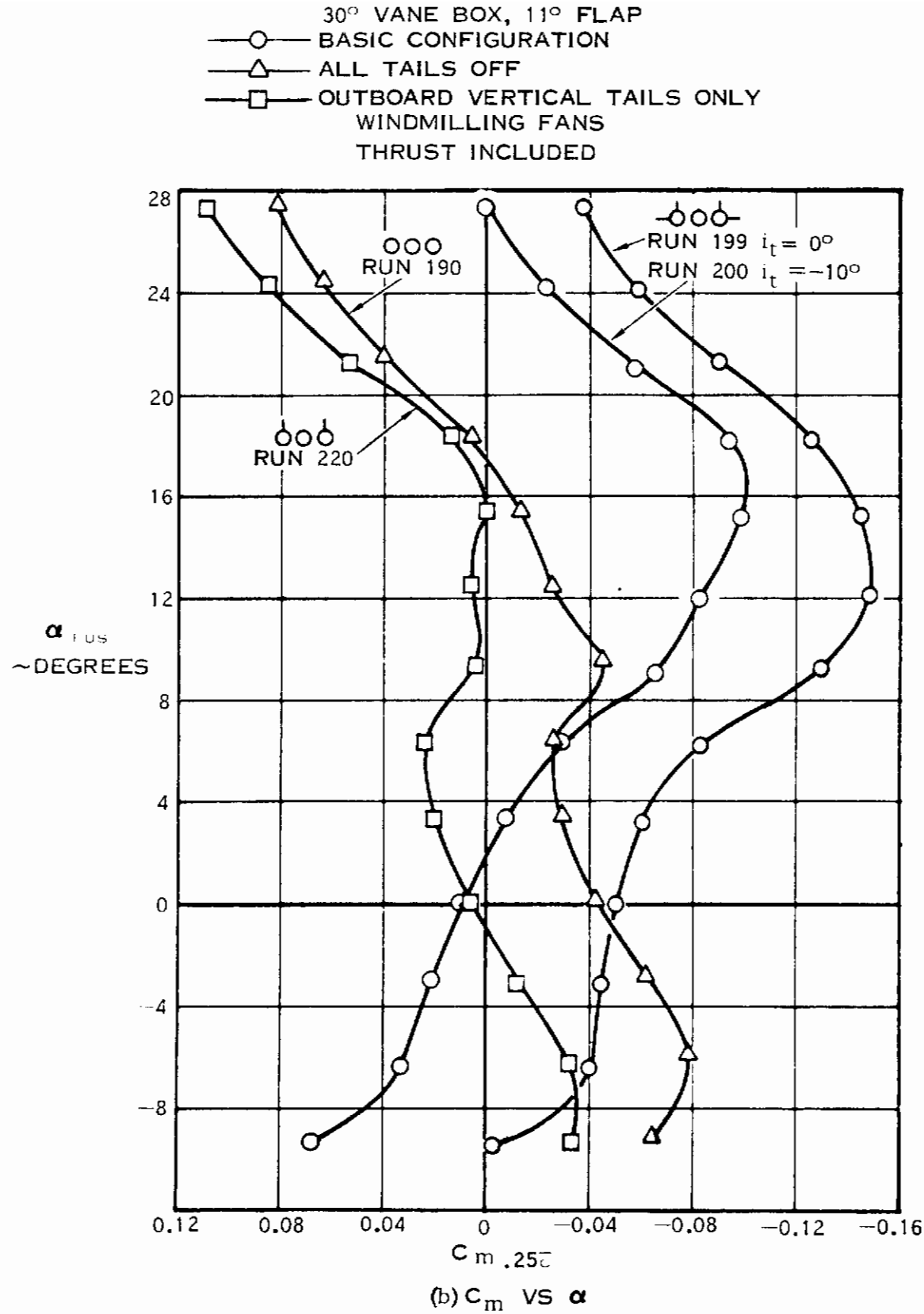

(b) C_m VS α

Figure 2. Effect of Tail Buildup on Longitudinal Characteristics - Windmilling (Continued)

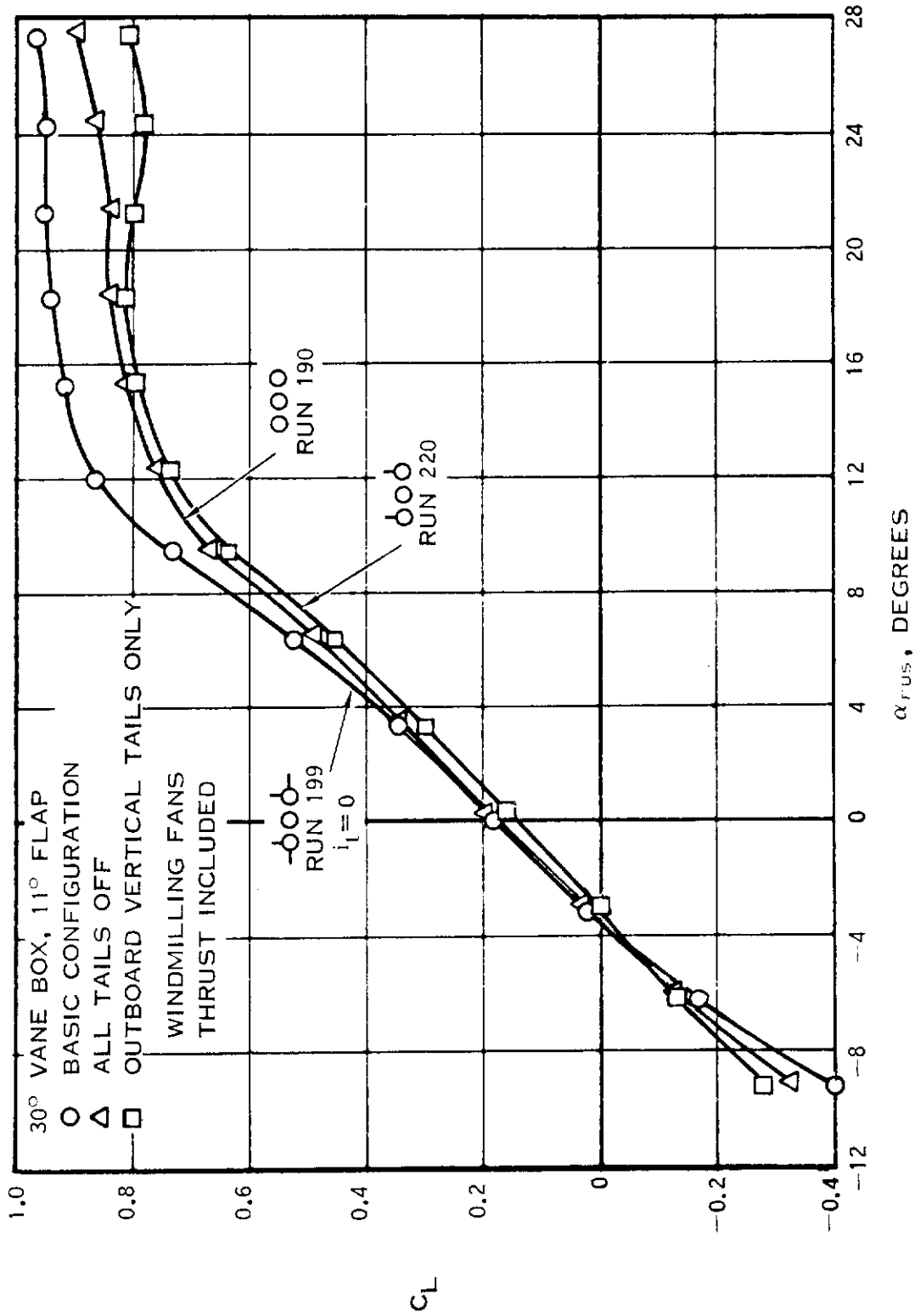

(c) C_L VS α

Figure 2. Effect of Tail Buildup on Longitudinal Characteristics - Windmilling (Concluded)

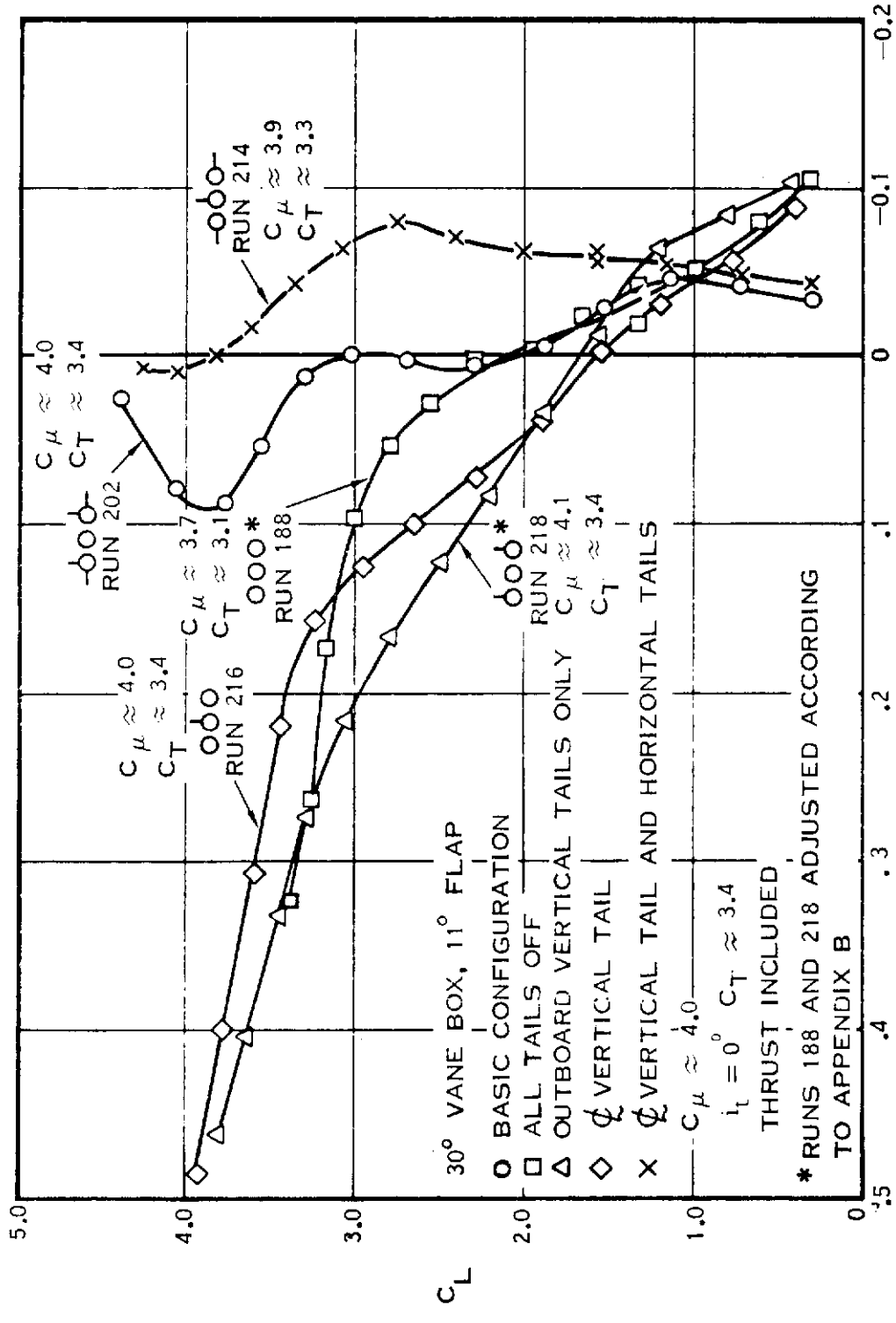

(a) C_L VS C_m

Figure 3. Effect of Tail Buildup on Longitudinal Characteristics - $C_\mu \approx 4$

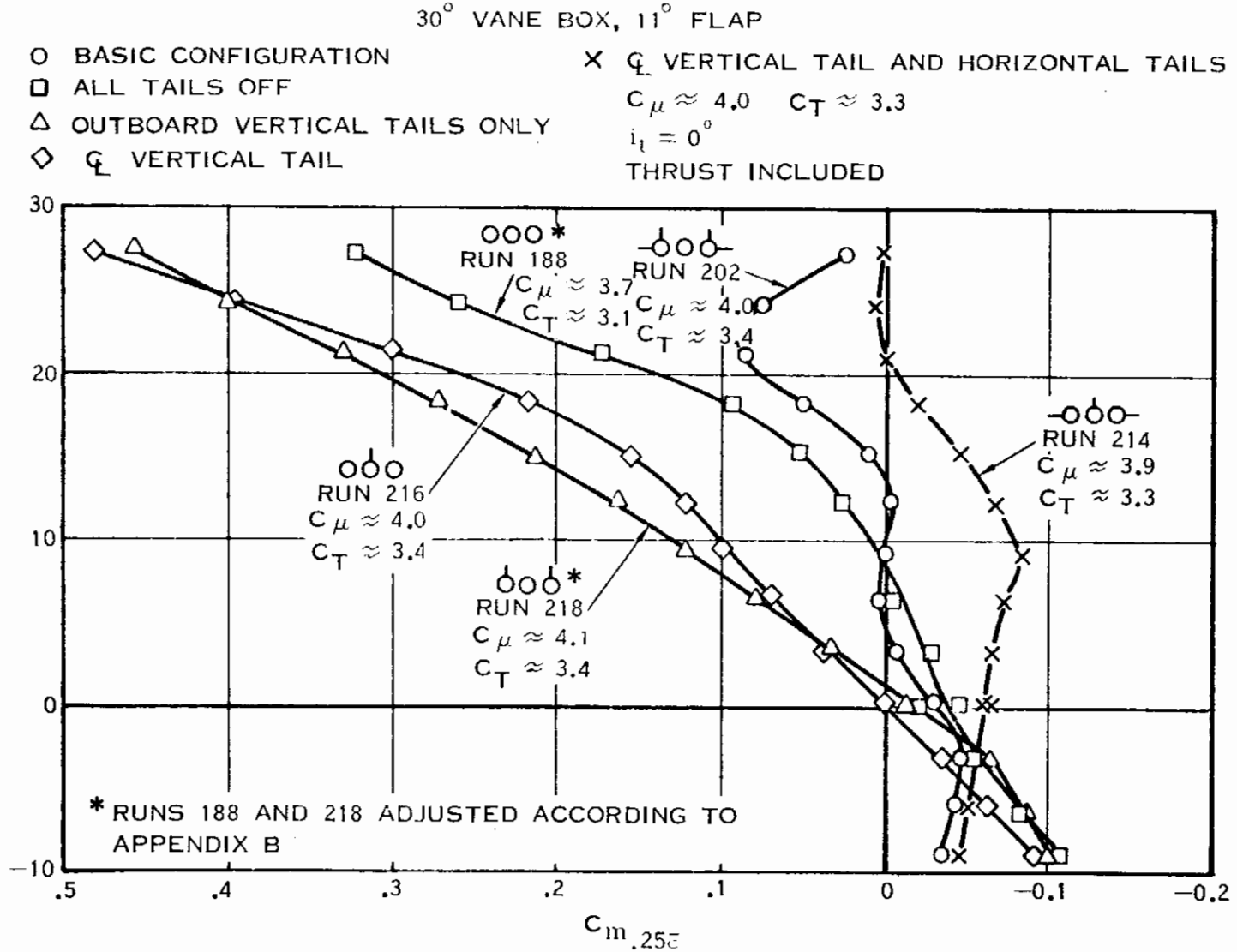

(b) C_m VS α

Figure 3. Effect of Tail Buildup on Longitudinal Characteristics - $C_\mu \approx 4$ (Continued)

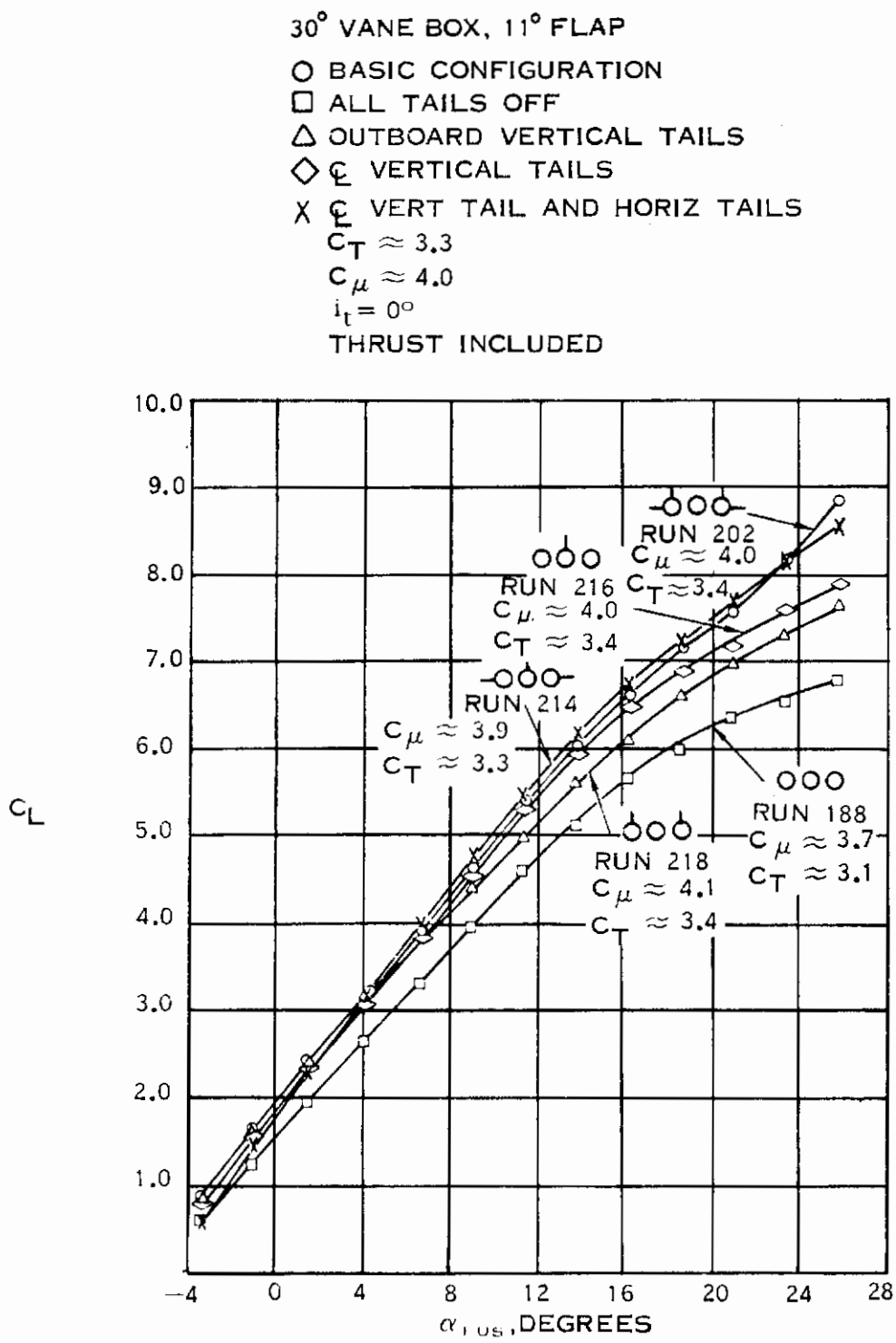

(c) C_L VS α

Figure 3. Effect of Tail Buildup on Longitudinal Characteristics - $C_\mu \approx 4$ (Concluded)

shows that the outboard vertical tails produce an abrupt reduction in stability and lift curve slope for both cases of horizontal tails on and off. At 10 to 12 degrees, all moment curves show a reduction in stability corresponding to the beginning of a gradual decrease in lift curve slope (Figure 3(c)). Since the aft fuselage is somewhat flat or "duck-billed" in shape, this change may be due to a gradual upper surface flow separation beginning at the aft end of the fuselage, progressing forward and perhaps engaging the center portion of the wing. Pressure data available does not show flap separation at this time. Comparison of run 218 with run 216 shows a much milder stability reduction at 12 degrees, indicating that the outboard vertical tails are providing an end plating effect to the wing. It is expected that pressure distribution data from the LRC high speed wind tunnel tests to be reported in Part IV will aid determination of the cause of the reduced stability.

At high angles of attack, with either the outboard vertical tails or the centerline vertical tail, the addition of the horizontal tails causes an increase in lift and a significant increase in stability, again indicating a wing vortex interaction with the horizontal tails.

Figure 4 presents pitching moment and lift data for a momentum coefficient increased to about $C\mu = 13.0$. Such a relatively large propulsive flow tends to mask the external aerodynamic forces, hence the causes for the nonlinearities in the data of Figure 4 are unknown. At $C\mu = 4.0$, there is not a large difference in pitching moment between the tails off and tails on data of runs 188 and 202. At $C\mu = 13.0$, the difference is large. Also shown on Figure 4(a) are runs 187 and 209, which vary $C\mu$ with angle of attack constant at zero. The end values of C_m and C_L of these runs correlate fairly well with the pitch runs except for $C\mu = 13.0$, tails off, where there is a large difference in C_m. Again, the consistency of the pitching moment data is in question. It is apparent, however, that the high velocity propulsive flow inclined 30 degrees downward induces additional down load on the horizontal tail as $C\mu$'s become large.

Longitudinal characteristics of the model with tare nose are presented in Figure 5 to show that it has no basic effect on pitching moment shape other than a moderate improvement in stability in the range of -3 to +9 degrees angle of attack. Above 9 degrees angle of attack, the tare nose has the same pitching moment characteristics as the fan nose. The C_{m_o} shift of +0.25 due to the nose fan correlates well with the calculated value based on nose fan thrust magnitude and location relative to the moment surface.

Figures 6 and 7 present horizontal tail control effectiveness for windmilling fans and for $C\mu \approx 4.0$ respectively. An average value for control effectiveness ($C_{m_{i_t}}$) is 0.0058/degree for fans windmilling and -0.0072/degree (considerably greater) for $C\mu \approx 4.0$. This compares with $C_{m_{i_t}}$ in the cruise configuration of -0.0054/degree for both windmilling and $C\mu \approx 2.0$ as reported in Part II. The increase in $C_{m_{i_t}}$ at $C\mu \approx 4.0$ indicates an increase in local dynamic pressure at the horizontal tails induced by the high propulsive flow exit velocity. A comparison of Figure 6 with Figure 7 shows a reduction in longitudinal stability with increasing

30° VANE BOX, 11° FLAP
$i_t = 0°$
THRUST INCLUDED

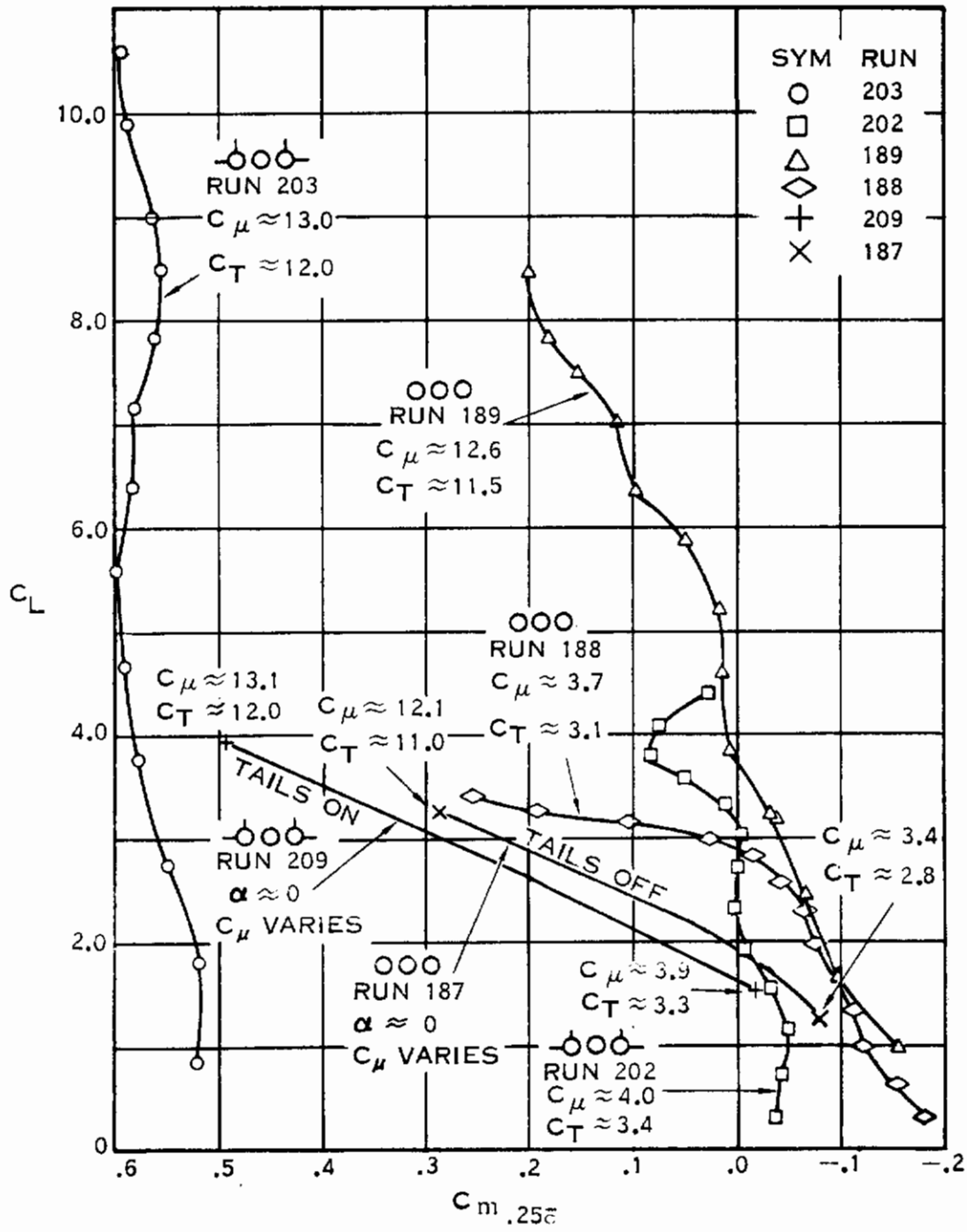

(a) C_L VS C_m

Figure 4. Effect of Tail Buildup on Longitudinal Characteristics - $C_\mu \approx 13$

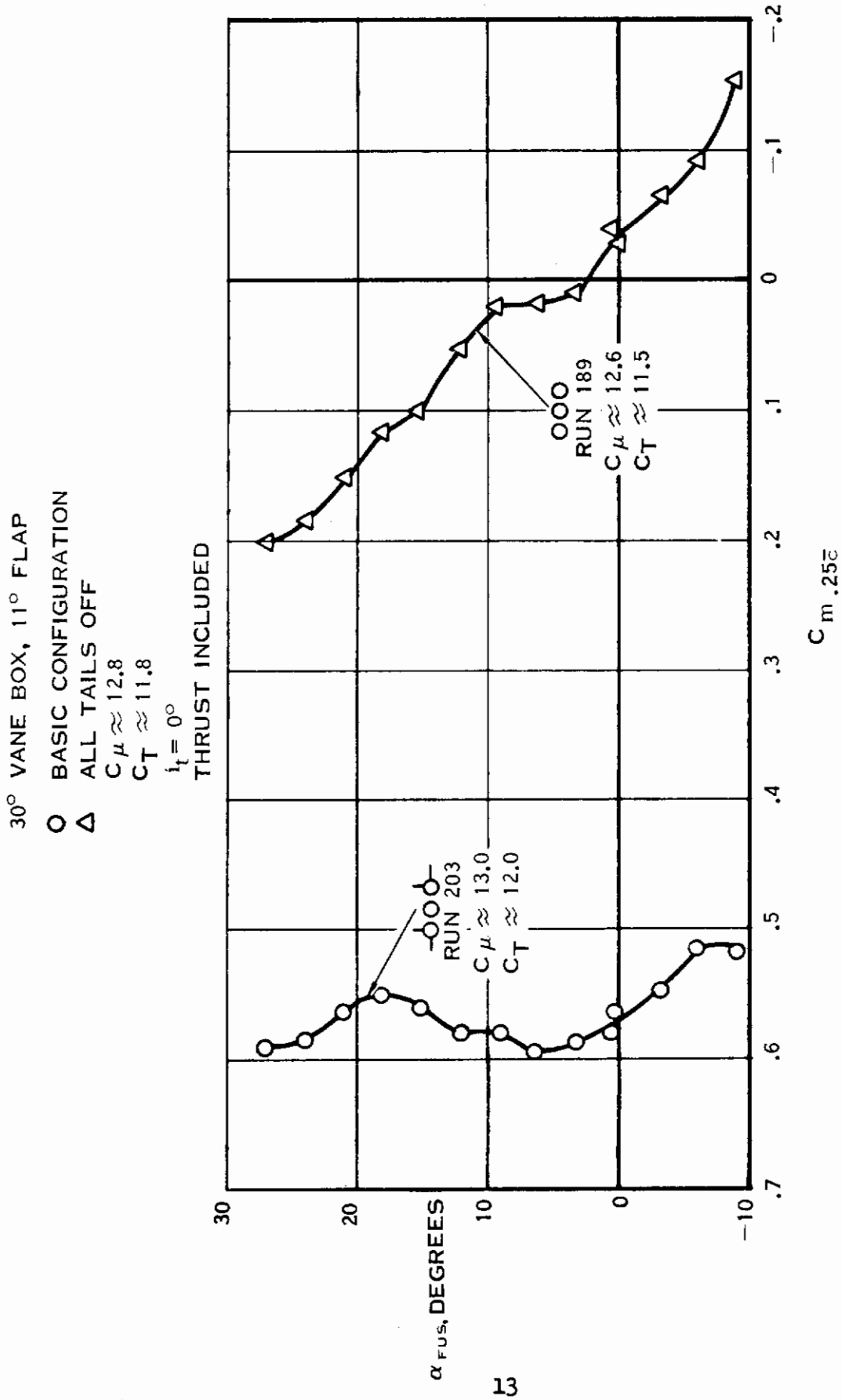

(b) C_m VS α

Figure 4. Effect of Tail Buildup on Longitudinal Characteristics - $C_\mu \approx 13$ (Continued)

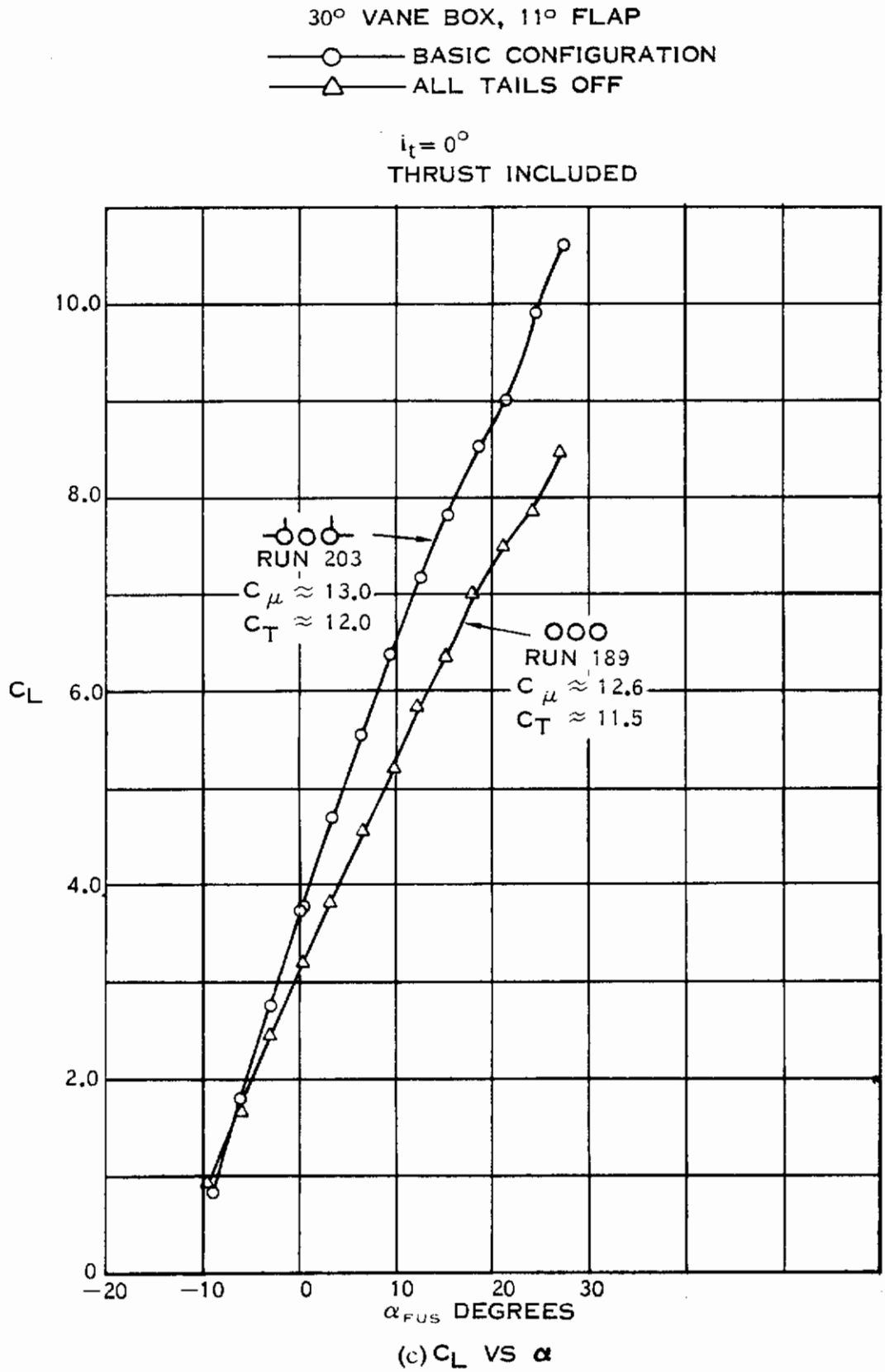

(c) C_L VS α

Figure 4. Effect of Tail Buildup on Longitudinal Characteristics - $C_\mu \approx 13$ (Concluded)

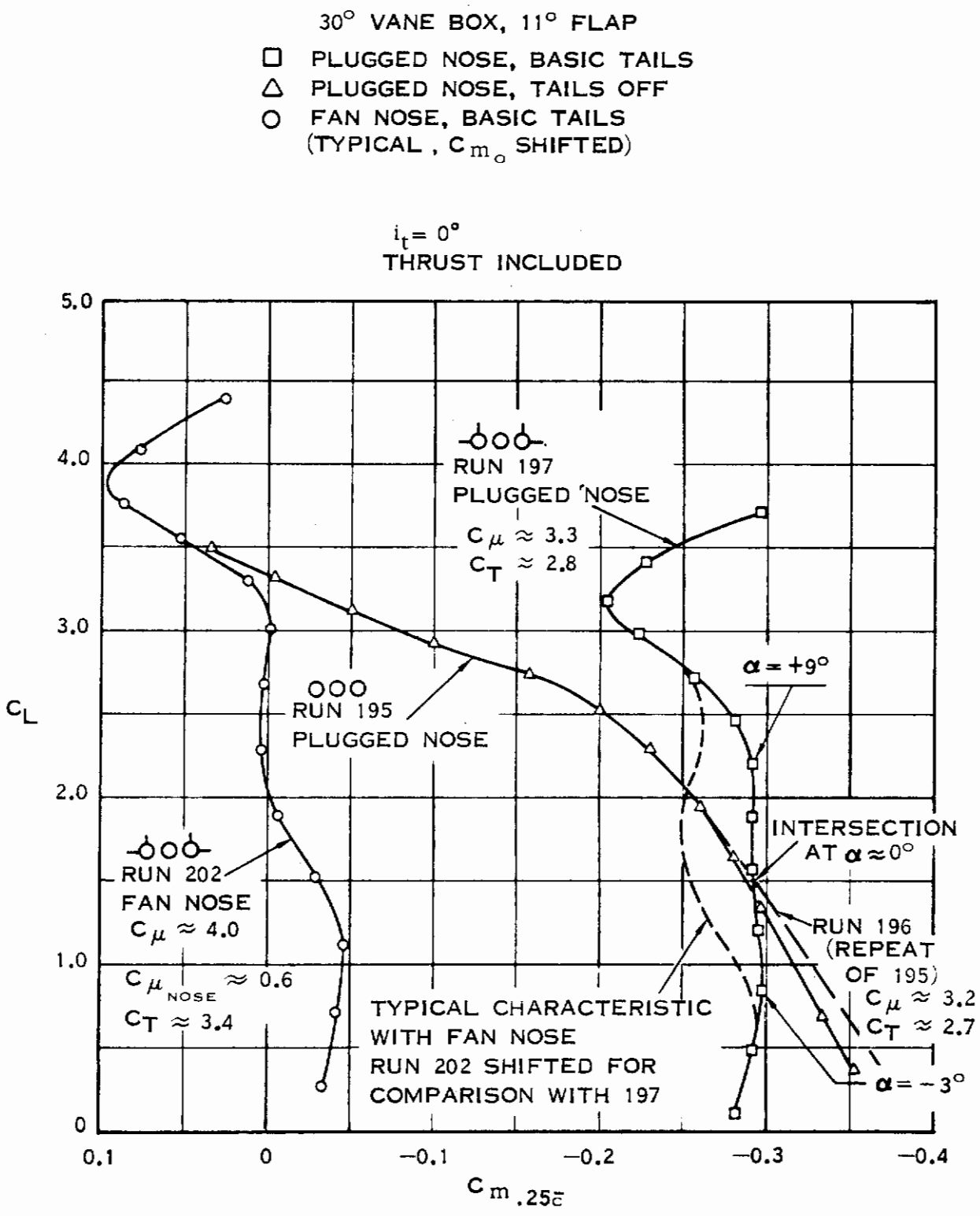

Figure 5. Effect of Plugged Nose on Longitudinal Characteristics

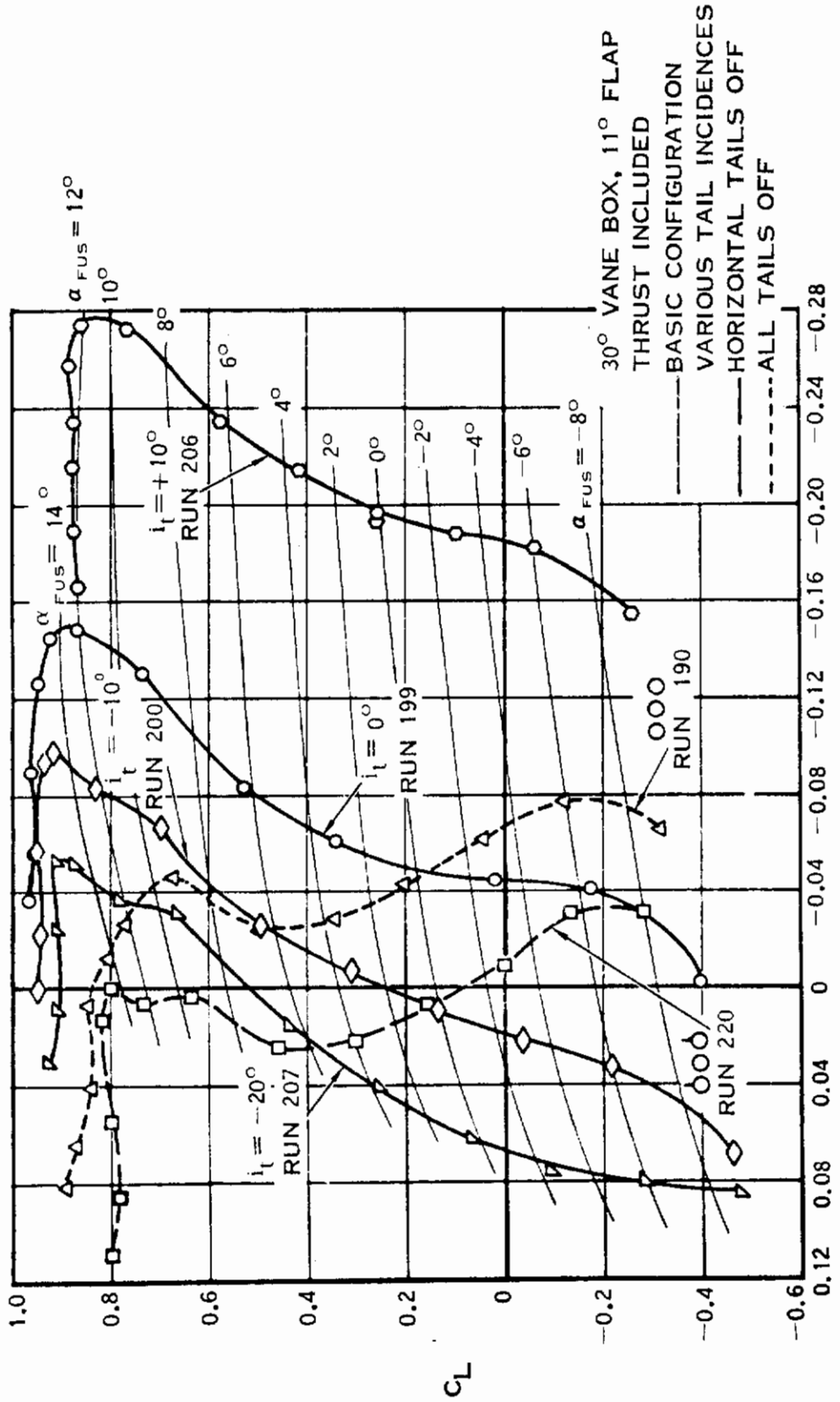

Figure 6. Longitudinal Control Effectiveness - Windmilling

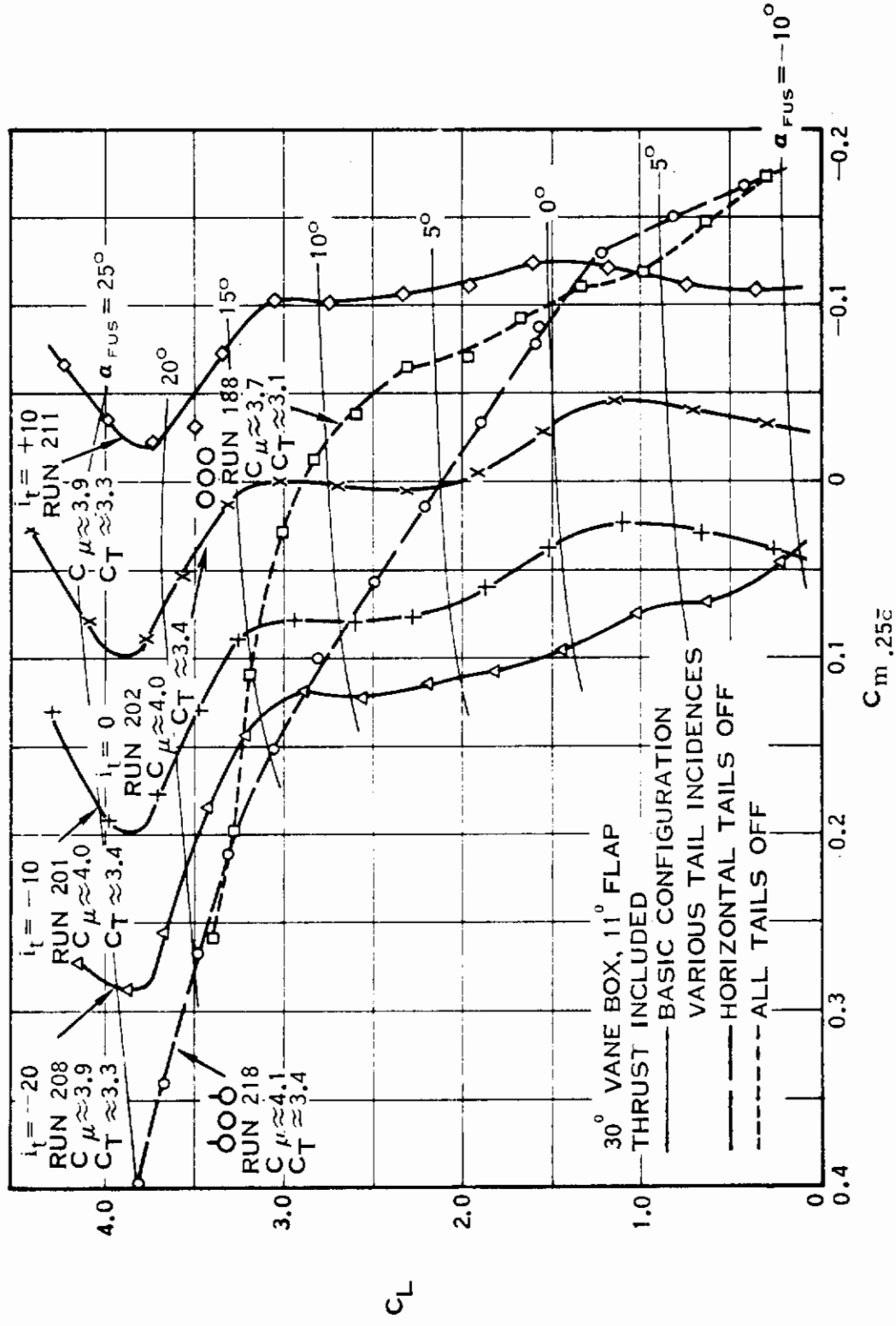

Figure 7. Longitudinal Control Effectiveness - $C_\mu \approx 4.0$, $C_T \approx 3.4$

C_μ. The increased stability and reduced tail effectiveness with fans windmilling limits maximum trimmed lift coefficient to $C_L = 0.55$ for this configuration, c.g. location, and maximum negative tail incidence.

The trim change due to power is shown in Figure 8. At 0.5 lift coefficient, the trim change of about 5 degrees i_t is small compared to 15 degrees i_t for the cruise configuration (Part II). As angle of attack is increased, the trim difference grows rapidly. The linearity of these curves would be expected to improve with incorporation of a centerline vertical tail instead of the outboard vertical tails and with improvements in fuselage shape.

Figure 9 presents the effectiveness of the flaps as a control device. Flap control effectiveness $C_{m_{\delta f}}$ is -0.035/degree, or about eight times that of the horizontal tails.

b. 60- and 90-Degree Vane Box

The basic longitudinal characteristics of the model with 60- and 90-degree vane box deflection are presented in Figure 10 for a $C_\mu \approx 3.9$. The thrust included effective aerodynamic center is located ahead of the leading edge of the MGC for both the all-tails-off and all-tails-on configurations. At approximately 13 degrees angle of attack, the data show a loss of lift and an increase in positive pitching moment which indicates wing stall or body aft separation. In comparing runs 89 and 126, the horizontal tails make an insignificant contribution to stability indicative of $d\epsilon/d\alpha = 1.0$ at high power coefficients. Some horizontal tail control effectiveness is, however, indicated by runs 26 and 27. The vane box thrust vector is located aft of the center of gravity as shown by the increase in positive pitching moment obtained by changing the vane box from 90 to 60 degrees with a 71-degree flap setting.

These high vane box deflections imply very low speeds or hover where the low dynamic pressure reduces the aerodynamic control authority and requires the use of the nose fan for pitch control. Figure 11 presents the nose fan thrust required to trim with the 90-degree vane box and a 71-degree flap deflection (90-degree flow turning). The thrust is calculated based on wind tunnel values of pitching moment, the geometric distance from the nose fan exit to the c.g. and the nose fan thrust assumed to be perpendicular to the fuselage reference line. Results show that adequate nose fan thrust is available for trim and approximately 30 pounds of excess thrust (model scale) are available for maneuvering at a_{2}c.g. = 25% $\bar{c}$. This excess thrust represents about 0.4 radians per second^2 pitch acceleration for a typical airplane.

Figure 12 presents the effects of flap deflection on the longitudinal characteristics of the 60-degree vane box. These data show the increase in the nose down pitching moment as the flap deflection is increased from 11 to 41 degrees. For flap deflections greater than 41 degrees the trend reverses, indicating that the primary flow separates from the flap and that the flow deflection decreases as the flap deflection increases. These data indicate that the 60-degree vane box configuration has reasonably linear

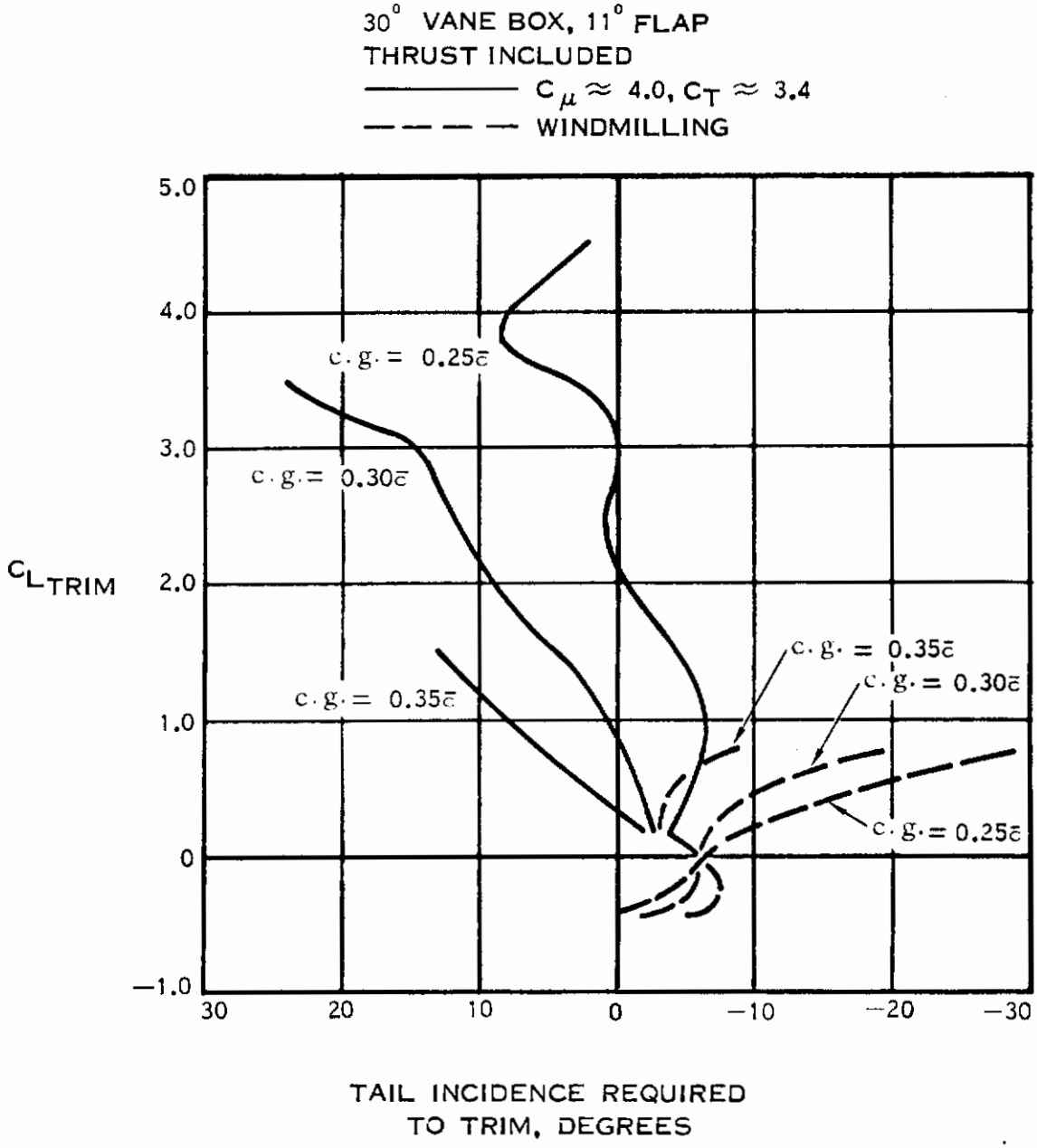

Figure 8. Effect of Power on Trim Requirements

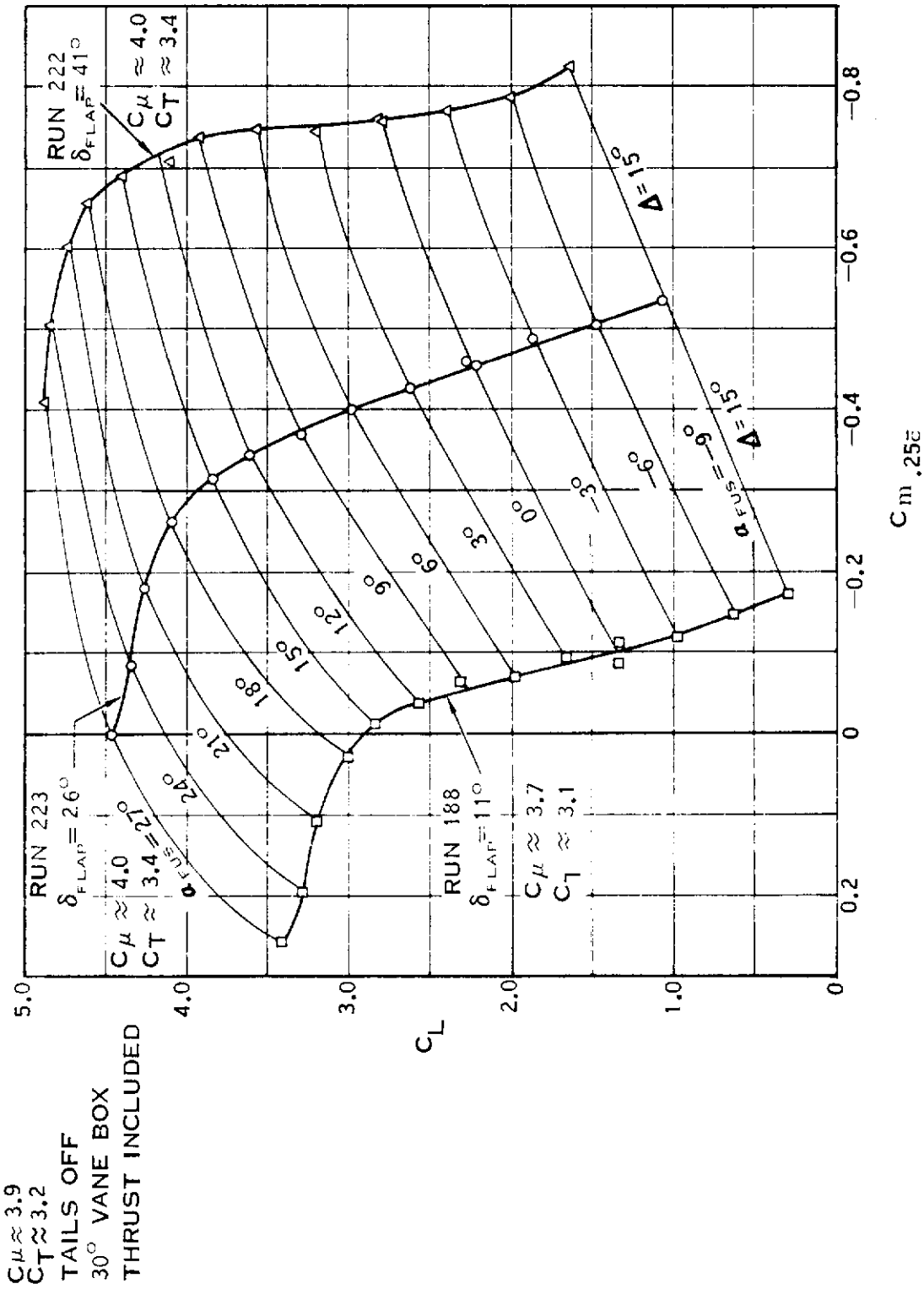

Figure 9. Variation of Pitching Moment and Lift Due to Flap Deflection

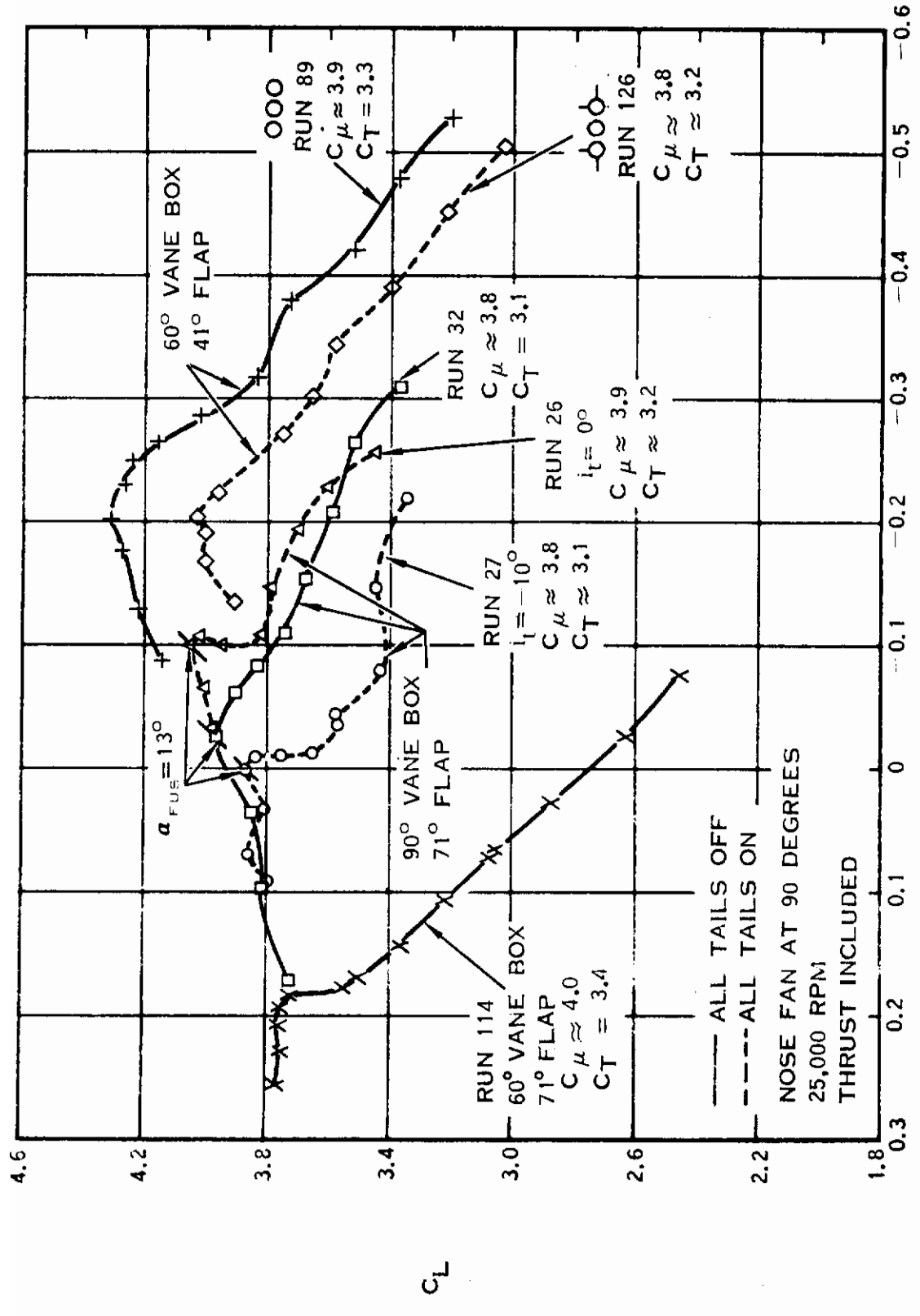

Figure 10. Longitudinal Comparison of 90-Degree and 60-Degree Vane Boxes with Tail On and Off at $C_\mu \approx 3.9$ $C_T = 3.3$

NOTES:

1. 90° VANE BOX (25,000 RPM)
2. FLAP DEFL = 71°
3. NOSE FAN EXIT AT 90°
4. TAILS OFF
5. GEOMETRIC MOMENT ARM USED
6. $C_\mu \approx 4.0$, $C_T \approx 3.4$, q = 10 PSF

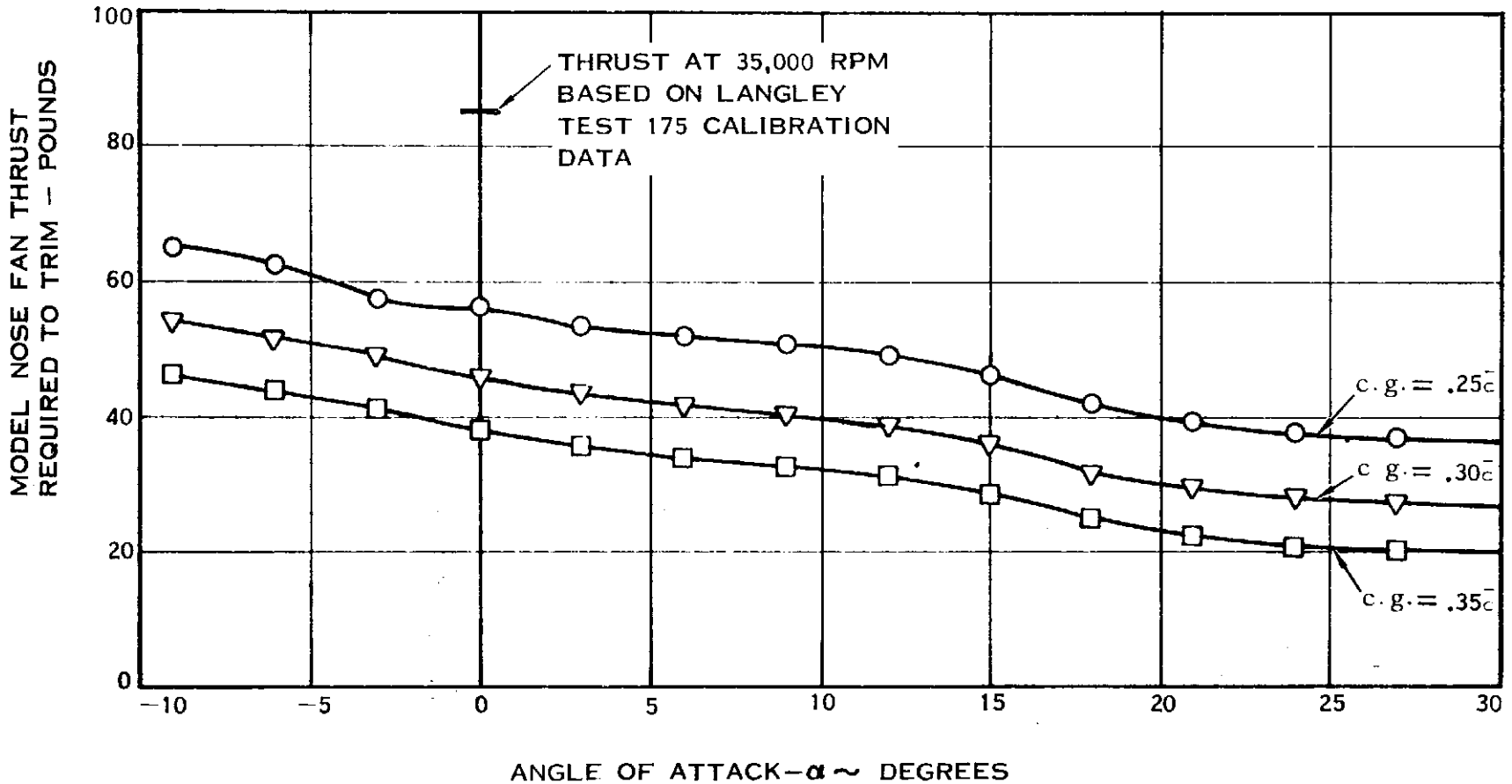

Figure 11. Model Nose Fan Thrust Required to Trim

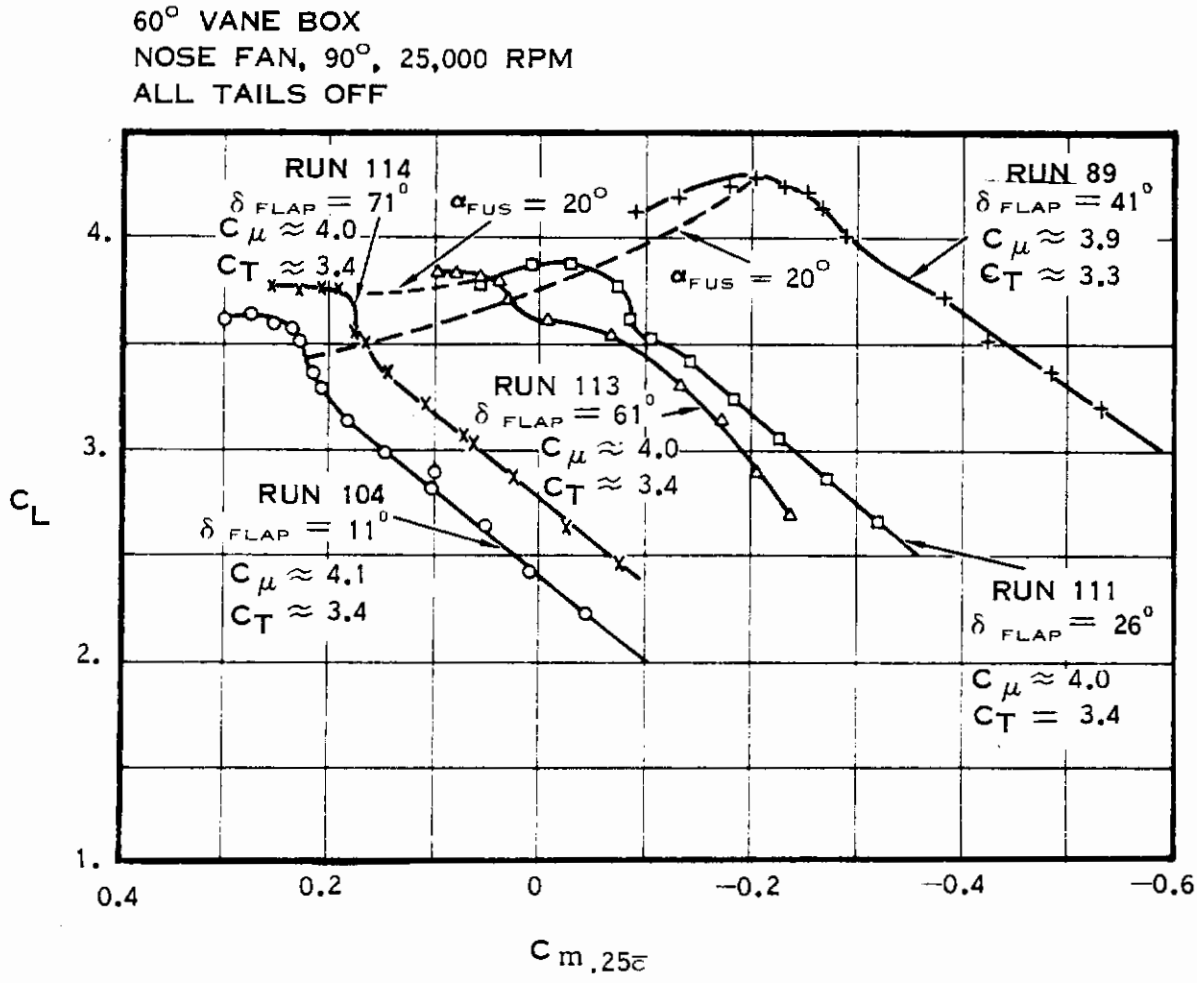

Figure 12. Effect of Flap Deflection on Longitudinal Characteristics, $C_\mu \approx 4.0$ $C_T \approx 3.4$

longitudinal characteristics at angles of attack up to approximately 20 degrees. At 20 degrees there is an increase in nose up pitching moment for all flap configurations. Figure 13 indicates the effects of C_μ on longitudinal stability. For high C_μ's, the thrust included aerodynamic center is ahead of the leading edge of the MGC and moves aft as C_μ decreases. The windmilling aerodynamic center is at 13% $\bar{c}$ aft of the leading edge of the MGC. The changes in aerodynamic center with C_μ are due to variations in the airplane pressure distribution caused by changes in inlet capture area affecting the leading edge stagnation point and changes in vortex patterns around the wing tips. There are large increases in the thrust-included lift coefficient and negative pitching moment as C_μ increases.

Horizontal tail effectiveness curves show that the horizontal tails do not stabilize the airplane but do provide some attitude control at the lower C_μ values.

2. DESCENT CAPABILITY

Flight path angles have been computed using the tabulated stability axes data. The results indicate that a 2,000 ft/min rate of descent can be made with the 60-and 90-degree vane box settings. The rate of descent was calculated by the following method.

For steady flight, the summation of forces along the flight path are zero; then

$$W\sin\gamma = C_D qS \cdot \text{(thrust included)} \tag{1}$$

For equilibrium perpendicular to the flight path

$$W\cos\gamma = C_L qS \cdot \text{(thrust included)} \tag{2}$$

From equations (1) and (2)

$$\gamma = \tan^{-1} \frac{-C_D}{\text{Trim } C_L} \tag{3}$$

By definition

$$q = \rho \frac{V^2}{2} \tag{4}$$

From equation (2)

$$q = \frac{W}{S} \frac{\cos\gamma}{\text{Trim } C_L} \tag{5}$$

Combining equations (4) and (5)

$$V_{knots} = \frac{1}{1.69} \sqrt{\frac{2}{\rho} \frac{W}{S} \frac{\cos\gamma}{\text{Trim } C_L}} = \sqrt{\frac{295\ W\cos\gamma}{\sigma S\ \text{Trim } C_L}}$$

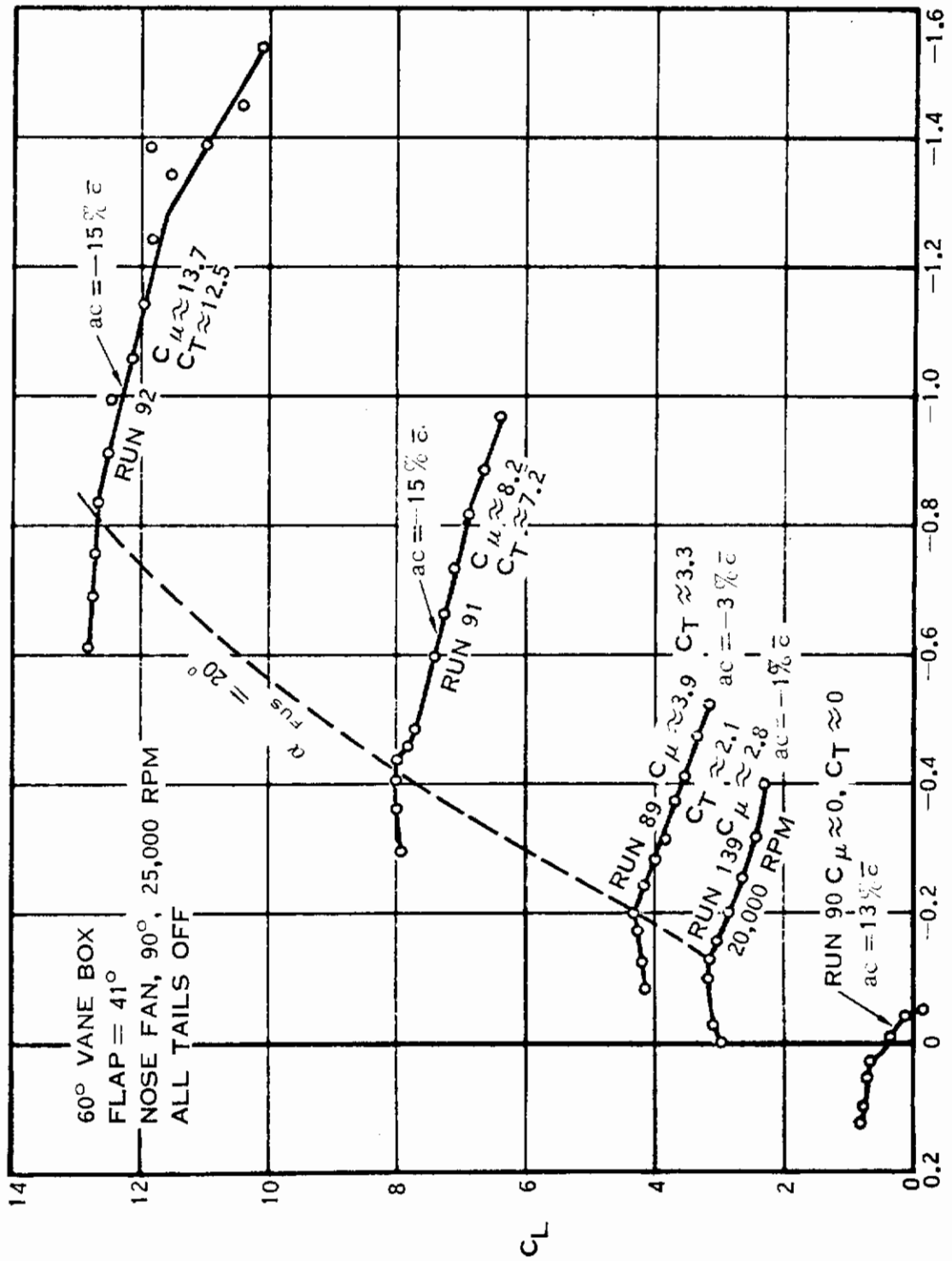

Figure 13. Effect of C_μ on Longitudinal Characteristics

Where

$$\text{Trim } C_L = C_L - \frac{C_m}{L_{NF/\bar{c}}}$$

L_{NF} = distance from c.g. to center of nose fan

$L_{NF/\bar{c}}$ = 1.2634 for a c.g. at 25% $\bar{c}$

Run selections for computation of descent are presented in Table I. A wing loading of 100 psf is assumed as typical. Descent capability with the 90-degree vane box is presented in Figure 14 which shows that flight path angle and attitude are roughly independent of velocity. For a constant value of C_μ = 32.0, flight path angle may be reduced from zero degree to -30 degrees with a change in pitch attitude of from -6 to -2 degrees. Descent angles for 60 degrees vane box deflection at four different flap deflections are presented in Figure 15(a) through 15(c). With 60 degrees of vane box deflection, descent angle is a function of airspeed at constant angle of attack, and reduced airspeed requires the usual increase in flight angle or angle of attack. Figures 15(a) through 15(c) are summarized in Figure 16, to demonstrate the effects of flap deflection on descent capability with the 60-degree vane box. Maximum descent angle is achieved with 50 degrees of flap deflection at a C_μ of 3.3. The limitations on descent capability due to buffet onset and power (thrust) available are undefined at this time; however, as shown by Figure 16, descent rates of 2,000 fpm seem attainable based on an angle of attack of 20 degrees which, according to Figures 12 and 13, is usable.

3. DIRECTIONAL STABILITY AND CONTROL

Tuft observations in the shakedown test reported in Part II indicated disturbed and possible stalled flow on the boom-mounted vertical tails. A fuselage-mounted centerline vertical tail of area equal to the sum of the boom-mounted vertical tails was constructed and tested. Results show this centerline vertical tail to be twice as effective as those on the boom acting together.

a. 30-Degree Vane Box

Side force and yawing moment characteristics with tail buildup are presented in Figures 17(a) and 17(b). The increment in $C_{Y\beta}$ due to adding the centerline vertical tail is greater than that of the outboard vertical tails, even though the total areas, aspect ratios, and tail arms are equal. With the centerline vertical tail, there is a reduction in $C_{Y\beta}$ and $C_{n\beta}$ at $\beta = -8°$ due to tail stall that does not appear for the outboard tails. The apparent lack of a stall for the outboard vertical tails indicates either: low effectiveness due to disturbed flow, strong sidewash gradient ($d\sigma/d\beta$), or a continuously stalled condition due to sidewash on one/both outboard tails. The improvement in directional stability due to the centerline tail is evident and is on the order of $\Delta C_{n\beta} \approx 0.0062$, more than twice the increment due to the outboard tails of $\Delta C_{n\beta} \approx 0.0029$. Since a V/STOL airplane can easily

TABLE I. RUN SELECTIONS FOR DETERMINATION OF γ VERSUS VELOCITY

RUN	WING BOX	FLAP	TAILS	C_μ	FIGURE
33	90°	71°	Off	39.0	14
37	90°	71°	Off	19.7	14
38	90°	71°	Off	13.0	14
36	90°	71°	Off	7.5	14
32	90°	71°	Off	3.8	14
78	90°	71°	Off	20.0	14
79	90°	71°	Off	7.8	14
31	90°	71°	Off	Range	14
114	60°	71°	Off	4.0	16
113	60°	61°	Off	4.0	16
93	60°	41°	Off	43.2	15
92	60°	41°	Off	13.7	15
91	60°	41°	Off	8.2	15
89	60°	41°	Off	4.0	15, 16
140	60°	41°	Off	9.0	15
139	60°	41°	Off	2.7	15
88	60°	41°	Off	Range	15
111	60°	26°	Off	4.0	15, 16
110	60°	26°	Off	Range	15
105	60°	11°	Off	13.0	15
104	60°	11°	Off	4.1	15, 16
103	60°	11°	Off	Range	15

SYMBOL	RUN	TUNNEL q	RPM	C_μ (EXCL NOSE FAN)
—○—	33	1	25,000	32.0
—○—	37	2	25,000	16.5
—○—	38	3	25,000	11.0
—○—	36	5	25,000	6.3
—○—	32	10	25,000	3.1
—△—	78	3	30,000	17.1
—△—	79	3	20,000	6.3
- - - -	31	RANGE	25,000	RANGE ($\alpha_{FUS} = 0°$)

—○— 25,000 RPM, C_μ CHANGED BY CHANGING TUNNEL q , α VARIES
—△— TUNNEL q = 3.0, C_μ CHANGED BY CHANGING RPM , α VARIES
- - - - - 25,000 RPM, $\alpha = 0$, C_μ VARIED BY VARYING TUNNEL q

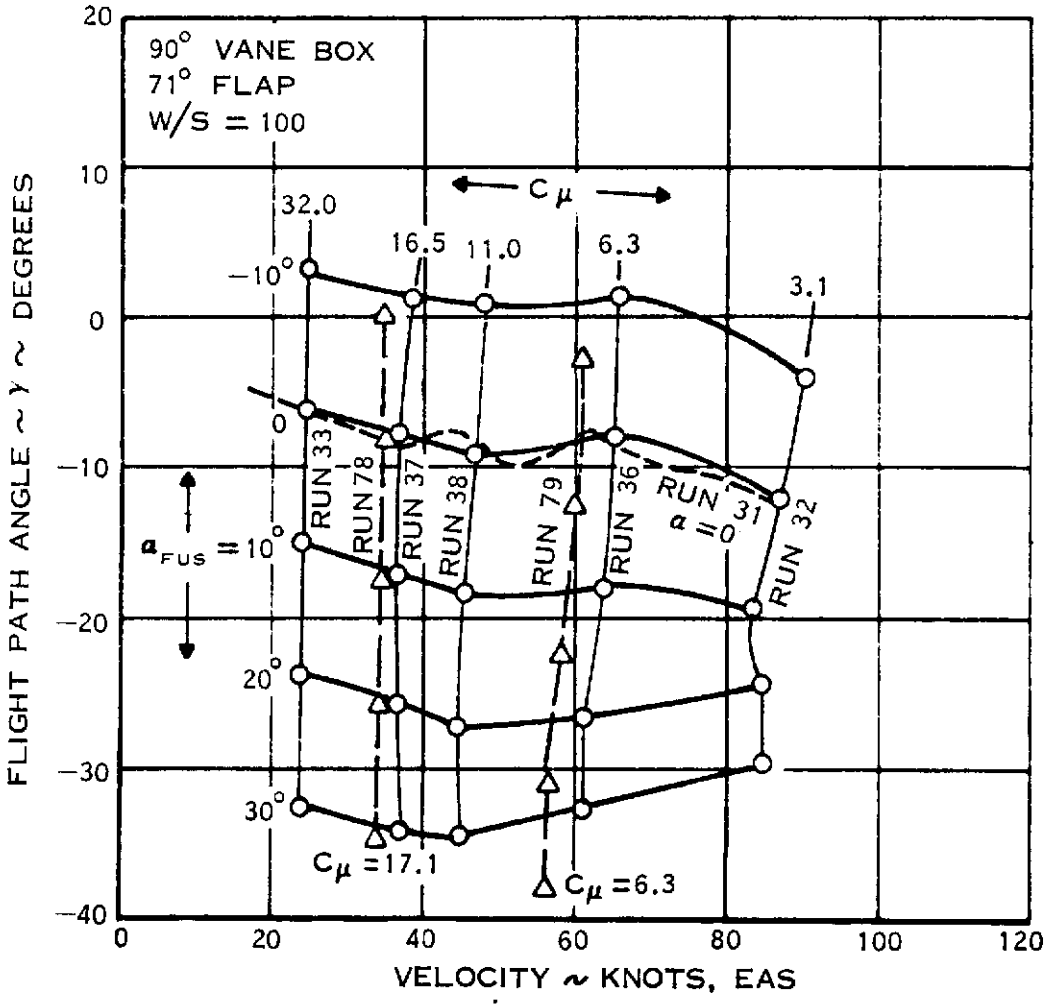

Figure 14. Descent Capability with 90-Degree Vane Box

RUN	q	RPM	C_μ (EXCL NOSE FAN)
93	1	25,000	36.5
92	3	25,000	11.6
91	5	25,000	7
89	10	25,000	3.3
140	3	20,000	7.3
139	10	20,000	2.2
88	RANGE	25,000	RANGE ($\alpha_{FUS}=0°$)

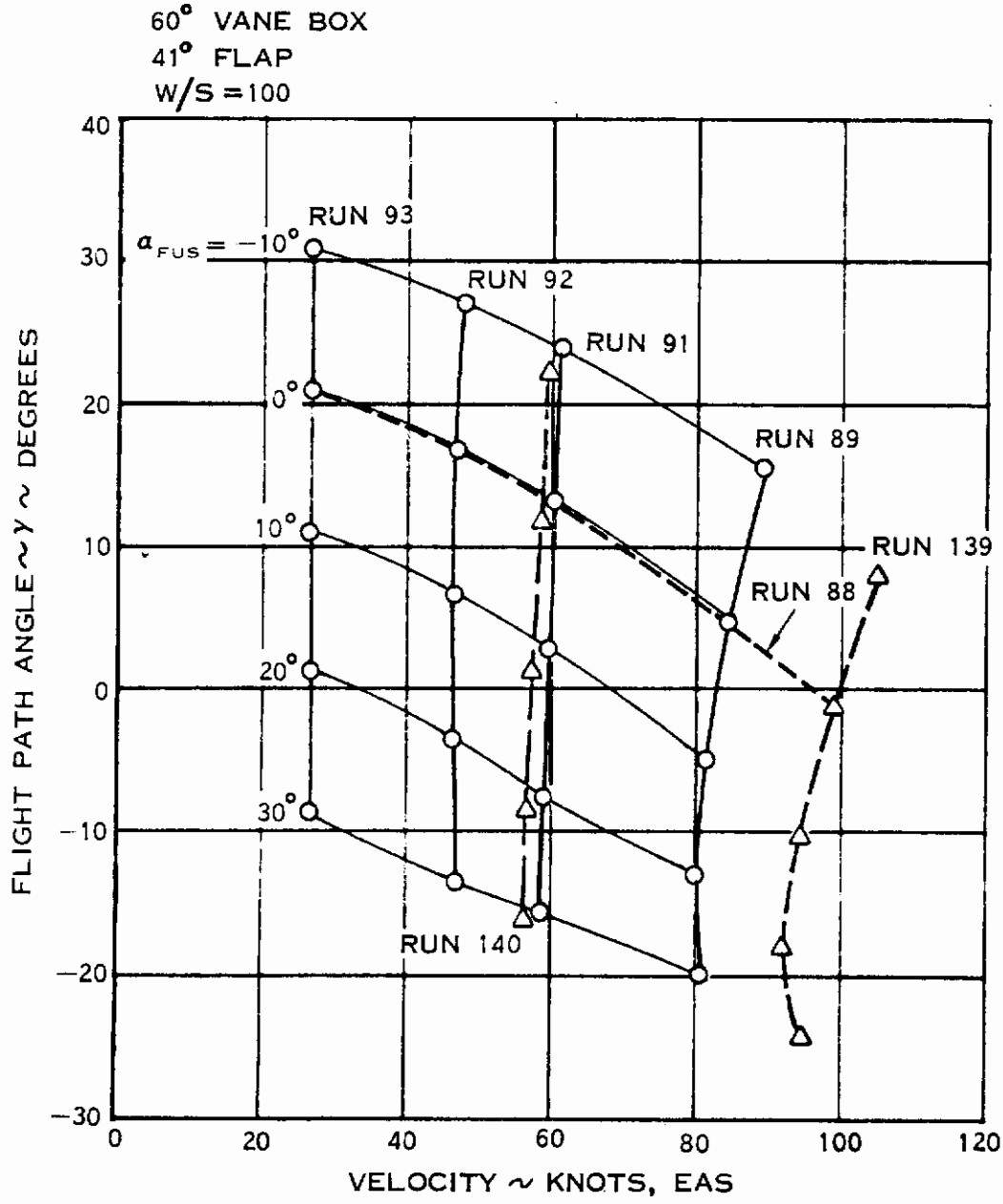

(a) 41 DEGREES FLAP

Figure 15. Descent Capability with 60-Degree Vane Box

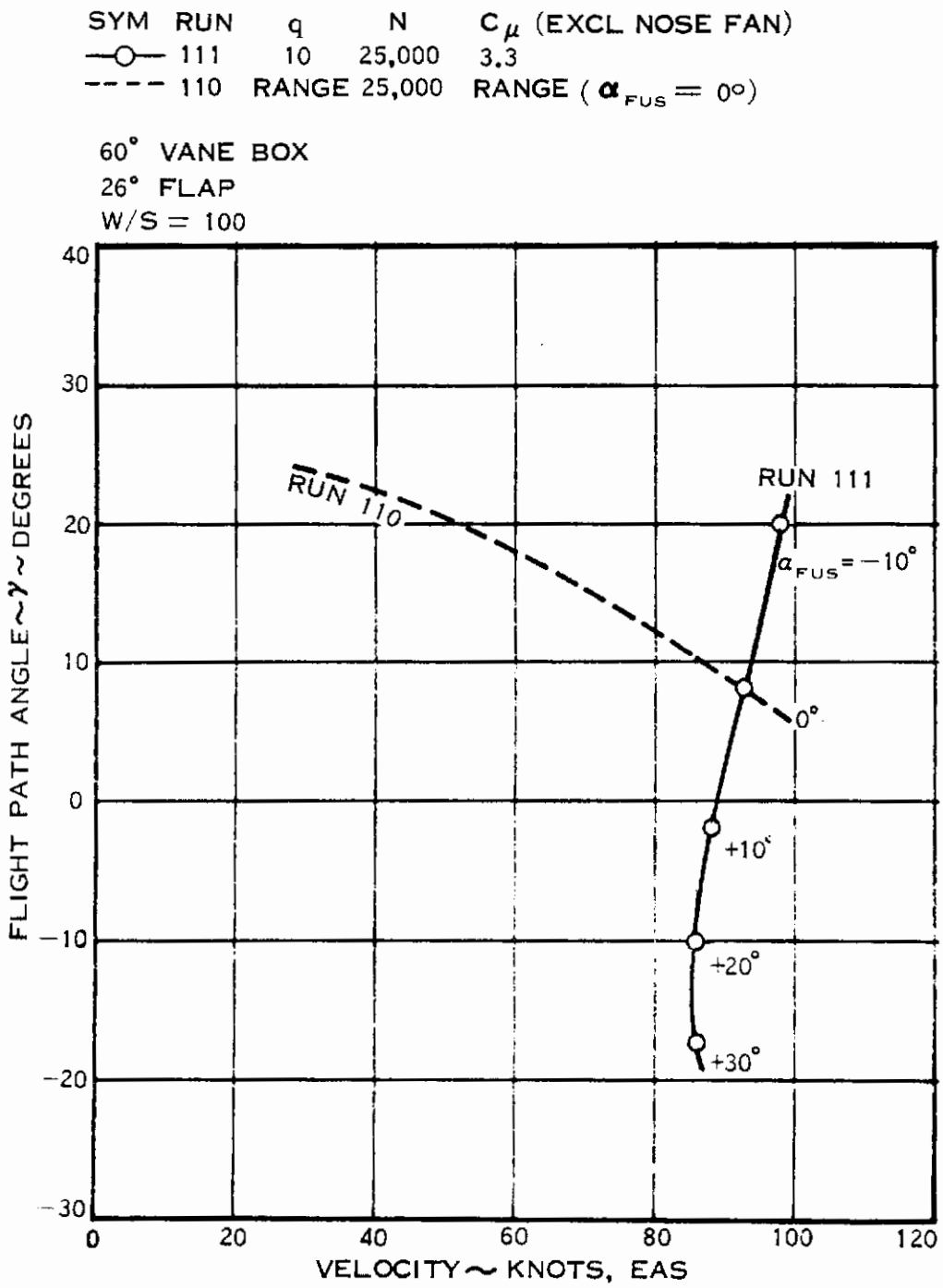

(b) 26 DEGREE FLAP

Figure 15. Descent Capability with 60-Degree Vane Box (Continued)

SYM	RUN	q	N	C_μ (EXCL NOSE FAN)
—○—	105	3	25,000	11
—○—	104	10	25,000	3.3
- - - -	103	RANGE	25,000	RANGE ($\alpha_{FUS} = 0^\circ$)

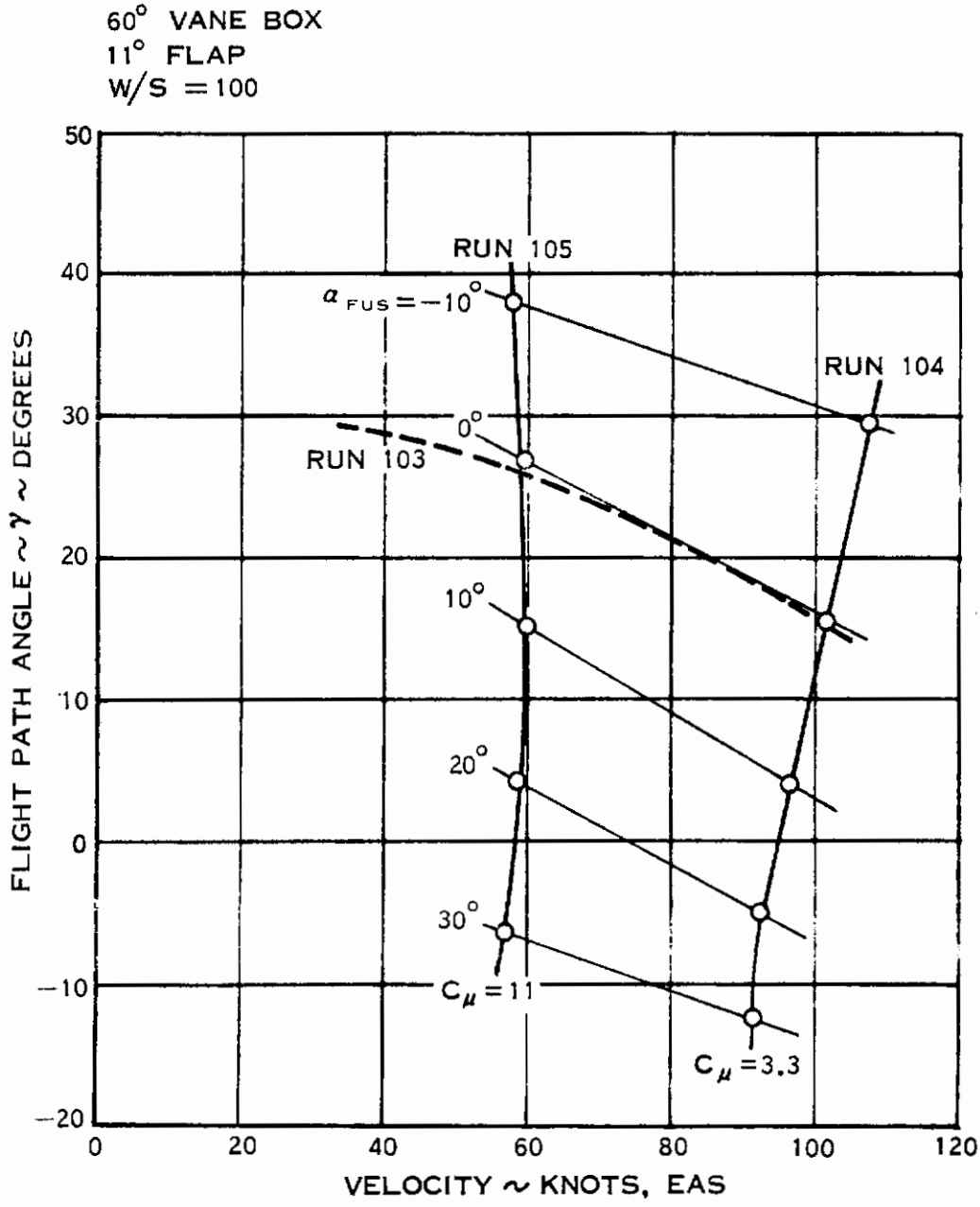

(c) 11 DEGREE FLAP

Figure 15. Descent Capability with 60-Degree Vane Box (Concluded)

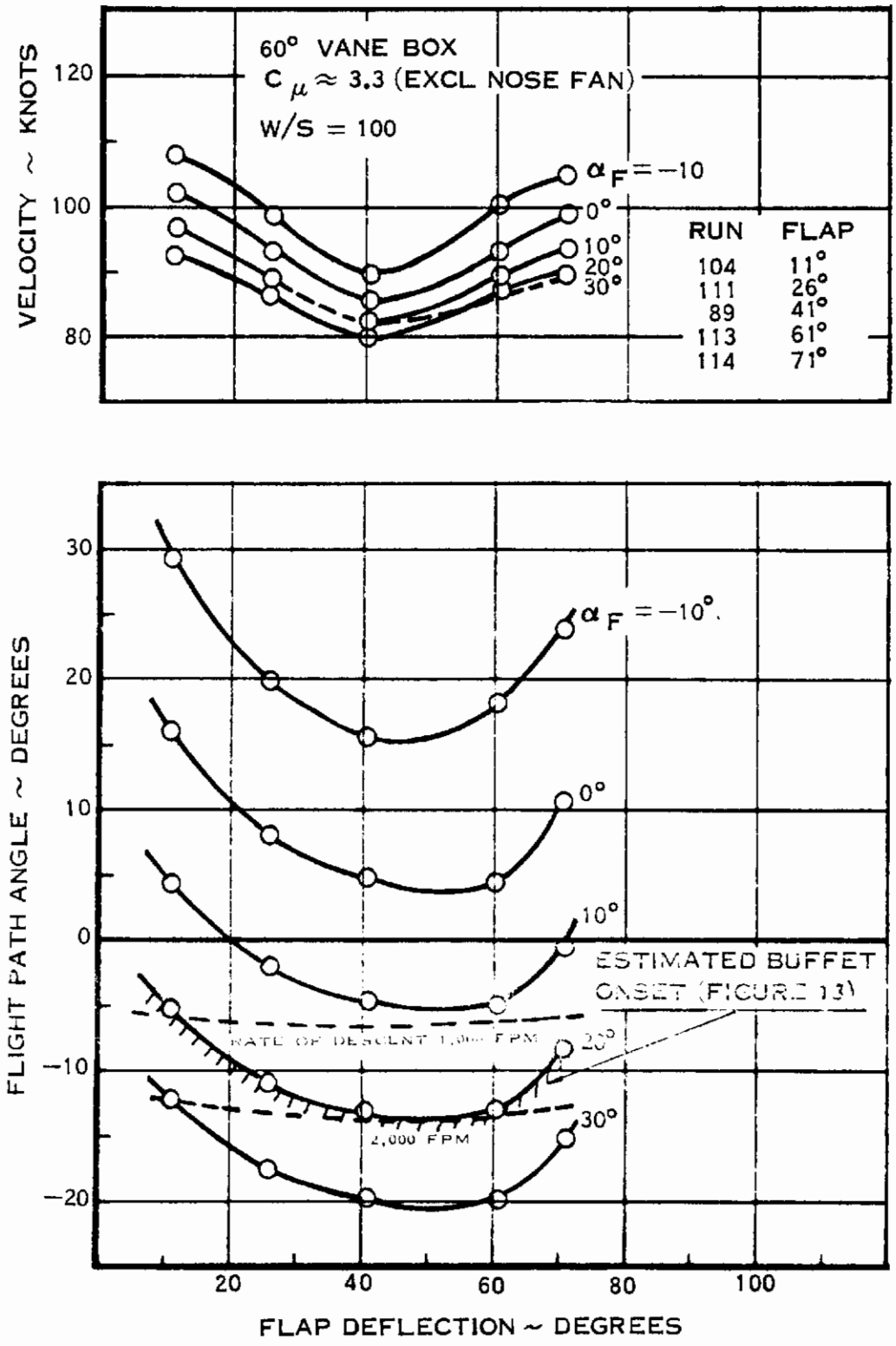

Figure 16. Effect of Flap Deflection on Descent Capability

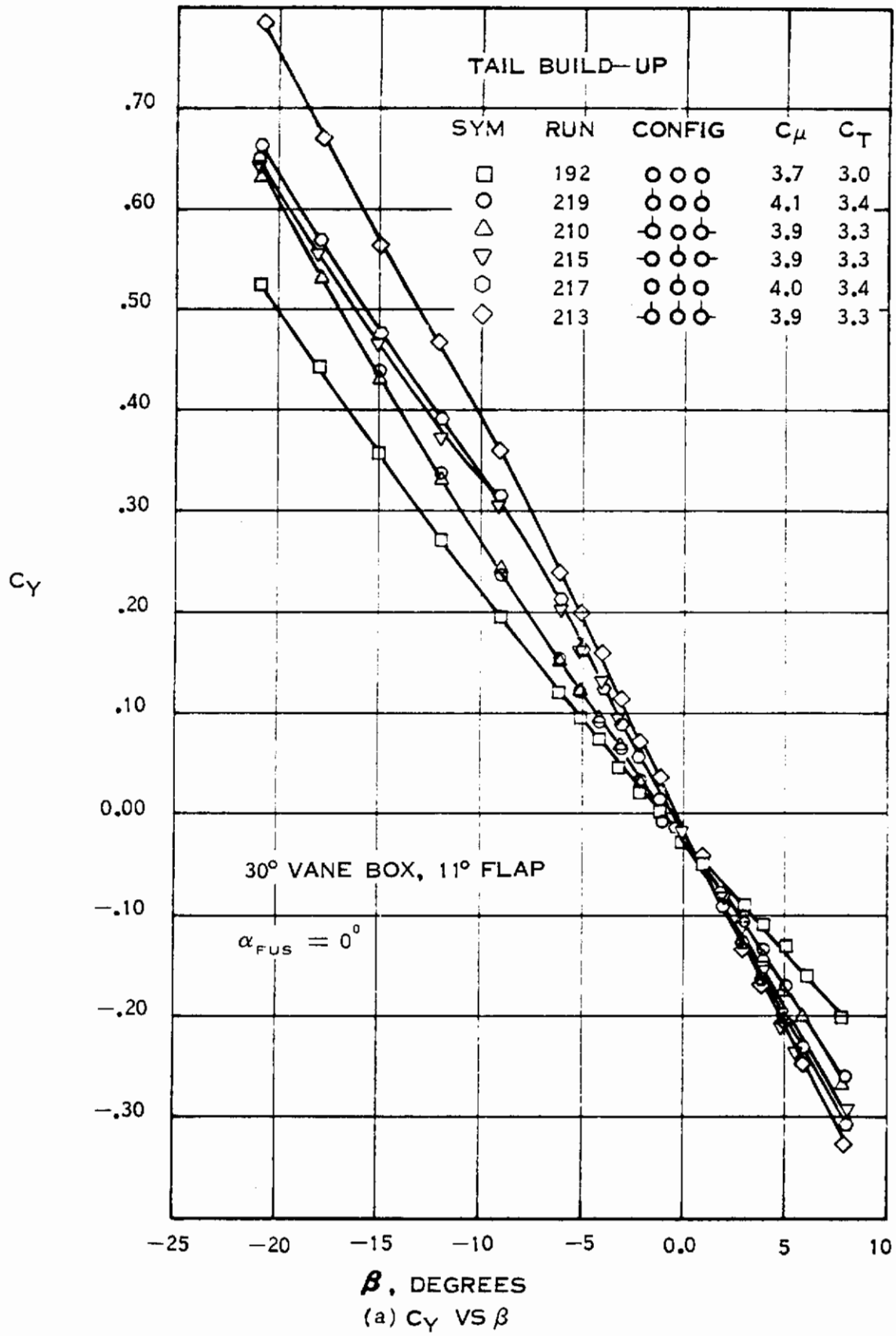

(a) C_Y VS β

Figure 17. Directional Characteristics with Tail Buildup

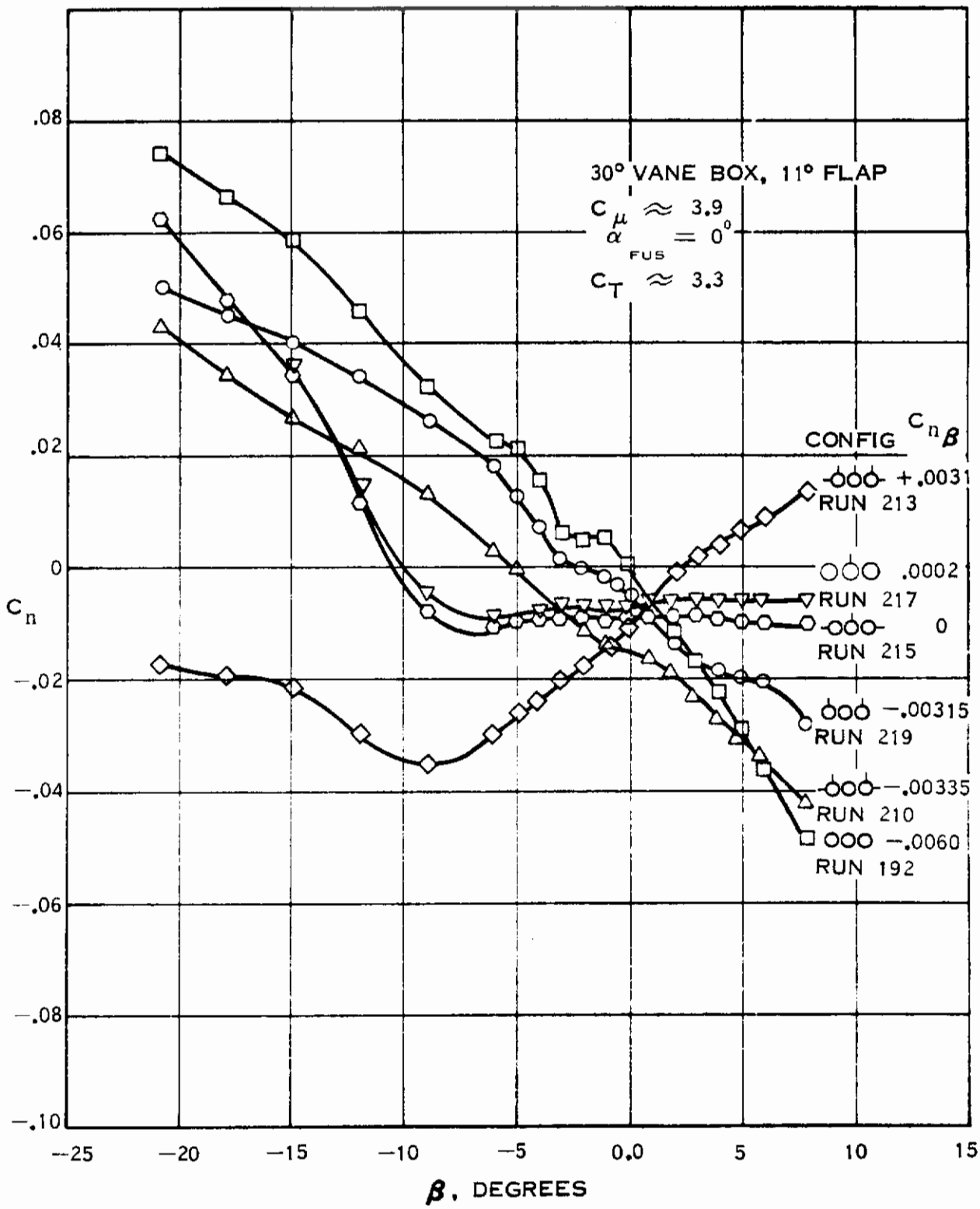

(b) C_n VS β

Figure 17. Directional Characteristics with Tail Buildup (Concluded)

exceed 8 degrees of sideslip, a modification of the centerline vertical tail is required such as an increase in sweep, a decrease in aspect ratio, or the addition of a dorsal to increase the effective sideslip range.

The effect of momentum coefficient on directional characteristics is presented in Figure 18. There is an unexplained reversal in trend of side force with $C\mu$. In going from windmilling fans to $C\mu \approx 3.8$, there is an increase in side force; however, increasing $C\mu$ from 3.8 to 13.0 results in a reduction in side force. The same trend applies to tails on or off. In Figure 18(b) the directional stability changes are more consistent; C_η becomes more negative with increasing $C\mu$ that implies an increasing sidewash gradient $d\sigma/d\beta$ which is normal for increasing thrust/momentum coefficient.

The effects of fairing the nose on directional characteristics are presented in Figure 19; tail off $C_{Y\beta}$ is reduced and the tail contribution to $C_{Y\beta}$ is greater than with the nose fan operating. These variations are also evident in Figure 19(b) showing a marked increase in $C_{\eta\beta}$ due to fairing the nose. The plugged nose also improves flow conditions ($d\sigma/d\beta$) over the outboard vertical tails increasing their contribution to stability.

b. 60-Degree Vane Box

Directional stability with the 60-degree vane box is presented in Figure 20. These data show a tails-off $C_{\eta\beta}$ of approximately -0.0066 for all momentum coefficients. Scatter in the data and zero shifts at $\beta = 0$ degree are believed to be caused by inability to set equal $C\mu$ on left- and right-hand wing fans or by variations in ambient conditions effecting balance zeros. Note also discontinuities in the trend lines (hysteresis) of Figures 17(b), 18(b), 19(b) and 20(b), which may be aerodynamic or equipment characteristics. The outboard horizontal and vertical tails-on data shown in Figure 20 show very little tail contribution to directional stability at $C\mu$'s from 3.6 to 12. There is a contribution for the windmilling case.

Lateral and directional control data were obtained by differential deflection of the vane box doors and differential fan rpm, see Figure 21. Note that differential vane box deflections and differential fan rpm as tested yielded additive yawing moments and opposing rolling moments. By proper matching of the differentials (i.e., programming), pure yaw control or roll control can be obtained.

c. 90-Degree Vane Box

Directional stability with the 90-degree vane box and all tails off is shown in Figure 22(a). Values of C_η at $\beta = 0$ are indicative of unintentional asymmetric power conditions and the low tunnel q used. The level of $C_{\eta\beta}$ is approximately -0.0095 for a tunnel q of 10. The horizontal and outboard vertical tails (Figure 22(b)) have a minor influence on $C_{\eta\beta}$ which, at the low flight speeds implied by the 90-degree vane box, is probably not significant to flying qualities compared to directional control. Directional control was demonstrated by asymmetrical deflection of the vane box doors. Figure 23 presents the yawing coefficient versus the momentum coefficient for a deflection of 100 degrees on the left and 80 degrees on the right. The

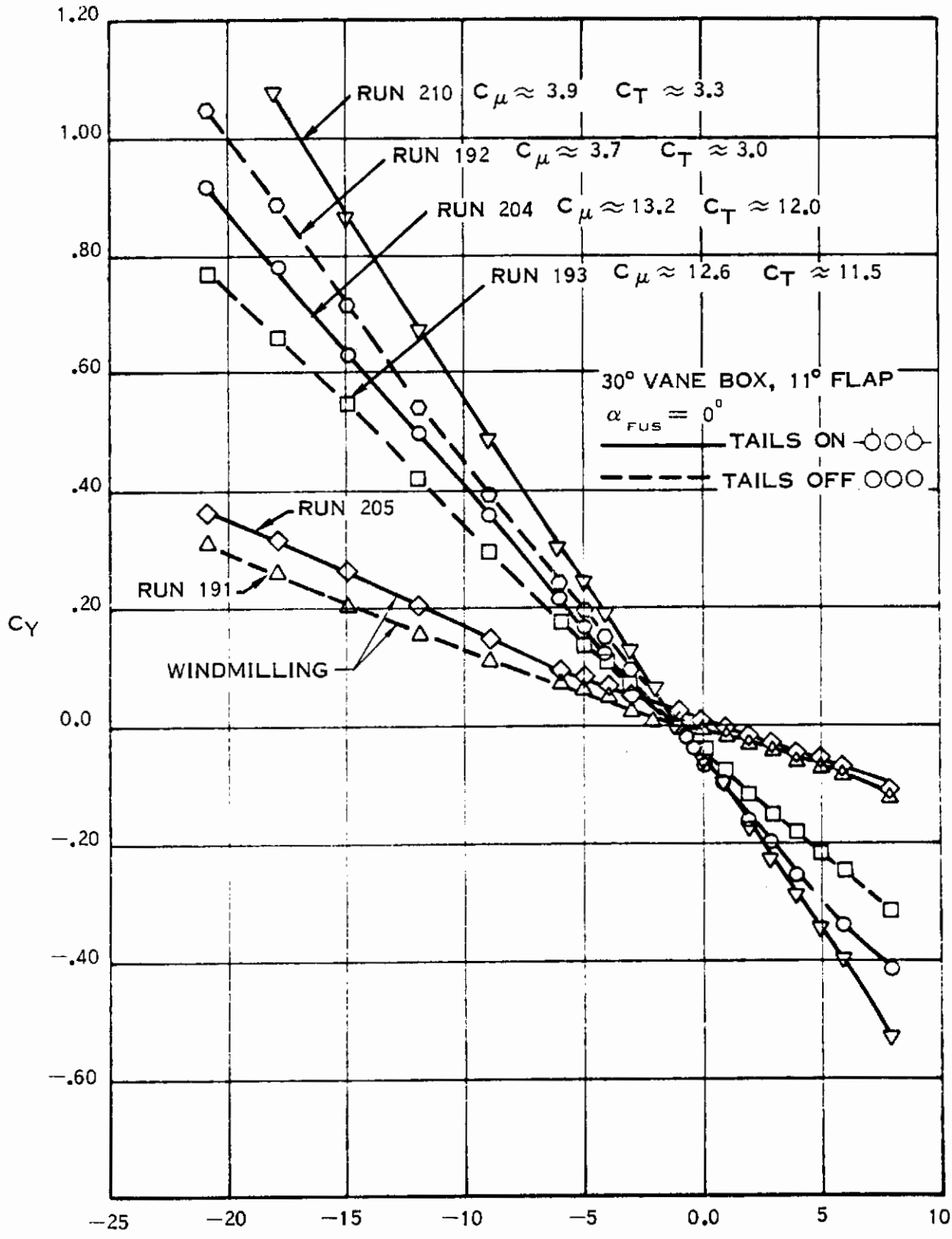

(a) C_Y VS β

Figure 18. Effect of C_μ on Directional Characteristics

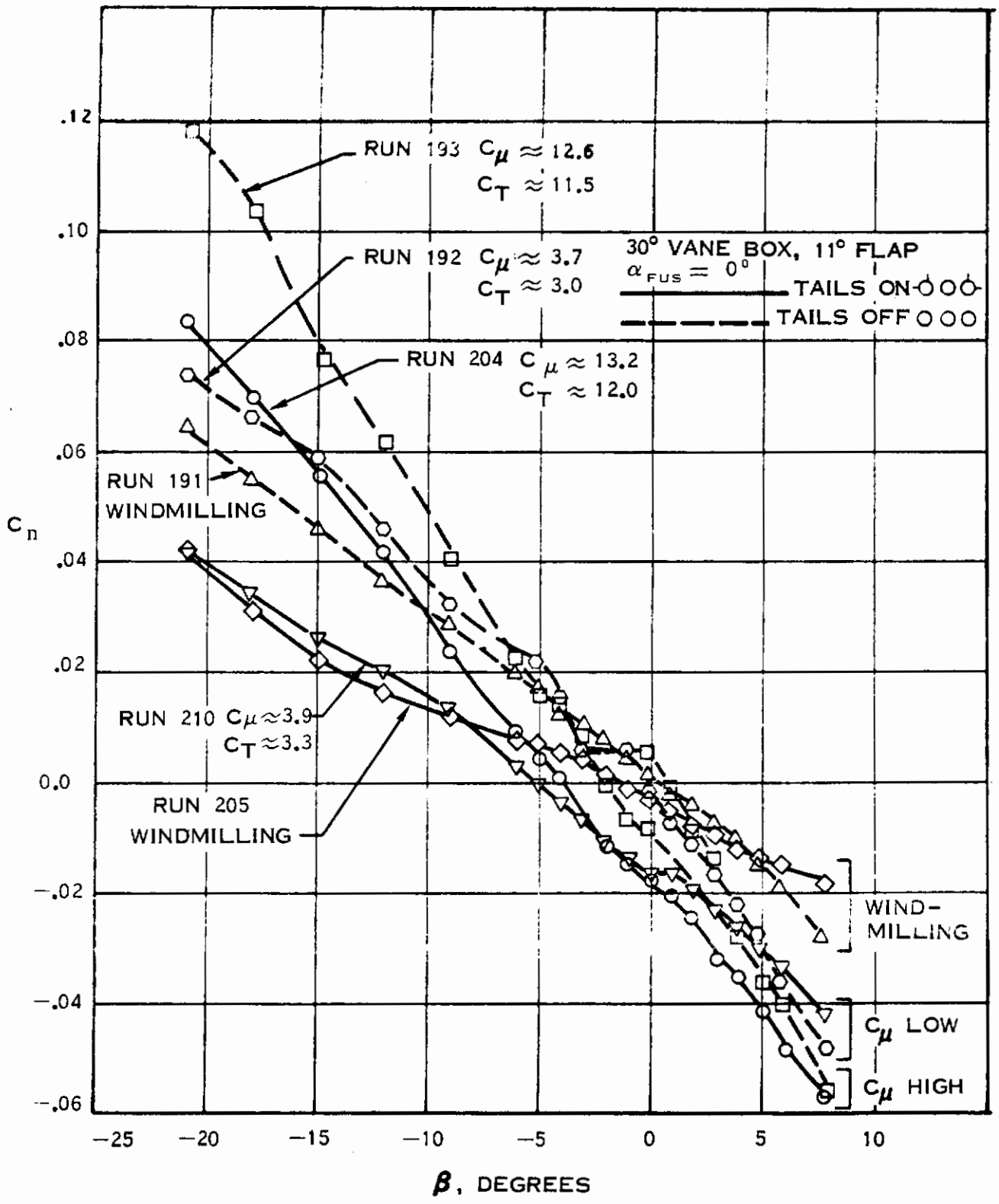

(b) C_n VS β

Figure 18. Effect of C_μ on Directional Characteristics (Concluded)

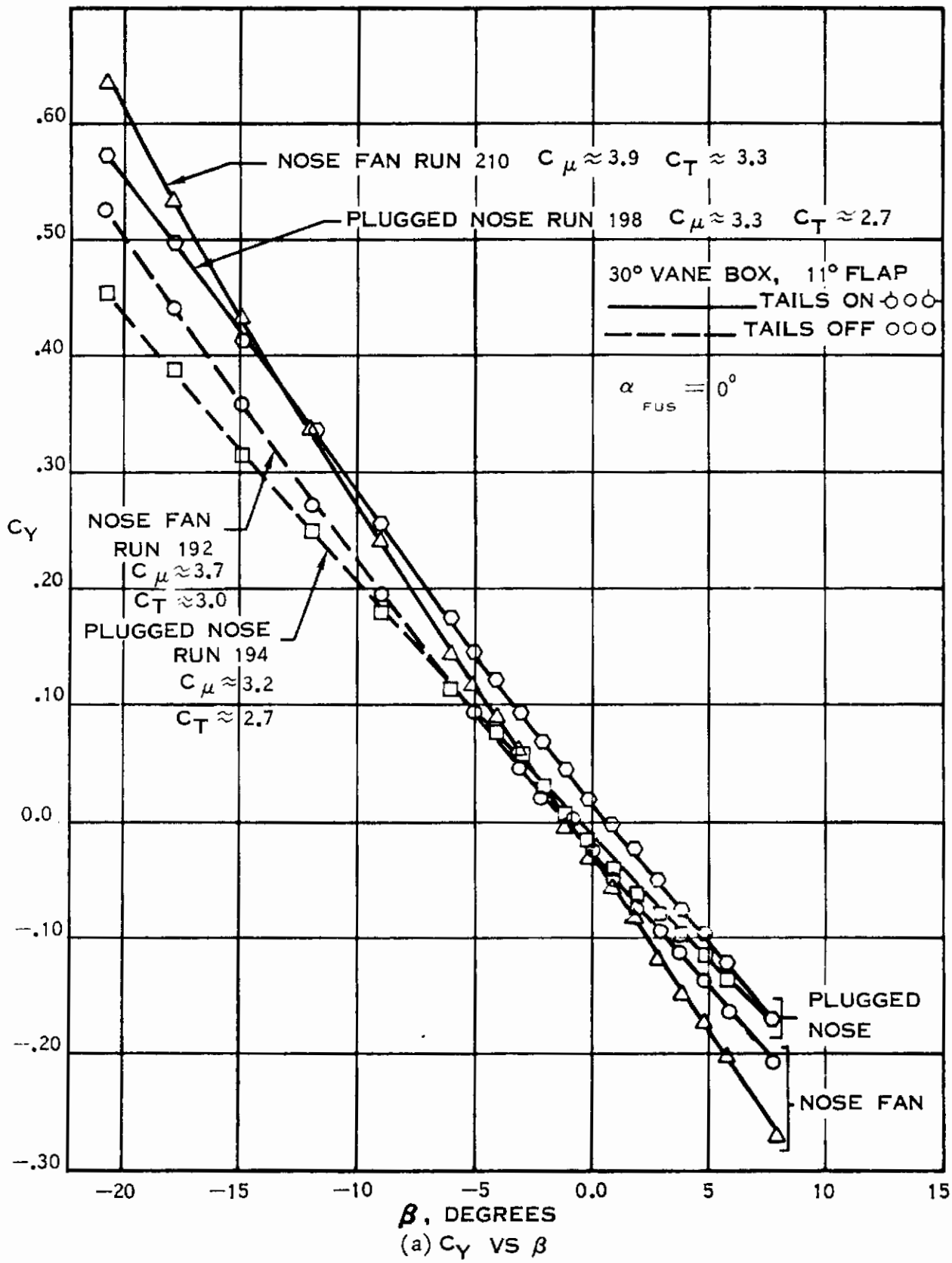

(a) C_Y VS β

Figure 19. Effect of Plugged Nose on Directional Characteristics

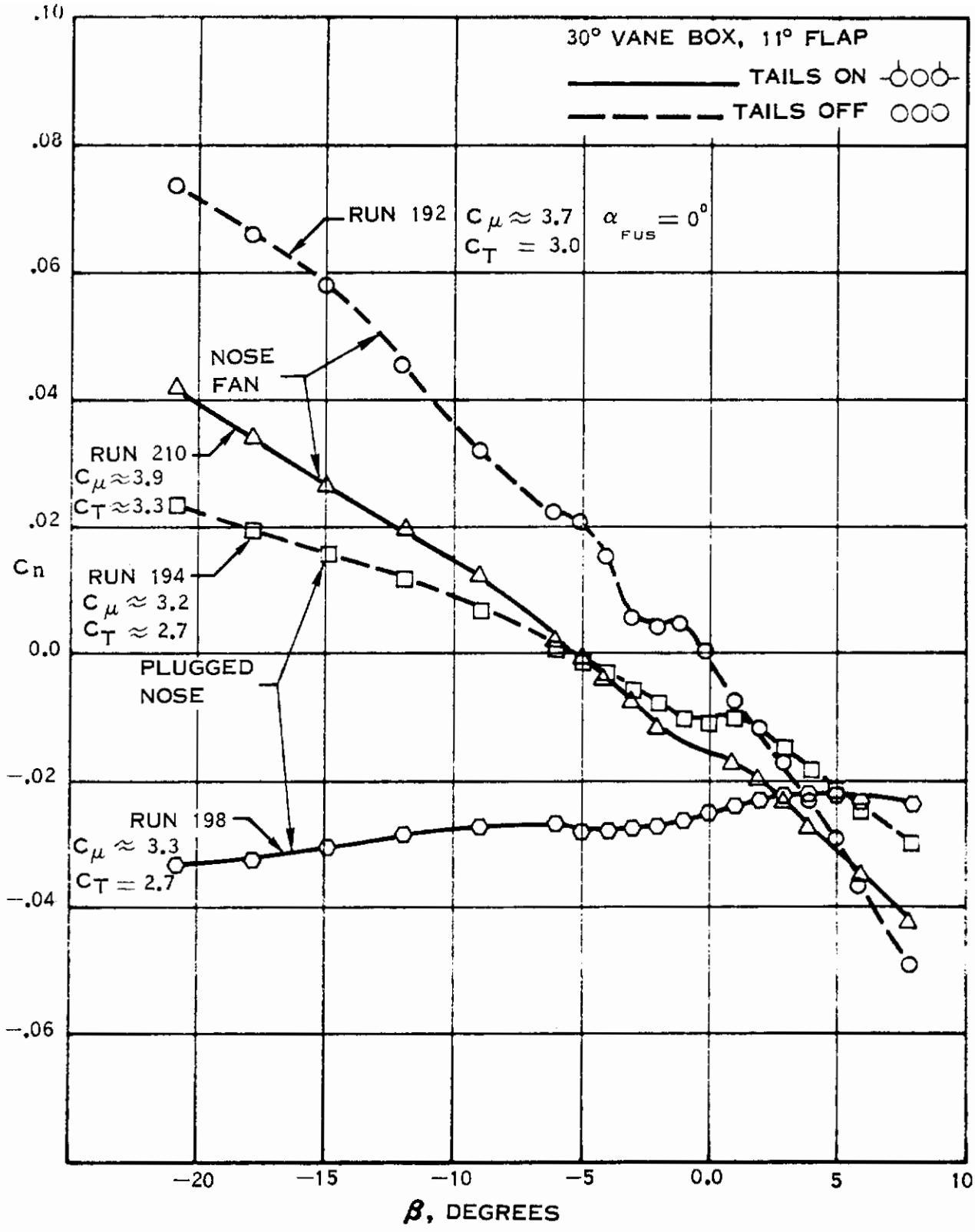

(b) C_n VS β

Figure 19. Effect of Plugged Nose on Directional Characteristics (Concluded)

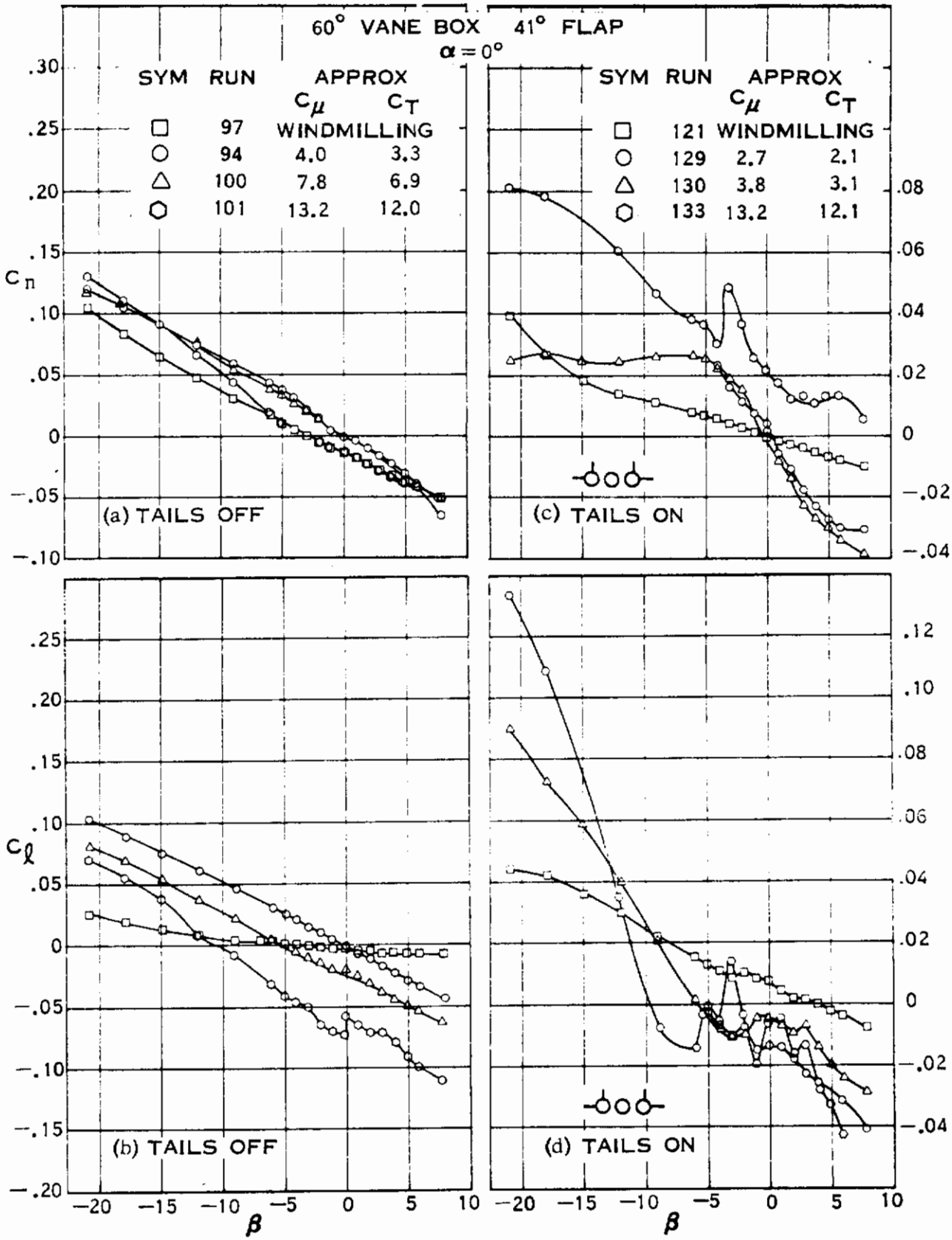

Figure 20. Effect of Cμ on the Lateral Directional Stability of the 60-Degree Vane Box

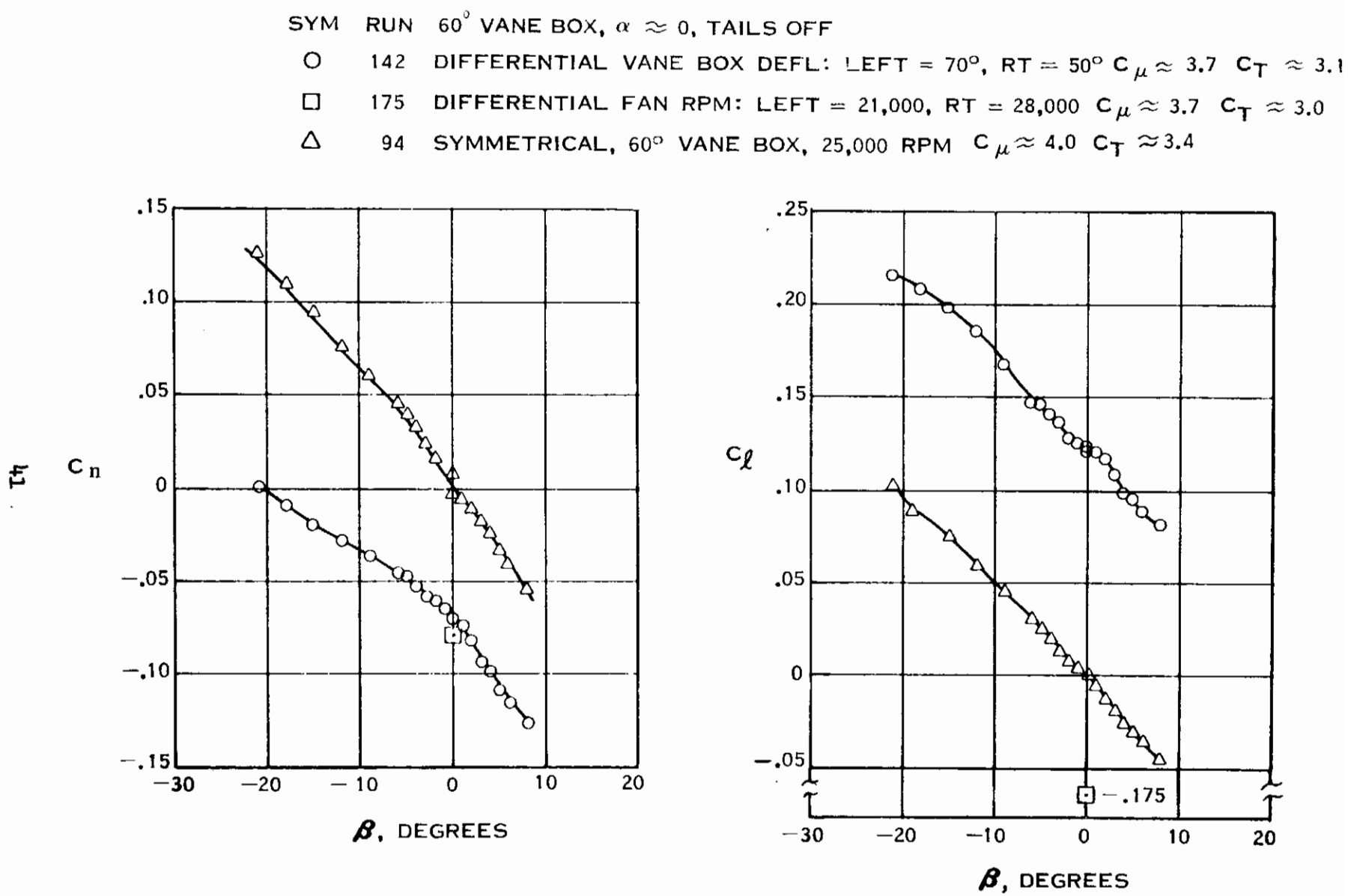

Figure 21. Control Effectiveness of Differential Vane Box Deflection and Fan RPM

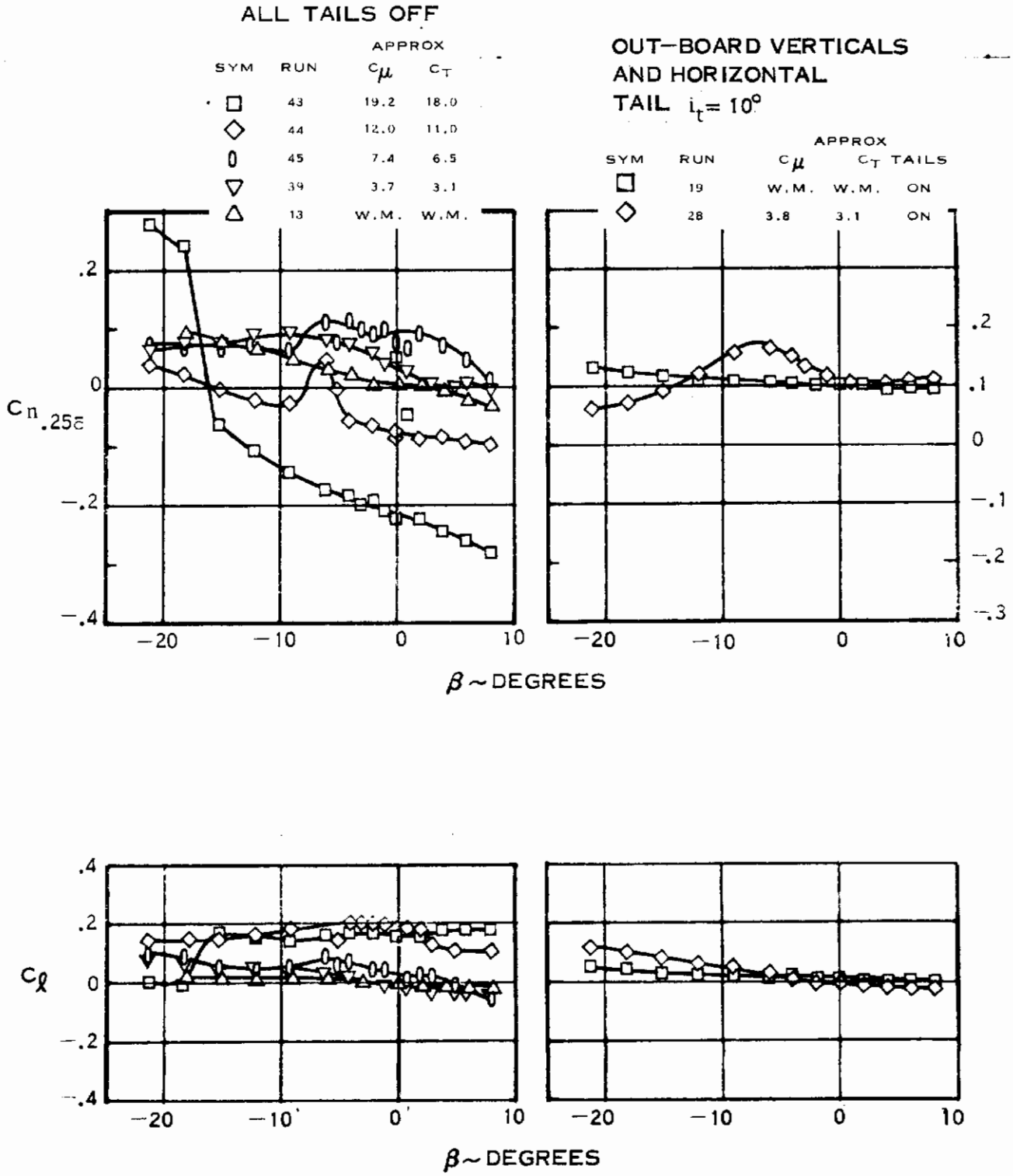

Figure 22. Lateral-Directional Stability of the 90° Vane Box with All Tails Off and All Tails On

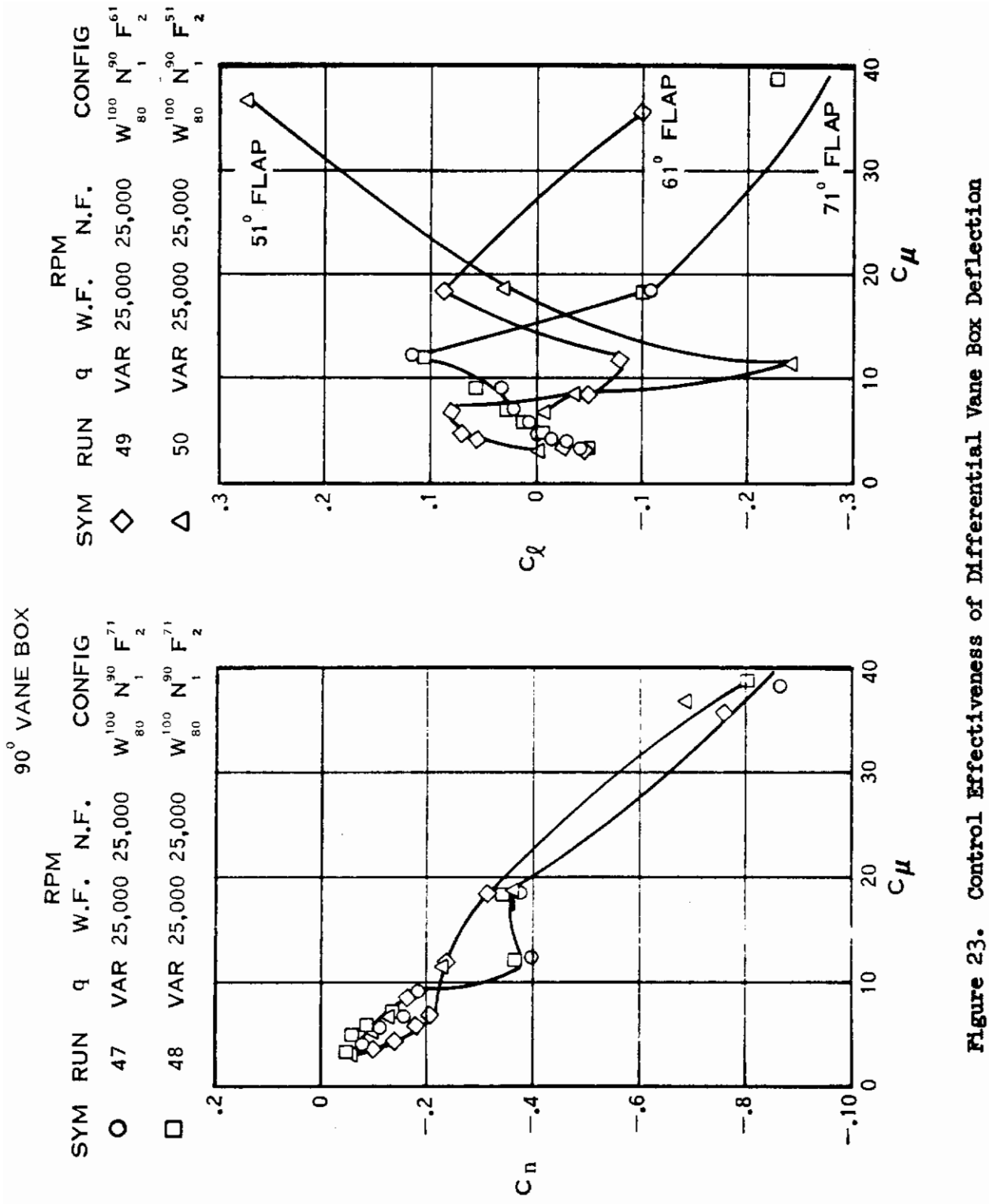

Figure 23. Control Effectiveness of Differential Vane Box Deflection

momentum coefficient was changed by varying the tunnel dynamic pressure. Reference to the basic yawing moment data shows characteristics approximately constant for all momentum coefficients tested, thereby indicating that the yawing moment is primarily caused by deflecting the vane box thrust with only minor aerodynamic effects. The rolling moment coefficient data are random with quite small values of actual rolling moment.

4. LATERAL STABILITY AND CONTROL

a. 30-Degree Vane Box

Lateral stability characteristics with the 30-degree vane box are presented in Figures 24, 25, and 26. Figure 24 shows the variations obtained with various tail combinations; all configurations have positive lateral stability. For the range of sideslip angles from zero to -10 degrees, tails off $C_{\ell\beta}$, run 192, is -0.0032, which increases to -0.0046 with the addition of the outboard vertical tails, run 219. Configurations with the centerline vertical tails have a $C_{\ell\beta}$ of the order of -0.0077. Beyond ±10 degrees of sideslip, the centerline vertical tail stalls and $C_{\ell\beta}$ reverts back to the level existing with the outboard vertical tails. Figure 25 demonstrates the increase in $C_{\ell\beta}$ arising from increases in momentum coefficient. The increasing C_ℓ at $\beta = 0$ with increases in C_μ indicates asymmetry in construction, left- and right-hand wing, or in the vane box angles. The negative rolling moment at $\beta = 0$ is increased upon addition of the tails which indicates either asymmetry in horizontal tail settings, left- and right-hand wing C_μ, or a strong influence of the wing exit flow on the local flow at the horizontal tails. Additional testing is required to investigate these asymmetries which may involve interactions with the wing tip vortex -- a vortex possibly existing around the edges of the exhaust flow -- and the pumping action of the high velocity deflected propulsive flow.

Figure 26 shows that the effect of plugging the nose on lateral stability is negligible.

b. 60-Degree Vane Box

The lateral stability with the 60-degree vane box and all tails-off is shown in Figure 20(b). The data show a $C_{\ell\beta}$ of 0.0007 fans windmilling and approximately -0.005 with momentum coefficient in the range 3.6 to 12.0. The outboard horizontal and vertical tails data shown in Figure 20(d) show no discernable effect of the tails on lateral stability.

Roll control effectiveness by differential vane box thrust is shown in Figure 21 which also shows a data point obtained with differential thrust at zero angle of attack and zero sideslip angle. This data point indicates a favorable yaw-to-roll relationship with differential thrust control in roll. Additional control effectiveness data with differential vane box doors and thrust were not obtained due to problems encountered with the roll gages of the balance.

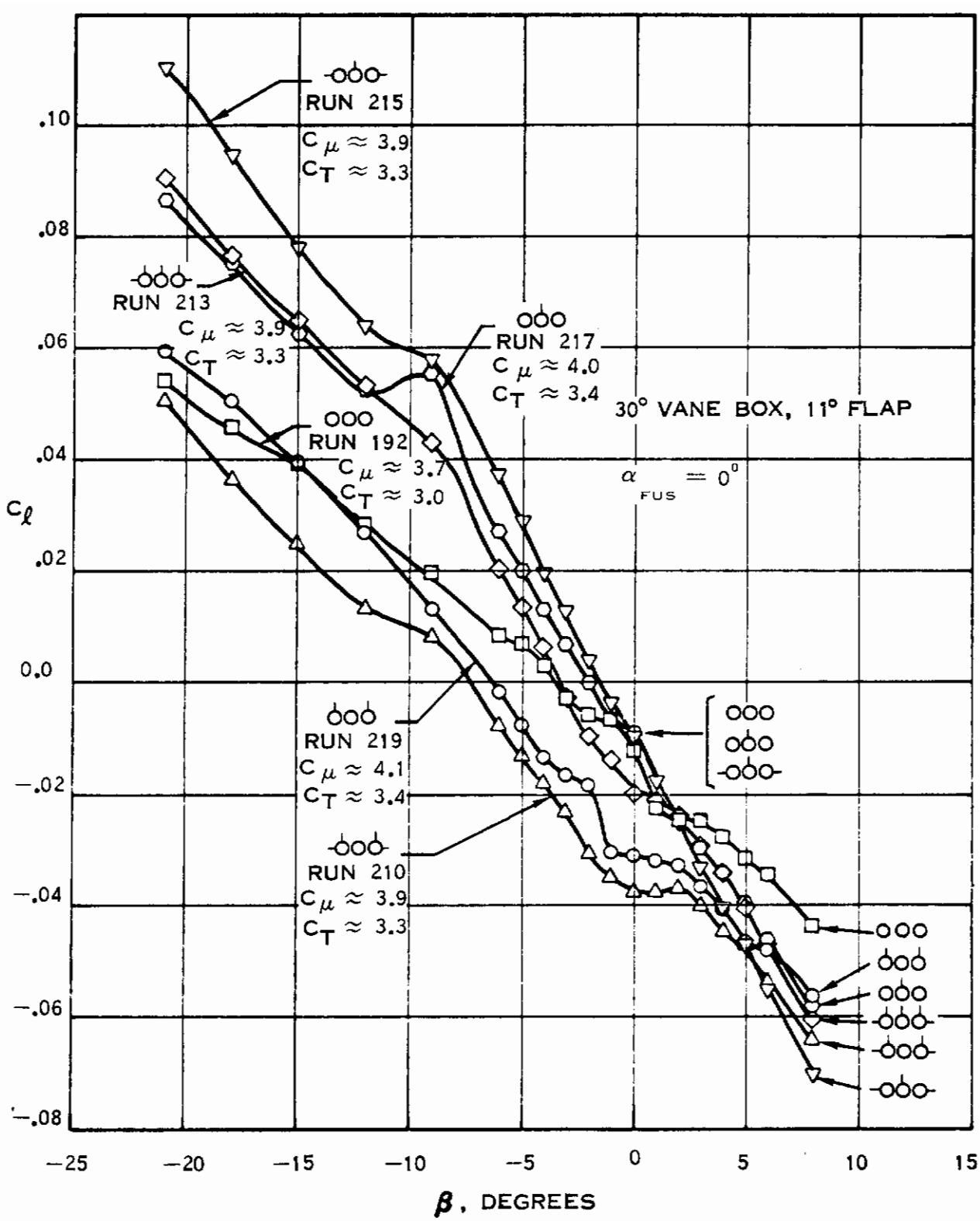

Figure 24. Lateral Characteristics with Tail Buildup

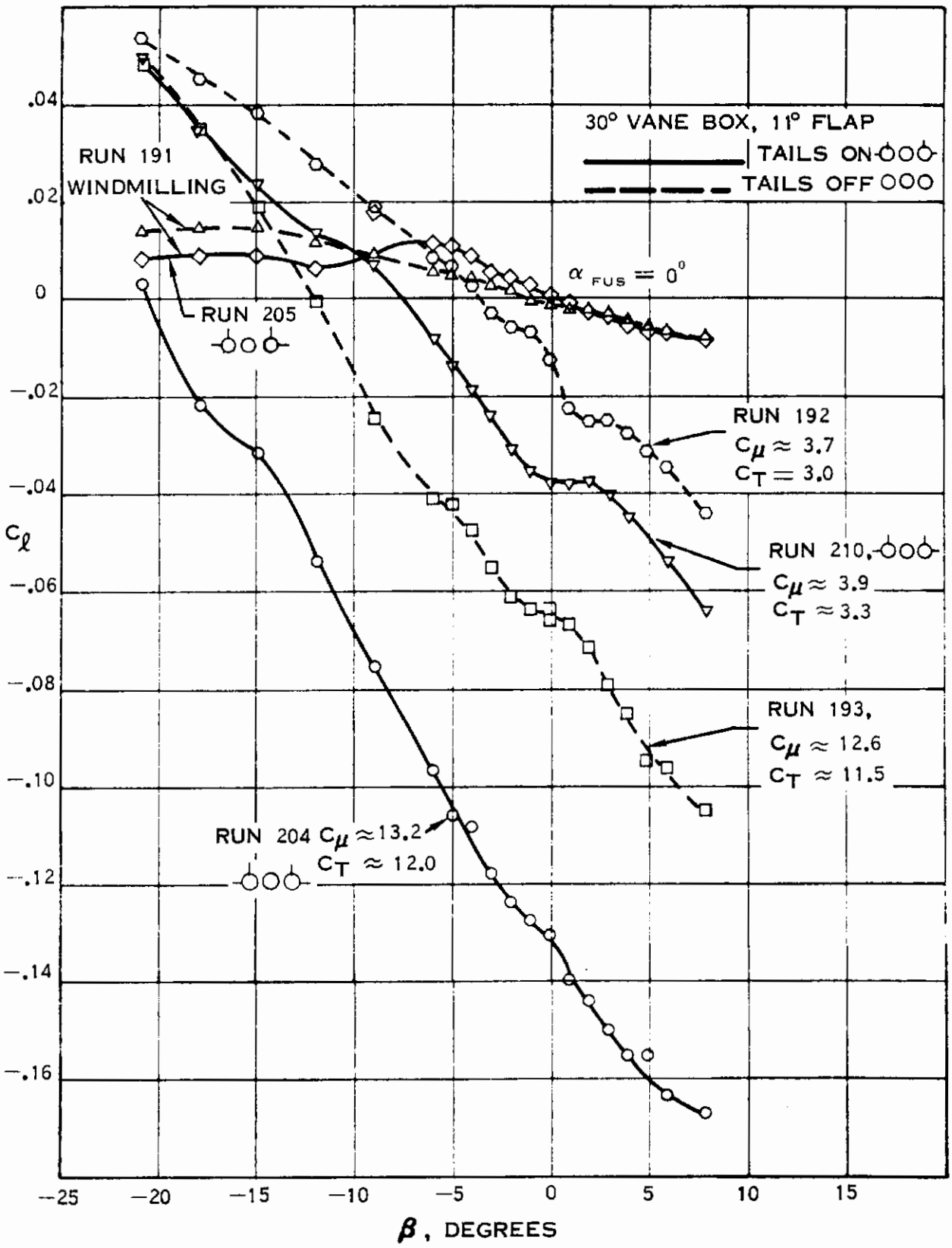

Figure 25. Effect of C_μ on Lateral Characteristics

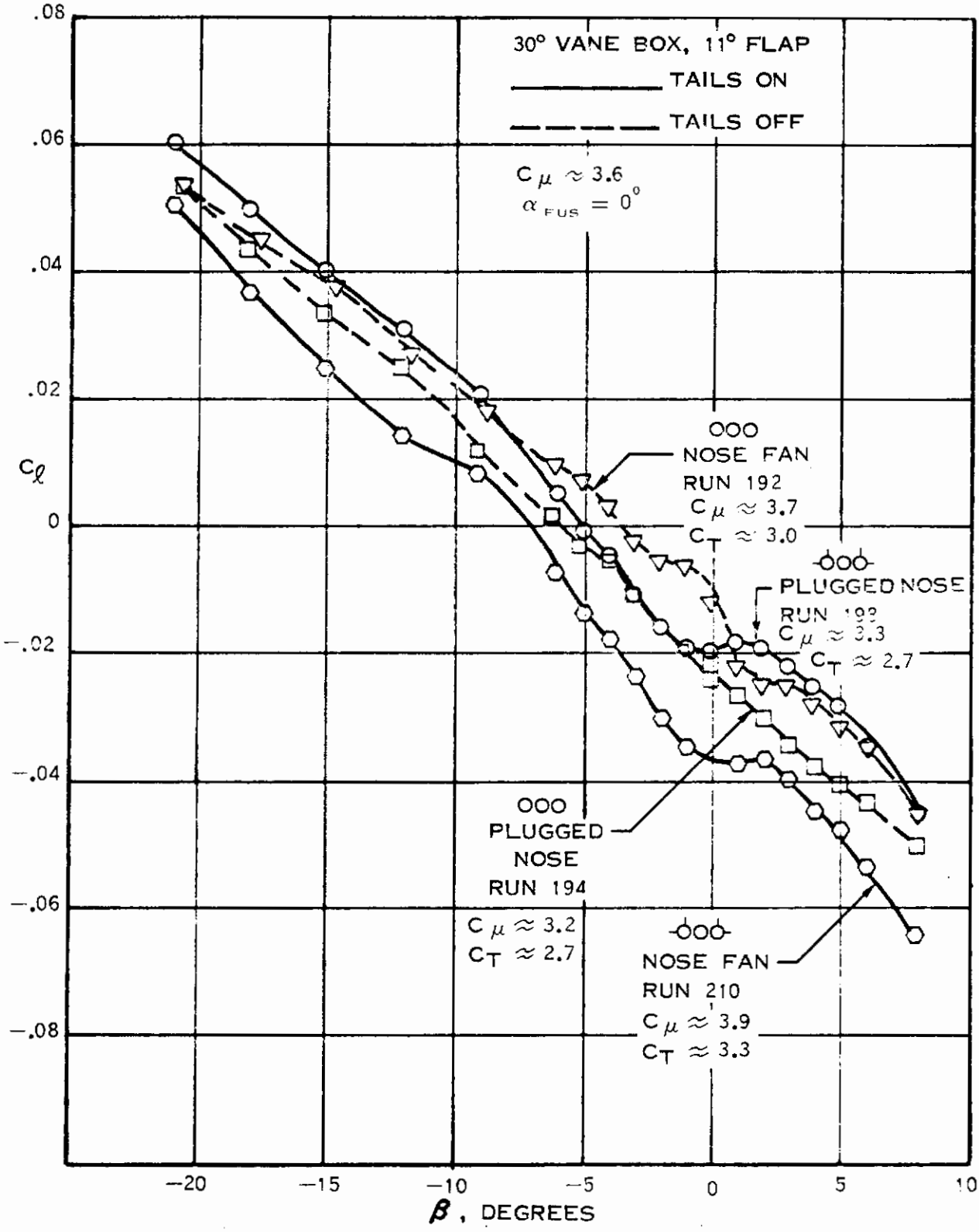

Figure 26. Effect of Plugged Nose on Lateral Characteristics

c. 90-Degree Vane Box

The lateral stability with the 90-degree vane box is shown in Figure 22. The influence of $C\mu$ and of outboard horizontal and vertical tails on $C_{\ell\beta}$ is negligible. Roll control by differential thrust and yaw control by differential vane box deflection is shown in Figure 27. This figure presents the rolling moment coefficient versus momentum coefficient for differential thrust of the two inboard fans and for all four fans. These data show that the rolling moment is well behaved and increases linearly with increasing $C\mu$ for both types of control. Differential thrust for all four fans produces about twice the rolling moment as for the two inboard fans, and the addition of differential vane box settings does not change rolling moment very much. Yawing moment is not as linear. However, it can be seen that the two types of control are fairly independent since differential thrust does not generally produce much yawing moment.

5. PRESSURE DISTRIBUTIONS

A total of 167 static pressure taps were installed in various areas of interest on the model fuselage, wing, flap, fan flow duct, inlets and boom; no static pressures were measured on the tail surfaces. The location of static pressure taps on the 0.167-scale ADAM II model may be found in Figure 28.

In general, static pressure measurements during the entire test were hindered and made questionable by the presence of ice and water on the model. Under conditions of high humidity and at low tunnel speeds, the expansion cooling of the high pressure air usually caused a one-eighth-inch thick layer of frost to form on the model wing before the first data point could be taken on a powered test run. At static thrust (tunnel $q = 0$) conditions and the lower tunnel speeds, the static pressure measurements are not considered reliable. For the 60° and 90° vane box angles, it is believed that only those pressures measured on the model fuselage during the ground effects tests are of value for data analysis.

The change in static pressure on the fuselage centerline with ground proximity is shown typically in Figure 29. The pressures shown here exhibit the irregularity often observed in static thrust test data from a deflected thrust model and show a change in pressure level with ground height. For constant model power, a growth in positive pressure along the bottom of the model fuselage occurs with decreasing ground height. The height at which the positive pressure increase begins is a function of model power. Figure 30 shows a typical variation of ground effects on fuselage centerline pressures with model power. The onset of the pressure growth along the bottom of the fuselage centerline occurs at greater heights as model power increases.

Due to the irregular nature of the pressure data and the limited number of pressure taps on the fuselage, no quantitative analyses have been attempted of the effect of the pressure growth on the model aerodynamic characteristics with ground proximity.

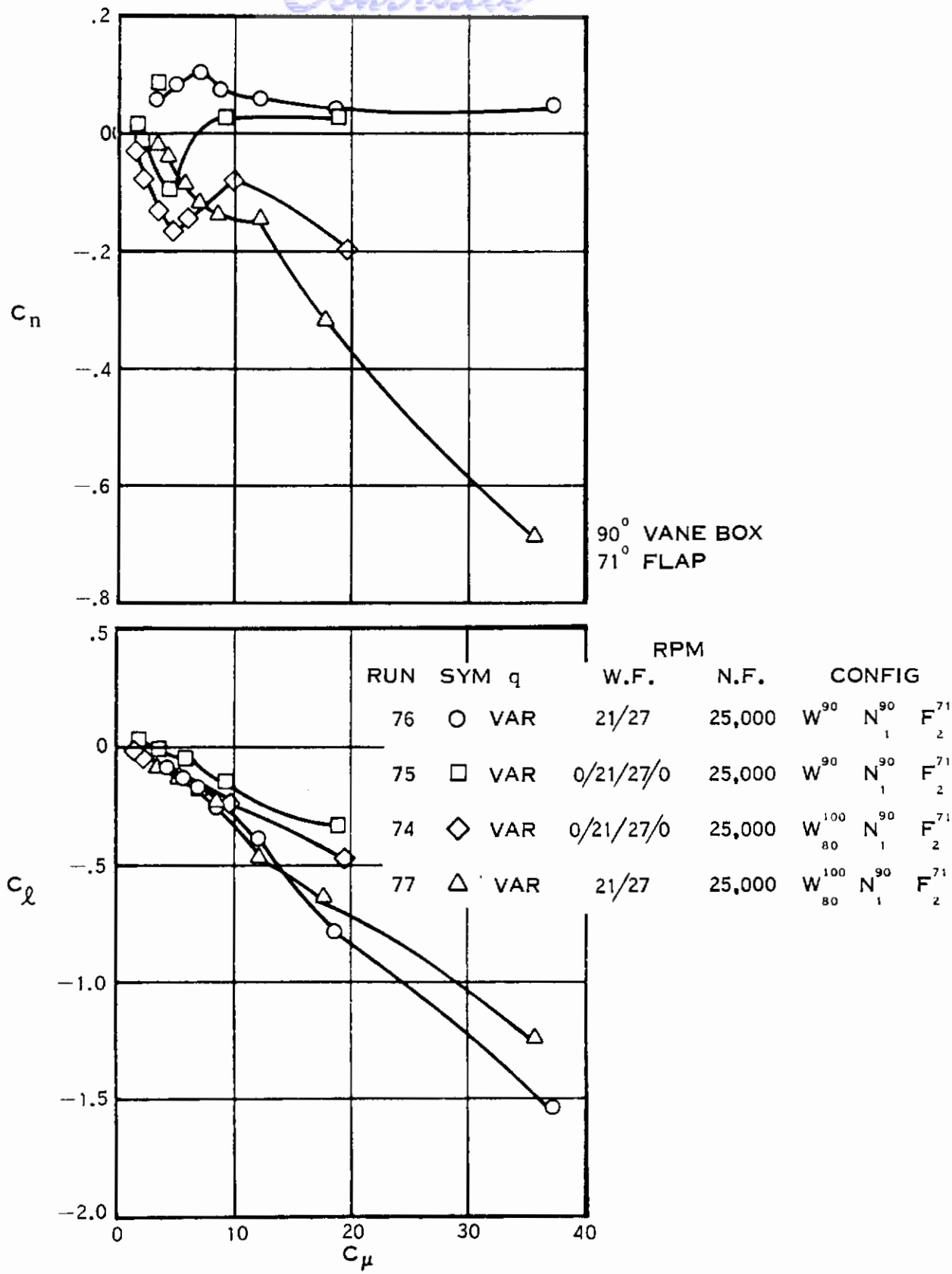

Figure 27. Control Effectiveness of Differential Vane Box Deflection and Wing Fan RPM

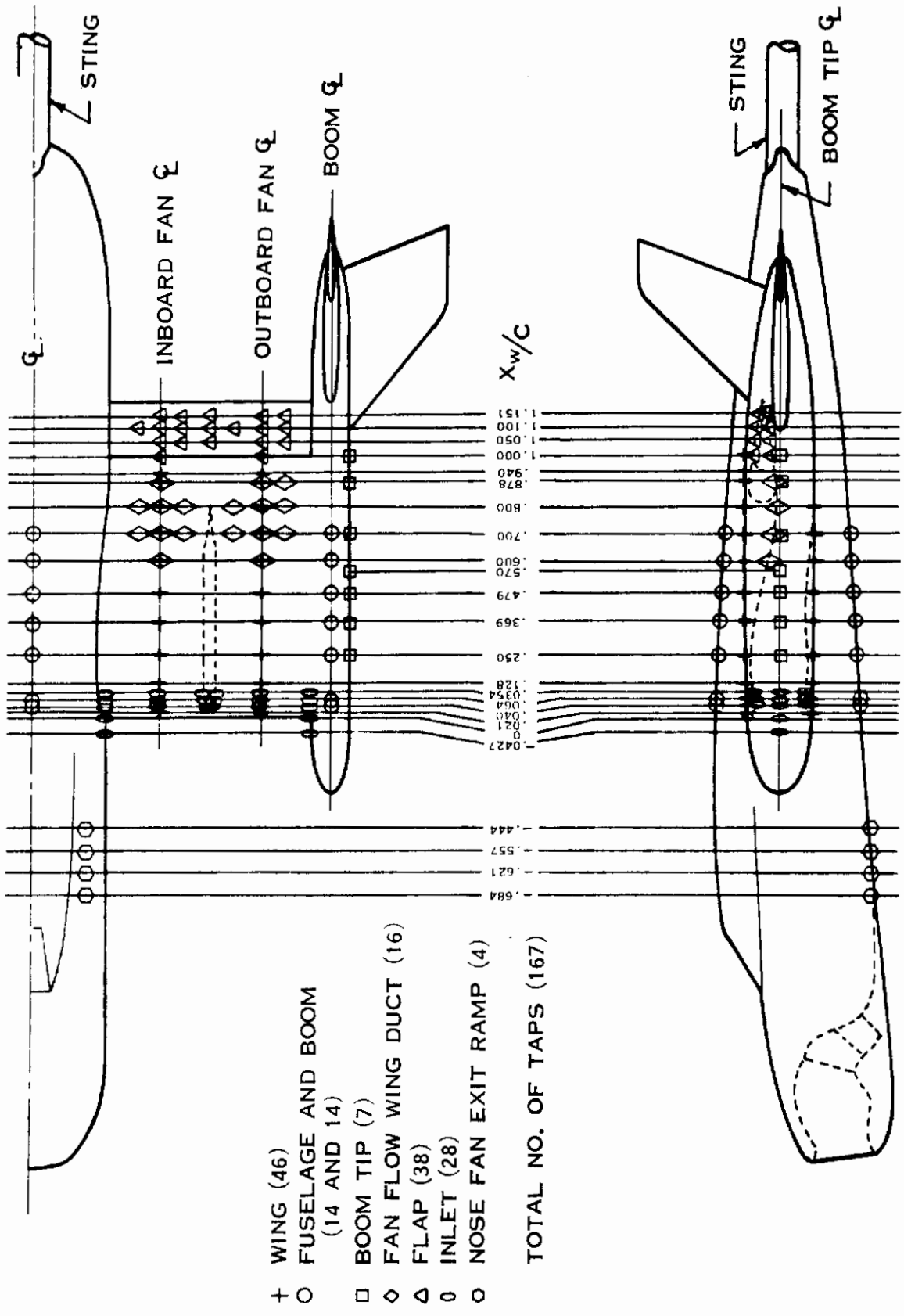

Figure 28. Static Pressure Tap Locations

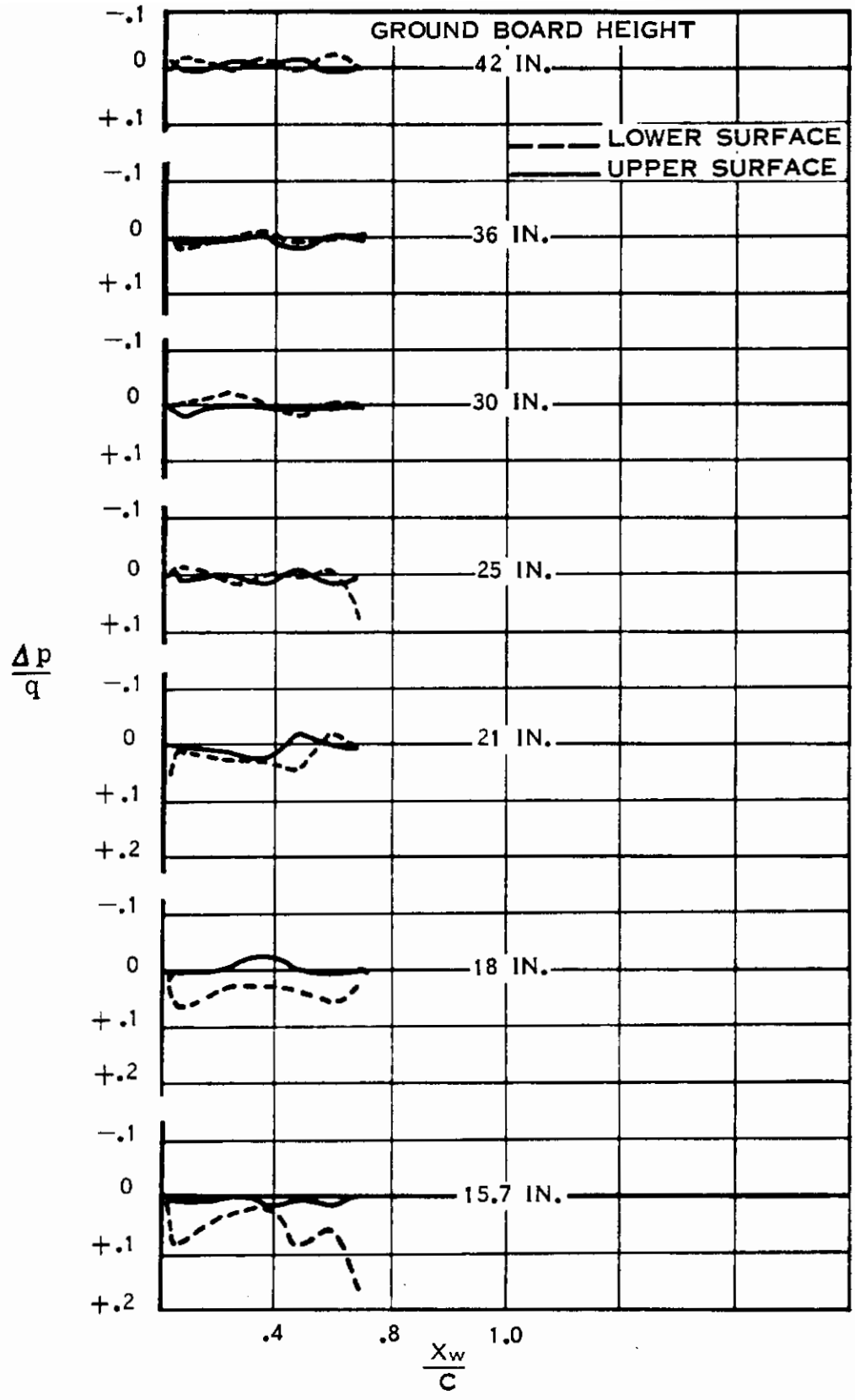

Figure 29. Variation of Pressure on Fuselage Centerline with Ground Height

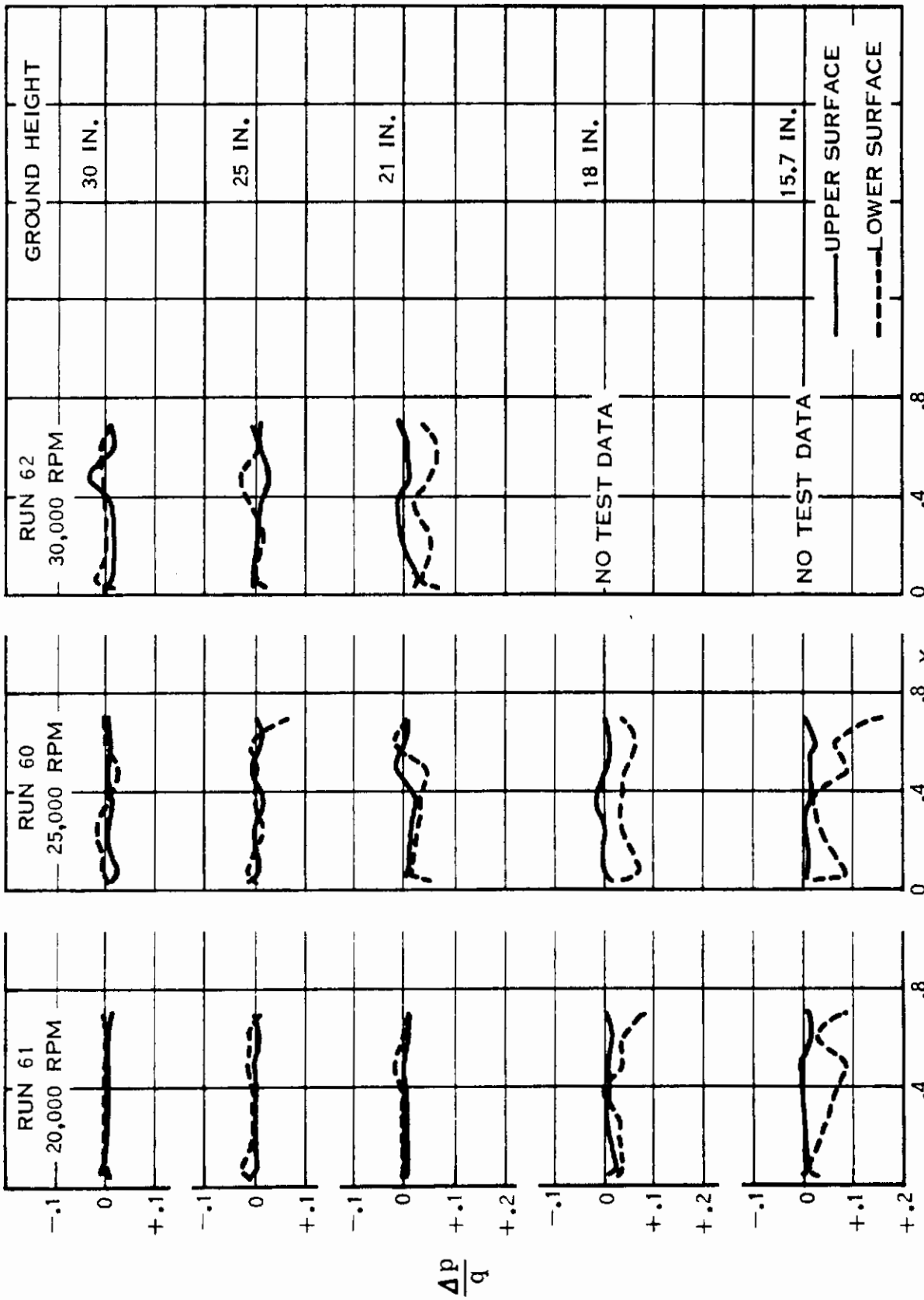

Figure 30. Variation of Positive Pressure Buildup on Fuselage Lower Surface with Ground Height

At the highest tunnel speed tested (q = 10) and the 30° vane box angle, there was less icing and the measured pressure data exhibited regions of reasonable behavior. See Figures 31, 32, and 33 for typical examples of these data. Figure 31 is a schematic diagram which shows where continuous segments of the wing pressure distribution were measured. Figure 32 shows the distribution of pressure coefficients over the model for a typical powered test run and Figure 33 shows the same type of data for a windmilling fans test run.

Figures 32 and 33 show a characteristic difference in pressure distribution that is due to the difference in the amount of air being drawn into the inlet for the powered fan and windmilling fans cases. For the windmilling case, the capture area ratio is less than one, and the stagnation point is located on the inside of the inlet lip. The resulting pressures on the top of the wing then resemble those of a normal airfoil at positive angle of attack. At higher powers, the stagnation point is outside the inlet lip and the upper surface acts as an airfoil at negative angles of attack, where the high negative pressures peak at the leading edge is absent. The pressure distributions at the inboard fan centerline and toward the leading edge are a good example of this effect. For the powered wing configuration of Figure 32, the capture area of the fans is greater than the inlet area and the external pressures very near the leading edge tend to be more positive at low angles of attack and change to negative at the higher angles as the stagnation points on the upper and lower wing surfaces change with pitch. For the unpowered wing configuration of Figure 33, the capture area is smaller than the inlet and the external pressures very near the leading edge tend to be negative on both upper and lower surfaces and to change little with angle of attack.

The pressures on the top wing surfaces, aft of the 40 percent chord station, exhibit an unexplained waviness which was not observed in any previous test and are not considered to be characteristic of the propulsive wing. These pressure variations could be the combined influence of ice and water that formed on the wing and a slight unsteadiness in the performance of the flap jet.

The power split between the wing fan flow (the secondary jet) and the flap jet (primary jet) was such that the secondary flow had a higher velocity than the primary flow. This resulted in a pressure level on the bottom aft surface of the wing and flap that was more negative than the pressure level on the top. This represents a down load on the flap and is inconsistent with the relative jet velocities envisioned for an actual ADAM aircraft. This unusual pressure gradient across the wing that was caused by the jets and flap setting did not exhibit a change with angle of attack; any vortex that resulted was, therefore, of a constant strength. If there is also a normal wing vortex on the forward portion of the wing, these two vortices could interact in the vicinity of the horizontal tail, and produce anomalies in lift, drag, and pitching moment data such as have been seen. Since the down load on the flap is both undesirable and inconsistent with a realistic aircraft concept, it is believed that an appropriate jet velocity simulation should be used for future model tests.

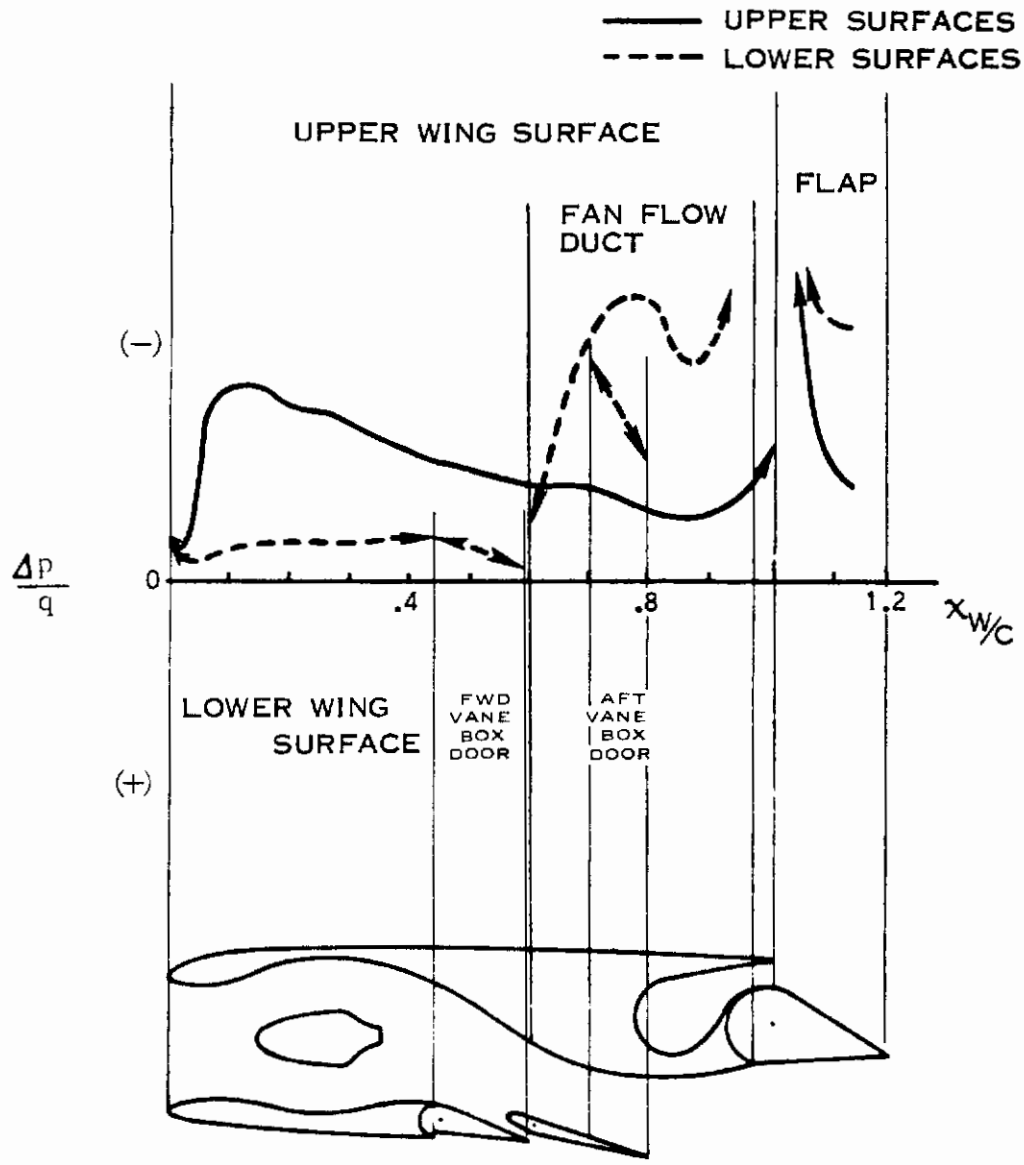

Figure 31. Key to Wing Pressure Distribution Plots for 30° Thrust Deflection Angle

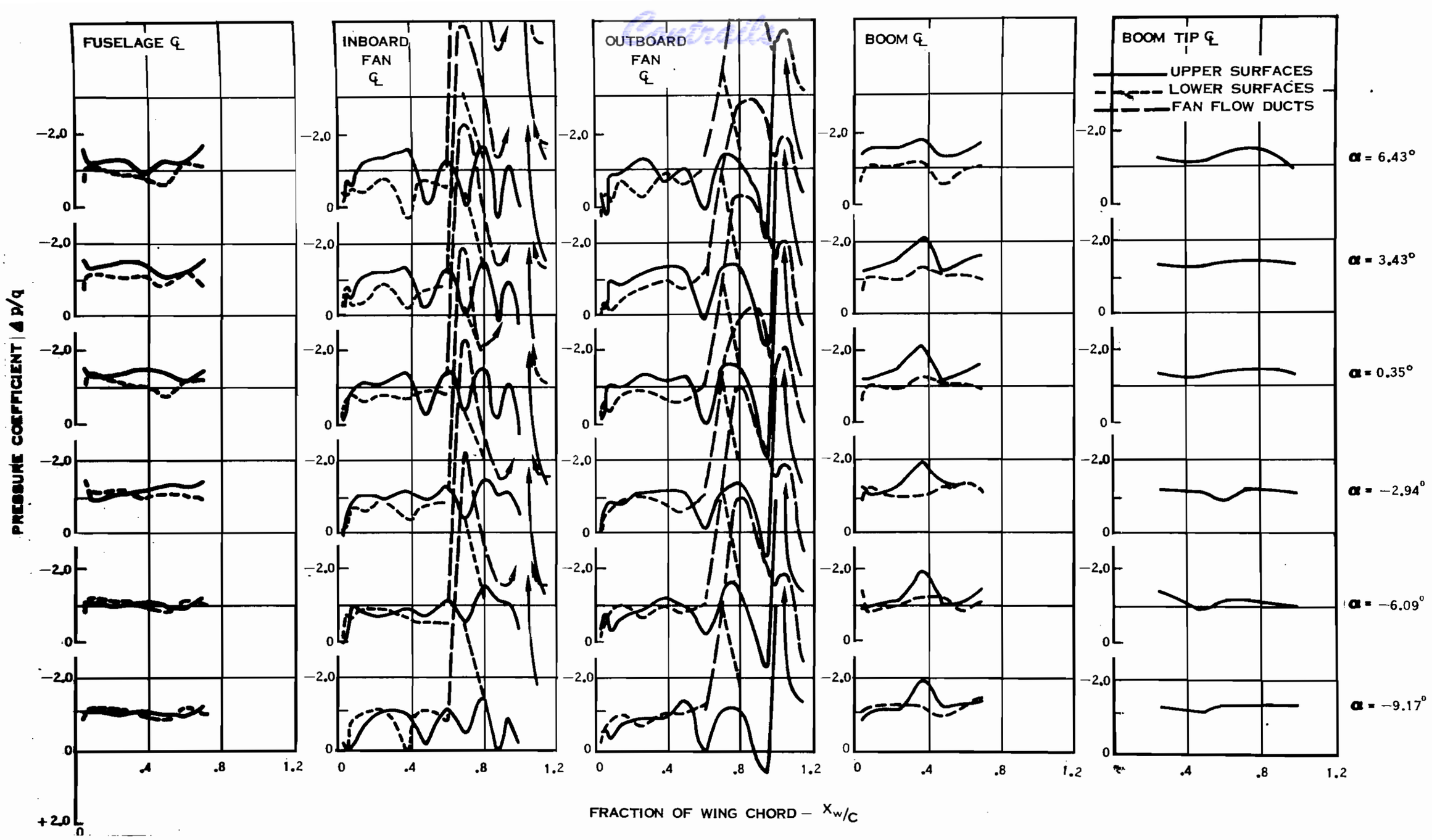

Figure 32(a). Typical Pressure Distributions for the 0.167-Scale ADAM II Model with Powered Fans 30° Thrust Deflection Angle

56 is blank

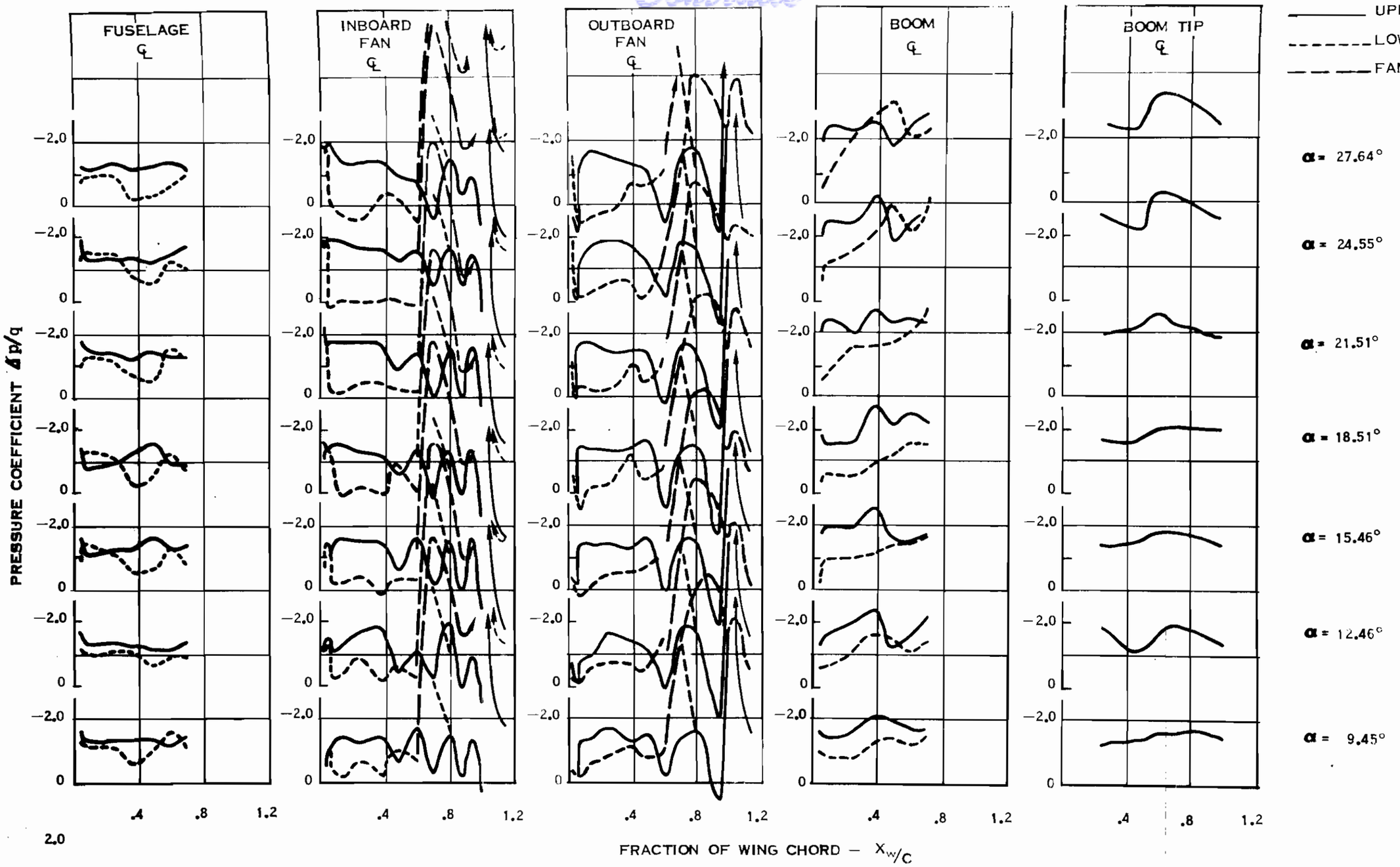

Figure 32(b). **Typical Pressure Distributions for the 0.167-Scale ADAM II Model with Powered Fans 30° Thrust Deflection Angle (Concluded)**

58 is blank

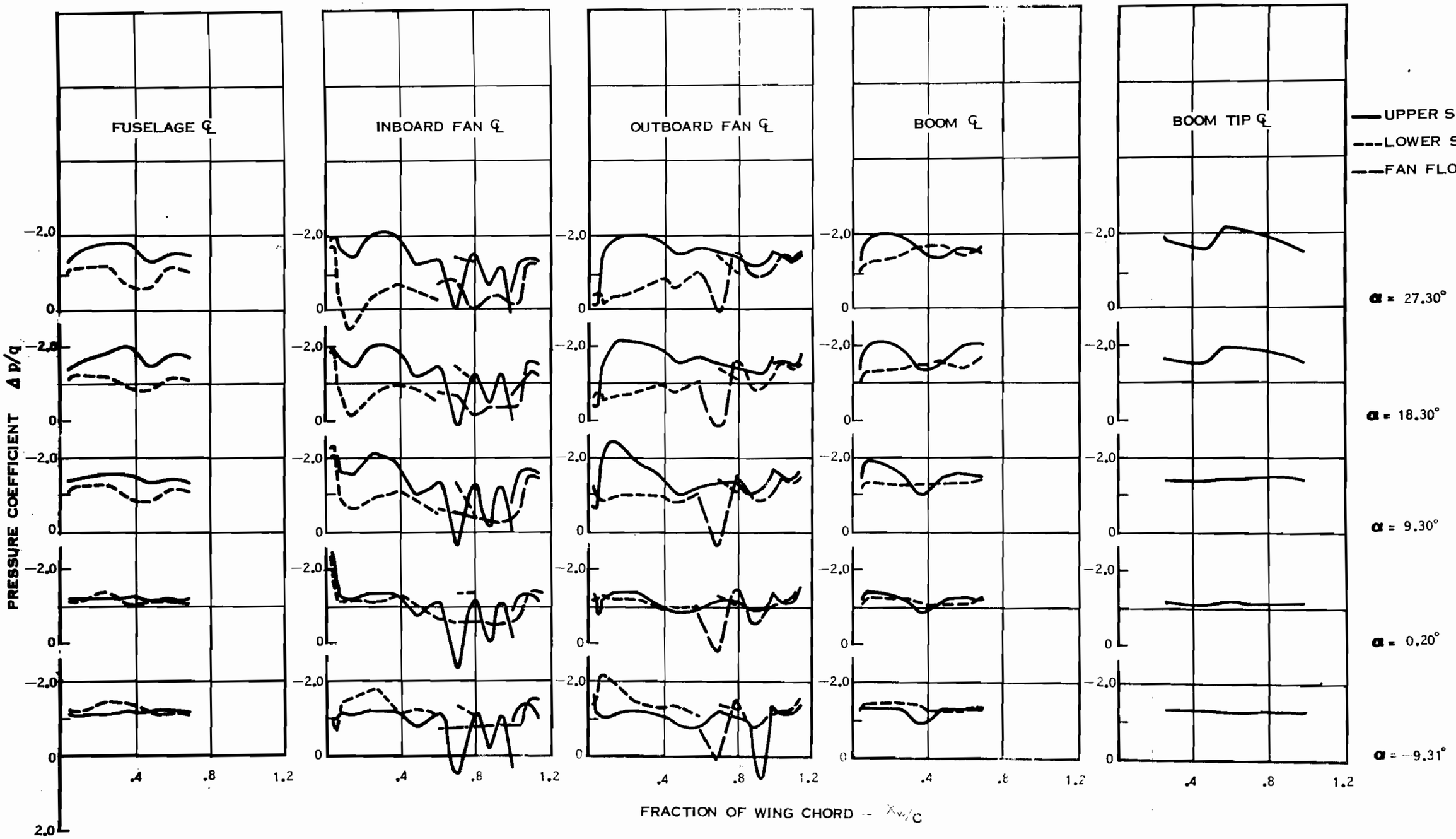

Figure 33. Typical Pressure Distributions for the 0.167-Scale ADAM II Model with Windmilling Fans 30° Thrust Deflection Angle

60 is blank

6. GROUND EFFECTS

Ground effects were investigated by two procedures to obtain the maximum data coverage in the minimum amount of tunnel occupancy time. The moving ground plane was synchronized with the tunnel wind speed to produce the most realistic ground effects.

At nominally constant dynamic pressure, angle of attack, and sideslip angle, the model height above the moving ground plane was varied from maximum (42", approximately 1.8 $\bar{c}$) to minimum (15.7", approximately 0.67 $\bar{c}$) with the sting extension removed. Out of ground effects height was 84 inches. At fixed model heights of 42 inches and 15.7 inches, pitch and yaw data were obtained. In the 90-degree vane box configuration, the dynamic pressure was also varied from static to a nominal value of ten. Additional model heights of 30 inches, 21 inches, and 12.3 inches were used for static pitch data in the 90-degree vane box configuration. Differential thrust vane box deflection angles were also investigated. Figures 34 through 36 show some of the ground effects. Additional ground effects plots were presented in the data report.

Under static conditions, the 90-degree vane box configuration develops increasing lift as the model height is lowered (Figure 34); however, a loss of up to approximately 15% in lift occurs at a total momentum coefficient of approximately 10. In general, for the 60° vane box configuration, lift increases from 10 to 15% (Figure 35); however, for the 30° vane box configuration, lift decreases up to 7% (Figure 36).

For the 90° vane box, statically, the drag increases with decreasing height down to approximately 1.3 $\bar{c}$, then increases with further decrease in height. At $C_\mu \approx 12$ the drag steadily decreases. In the 60° vane box configuration drag steadily decreases, while a steady increase in drag results with the 30° vane box.

As the model height is decreased, a decreasing nose down pitching moment results with the 90° vane box, but 60° and 30° vane boxes produce an increasing nose down pitching moment. With the 30° vane box, a decrease in longitudinal stability occurs as model height is lowered.

The variation of rpm with height variations is small; therefore, the thrust variation should be small, indicating a resultant thrust angle change to account for the magnitude of the variation in drag with the 60° vane box data. An aerodynamic lift increase would also have to occur and pressure data on the fuselage lower surface tends to bear out this effect. The variation of lift and drag as model height is decreased gives total longitudinal thrust vector angular changes consistent with the drag changes for 90° and 60° vane box configurations, also indicating a decrease in thrust deflection angle.

62 is blank

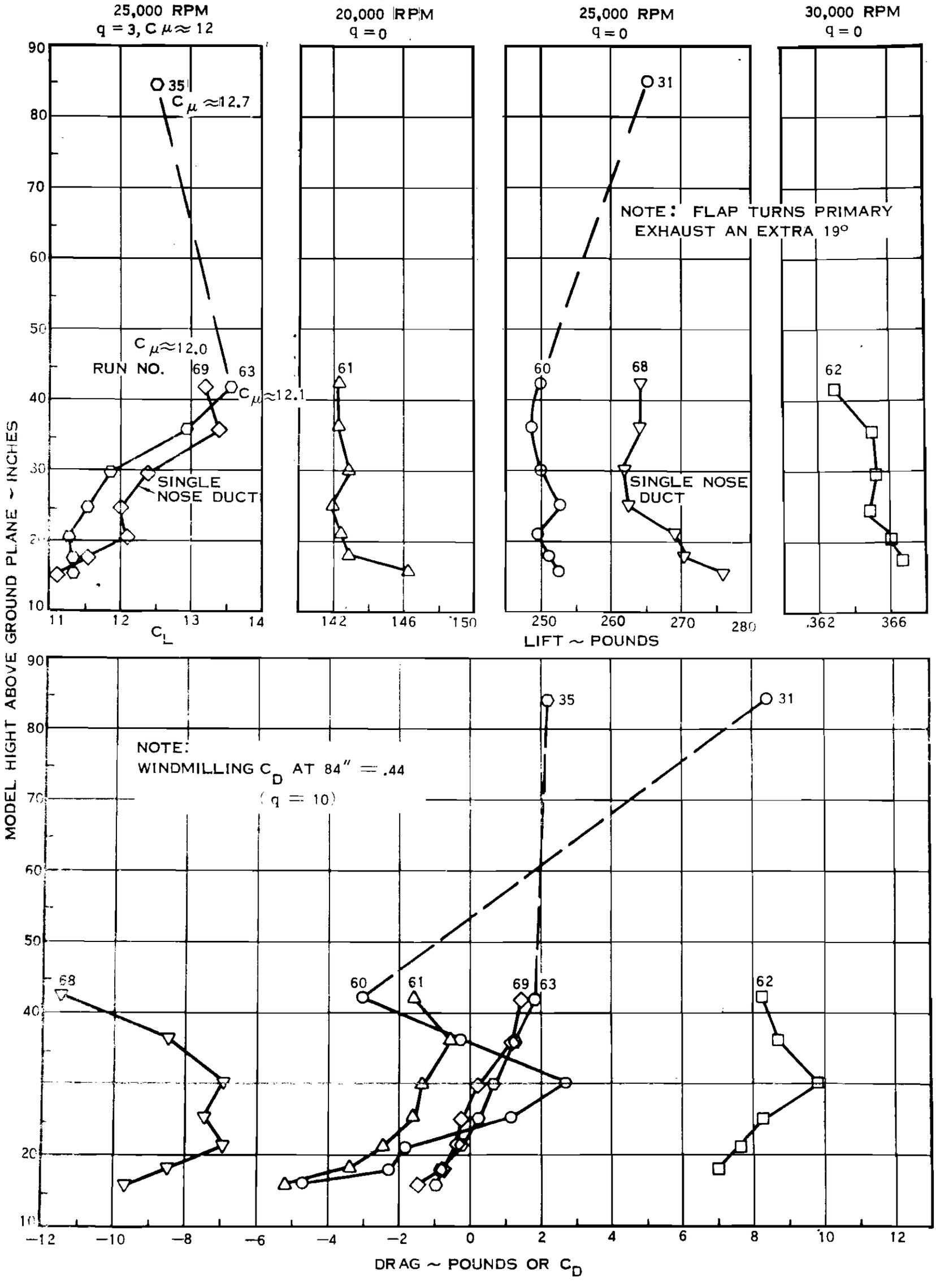

Figure 34(a). Effect of Distance to Ground on Longitudinal Characteristics, 90° Vane Box

64 is blank

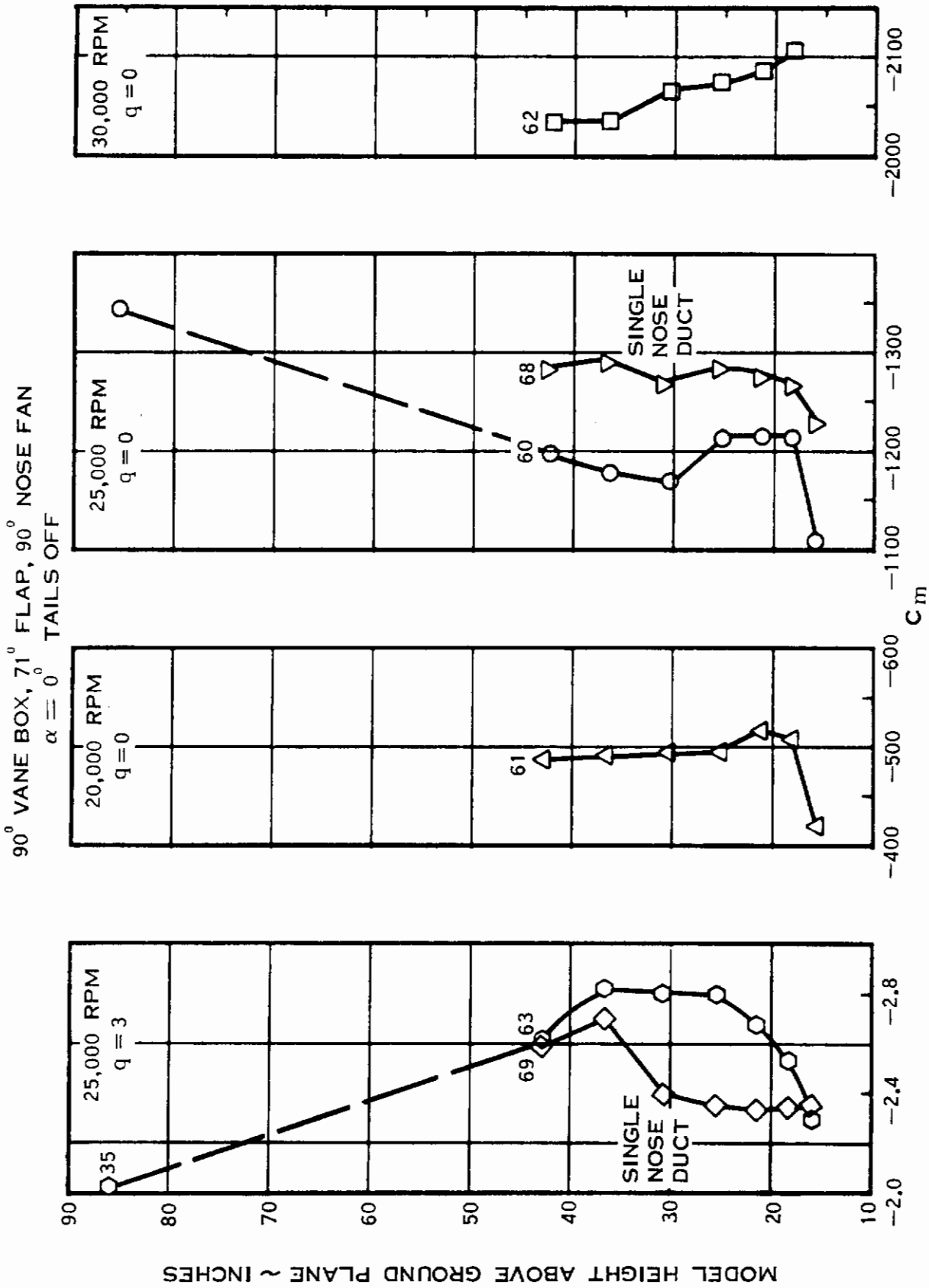

Figure 34(b). Effect of Distance to Ground on Longitudinal Characteristics, 90° Vane Box

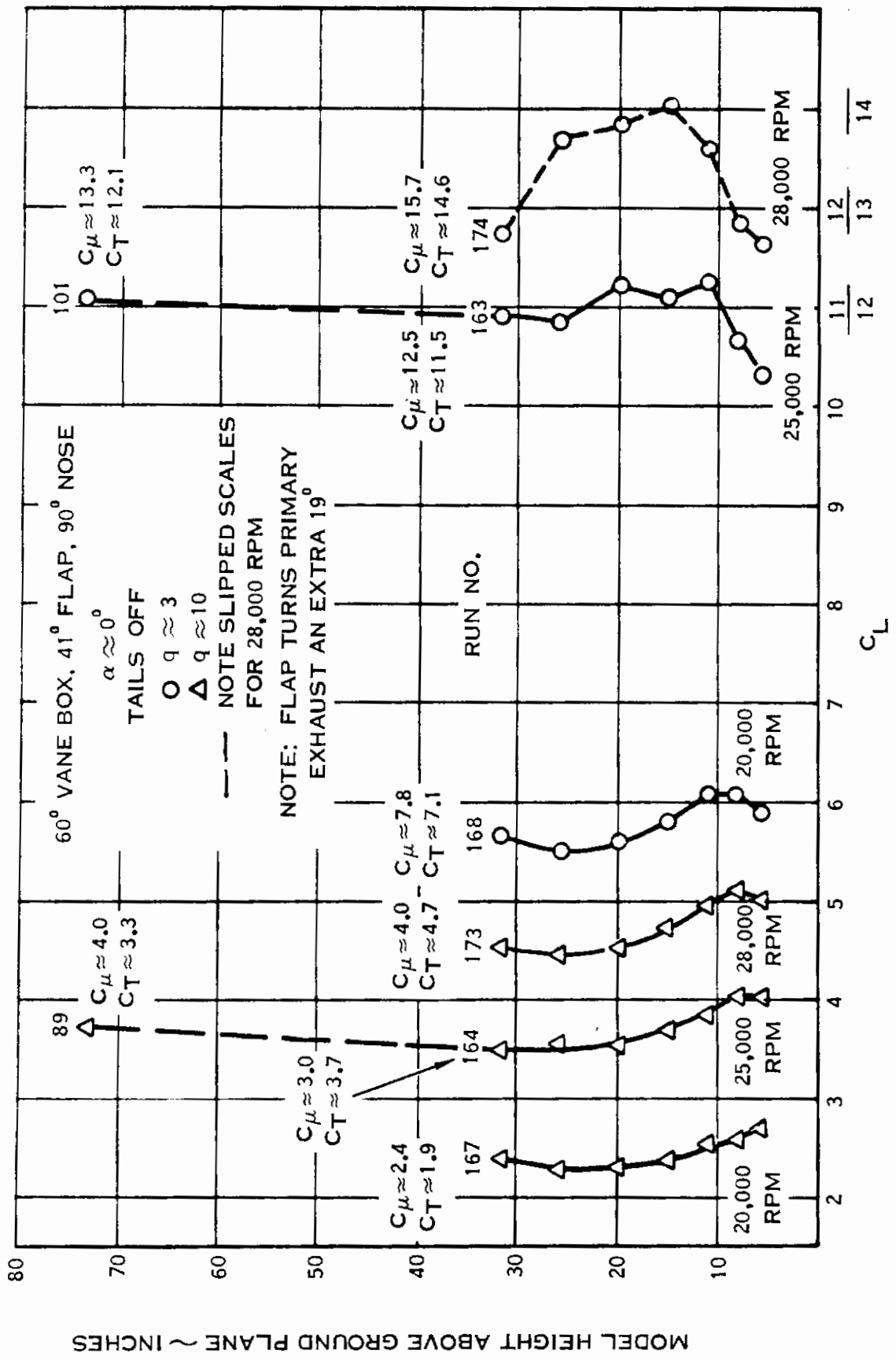

Figure 35(a). Effect of Distance to Ground on Longitudinal Characteristics, 60° Vane Box

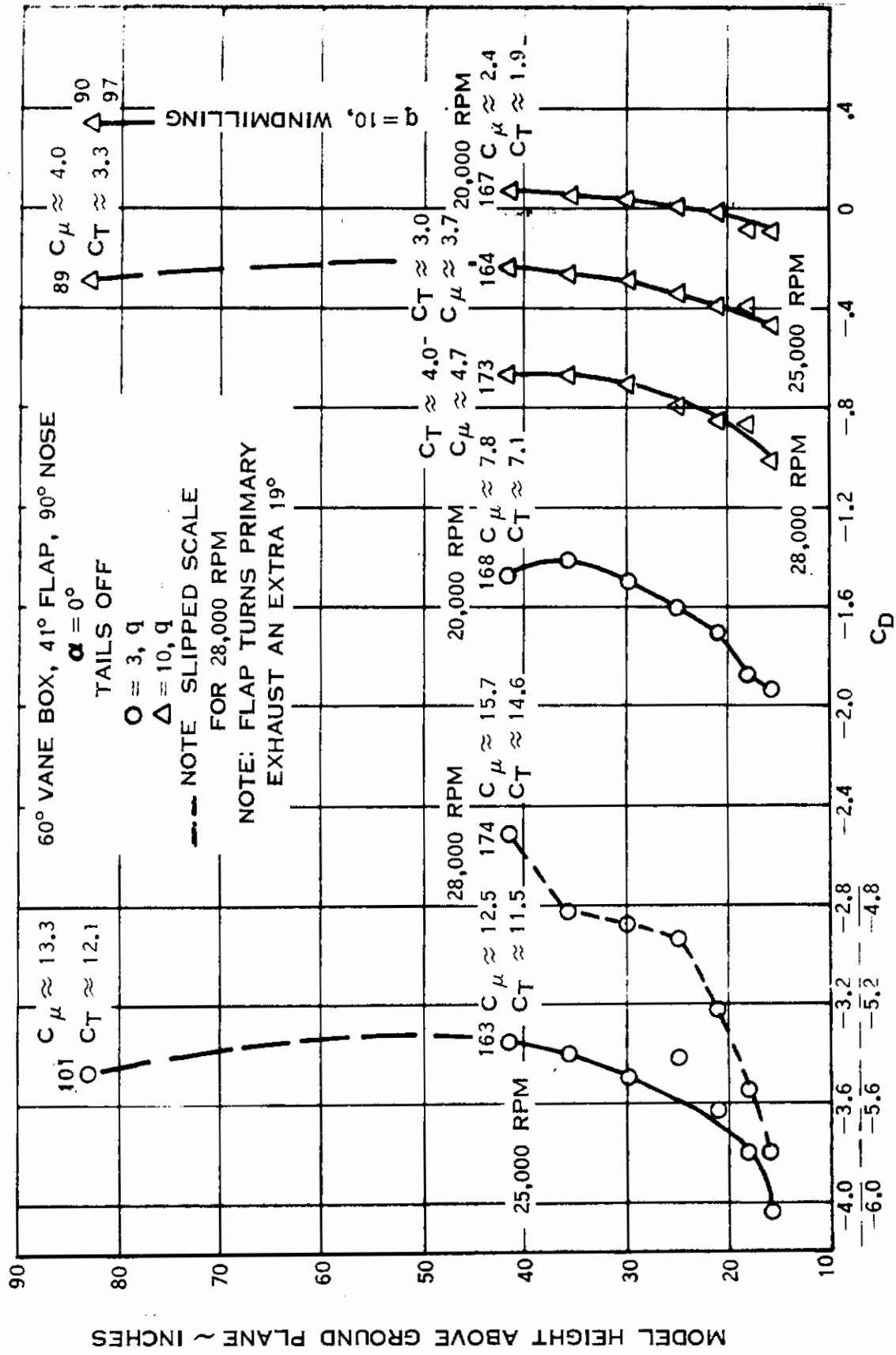

Figure 35(b) Effect of Distance to Ground on Longitudinal Characteristics, 60° Vane Box (Continued)

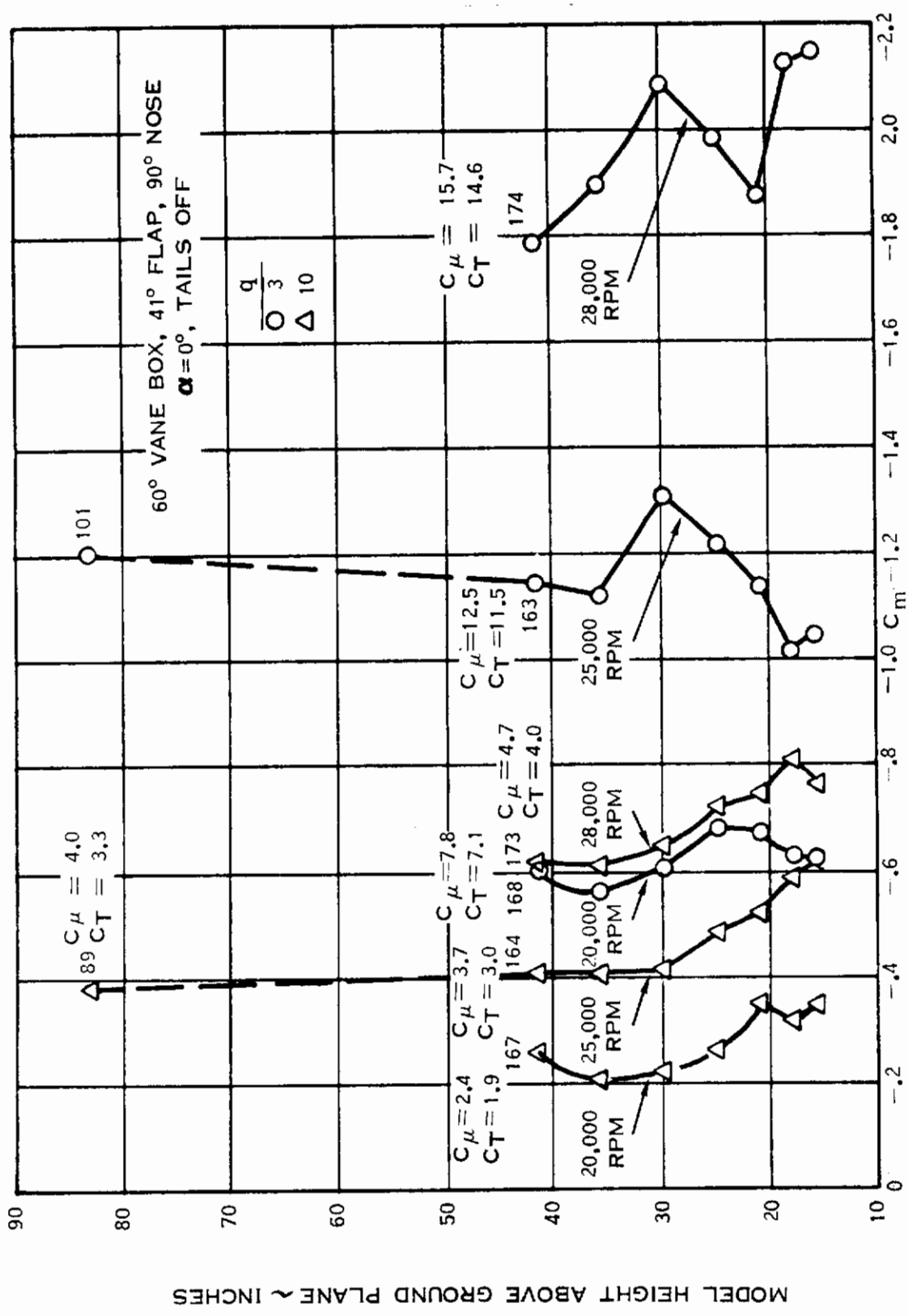

Figure 35(c) Effect of Distance to Ground on Longitudinal Characteristics, 60° Vane Box (Concluded)

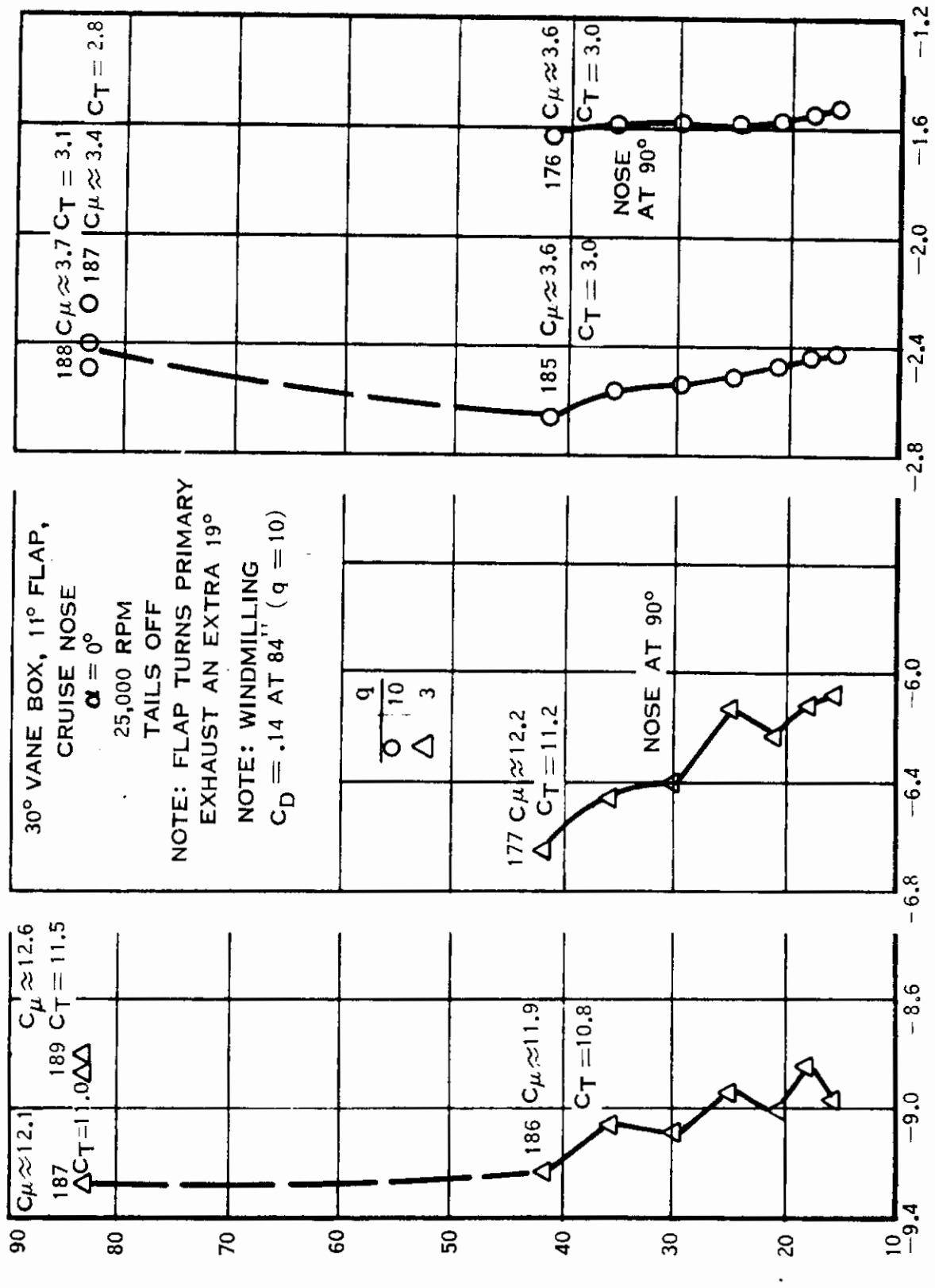

Figure 36(a). Effect of Distance to Ground on Longitudinal Characteristics, 30° Vane Box

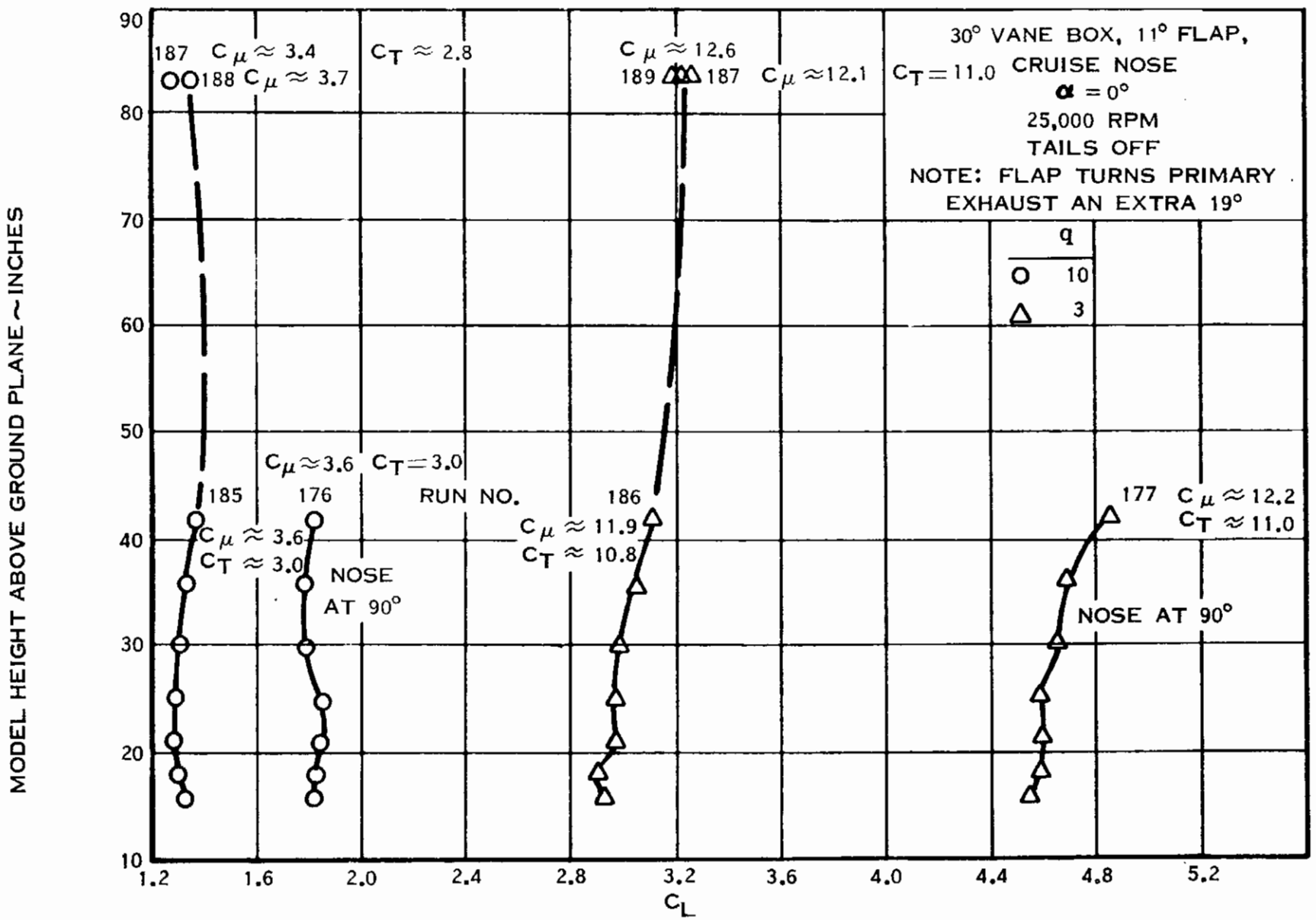

Figure 36(b). Effect of Distance to Ground on Longitudinal Characteristics, 30° Vane Box

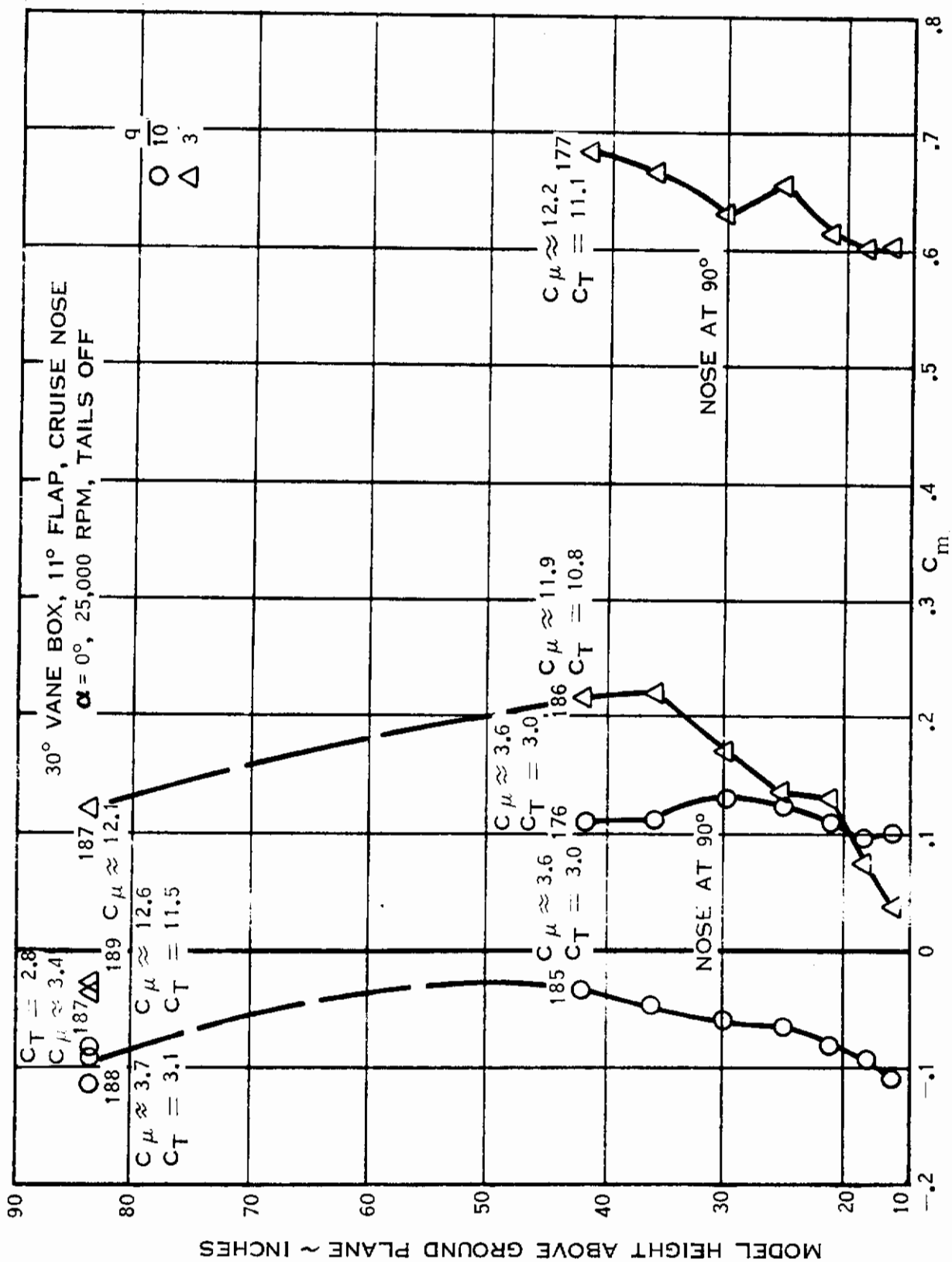

Figure 36(c). Effect of Distance to Ground on Longitudinal Characteristics, 30° Vane Box

72 is blank

SECTION III

CONCLUSIONS AND RECOMMENDATIONS

1. CONCLUSIONS

These test results represent the most complete set of low speed data taken to date on the ADAM concept. These tests were the first full-span powered tests conducted on a modern ADAM design. These results have provided a base line of data upon which to build. Much has been learned about the flow conditions that exist. The tests have also served to closely identify areas requiring additional testing. These areas are outlined in the recommendations below. The LRC transonic test results to be included in Part IV will provide additional information.

a. General

1. Substituting a centerline vertical tail for the outboard vertical tails results in improved longitudinal and directional stability.

2. For large momentum coefficients, the high velocity propulsive flow induces additional velocity over the boom-mounted tails, increasing control effectiveness.

3. The flaps are very strong trim devices.

4. For $C_\mu \approx 4.0$, flow over the flaps separates at deflections greater than approximately 41 degrees.

b. 30-Degree Vane Box

1. Horizontal tail effectiveness is reduced at low momentum coefficients.

2. Increase in momentum coefficients reduces directional stability.

c. 60-Degree and 90-Degree Vane Boxes

1. The control power of the nose fan can be made adequate.

2. Propulsive forces and moments become dominant compared to aerodynamic contributions.

3. The presence of the ground generally increases lift and reduces the resultant force angle.

2. RECOMMENDATIONS

a. Replace the boom-mounted vertical tails with a fuselage-mounted vertical tail.

b. Perform additional testing using a heated air supply to minimize icing, and use flow visualization techniques with the following objectives:

   1. Determine the role of the booms and aft fuselage on longitudinal stability.

   2. Determine the additional control effectiveness to be obtained from larger horizontal tails.

   3. Determine the effect of a more realistic velocity ratio between the primary and secondary flows.

   4. Determine the effectiveness of end plating the flaps on preventing flap separation at high deflections.

REFERENCES

1. Beissner, F. L., Jr.; Application of Three Dimensional Lifting Surface Theory to the Determination of Span Efficiency Factor for Wing and Outboard Tails (U), LTV Report No. 2-53310/4R-50249, dated 18 December 1964. Unclassified

76 is blank

APPENDIX I

RUN SCHEDULE FOR TEST NO. 175
IN 17-FOOT SECTION OF 7 X 10 FOOT LOW SPEED WIND TUNNEL, NASA, LANGLEY RESEARCH CENTER, VA.

RUN NO.	q	α	β	RPM			δ_T *		δ_N *	δ_F *	i_v *	i_h *	GROUND PLANE HEIGHT	REMARKS
				LEFT	RIGHT	NOSE	LEFT	RIGHT						
1	OFF	0°	0°	15000	15000	15000	90°	90°	90°	71°	OFF	OFF	OGE	N (BIFURCATED NOSE DUCTS)
2				32000	32000	32000								OGE = OUT OF GROUND EFFECTS
3				30000	30000	30000								RNG = RANGE (VARIED)
4				25000	25000	25000								WM = WINDMILLING
														THRUST
5				20000	20000	20000								CALIBRATION
6	RNG			WM	WM	WM								RAKES
7				15000	15000	15000								INSTALLED
8				20000	20000	20000								
9				25000	25000	25000								
10	10	0/26°												
11	RNG	0°		30000	30000	30000								CALIB RAKES REMOVED
12	10	RNG		WM	WM	WM								
13		0°	RNG											
14		8°												
15		16°												
16		RNG	0°								0°	−10°		*
17												+10°		δ_T = VANE BOX DEFLECTION (POS T E. DOWN)
18												+30°		
19		0°	RNG									+10°		δ_N = NOSE FAN EXIT DEFLECTION (POS T E. DOWN)
20		8°												
21		16°												δ_F = FLAP DEFLECTION (POS T E. DOWN)
22	RNG	0°	0°	25000	25000	25000								
23	10	RNG												i_v = VERTICAL TAIL INCIDENCE ANGLE (POS WITH TOE-OUT)
24												+30°		
25				WM	WM	WM						0°		i_h = HORIZONTAL TAIL INCIDENCE ANGLE (POS L E. UP)
26				25000	25000	25000								
27												−10°		
28		0°	RNG									+10°		
29		8°												
30		16°												
31	RNG	0°	0°								OFF	OFF		
32	10	RNG												
33	1													
34	2													CHECK ON RUN 34
35	3													CHECK ON RUN 35
36	3													
37	2													
38	3													
39	10	0°	RNG											
40		8°												
41		16°												

78 is blank

RUN SCHEDULE FOR TEST NO. 175
IN 17-FOOT SECTION OF 7 X 10 FOOT LOW SPEED WIND TUNNEL, NASA, LANGLEY RESEARCH CENTER, VA. (CONTINUED)

RUN NO.	q	α	β	RPM			δ_T		δ_N	δ_F	i_v	i_h	GROUND PLANE HEIGHT	REMARKS
				LEFT	RIGHT	NOSE	LEFT	RIGHT						
42	1	0°	RNG	25000	25000	25000	90°	90°	90°	71°	OFF	OFF	OGE	
43	2	↓	↓	↓	↓	↓	↓	↓	↓	↓	↓	↓	↓	
44	3													
45	5													
46	OFF	RNG	0°											
47	RNG	0°	↓				100°	80°						
48	↓	↓					↓	↓		↓				
49										61°				
50										41°				
51										↓			42 IN	
52													15.7 IN	
53										71°			42 IN	
54										↓			15.7 IN	
55	OFF	RNG					90°	90°					42 IN	
56	↓	↓					↓	↓					30 IN	
57													21 IN	
58													15.7 IN	
59													12.3 IN	
60		0°		↓	↓	↓							RNG	
61		↓		20000	20000	20000							↓	
62				30000	30000	30000								
63	3			25000	25000	25000								
64	↓			↓	↓	↓					0°	+10°		
65	OFF										↓	↓		
66	↓											-10°		
67	3											↓		
68	OFF										OFF	OFF		N_2 (SINGLE NOSE DUCT)
69	3													
70	RNG			21000	26000								42 IN	N_1 (BIFURCATED NOSE DUCTS)
71	↓			↓	↓								15.7 IN	
72							100°	80°					42 IN	
73							↓	↓					15.7 IN	
74				0/21	27/0								OGE	
75				↓	↓		90°	90°					↓	
76				21000	26000		↓	↓						
77				↓	↓		100°	80°						
78	3	RNG		30000	30000	30000	90°	90°						
79	↓	↓		20000	20000	20000	↓	↓						
80	RNG	0°		30000	30000	30000	60°	60°		41°				THRUST CALIBRATION RAKES INSTALLED
81	↓	↓	↓	25000	25000	25000	↓	↓	↓	↓	↓	↓	↓	
82				27500	27500	27500								
83				22000	22000	22000								
84				20000	20000	20000								

80 is blank

APPENDIX I

RUN SCHEDULED FOR TEST NO. 175

IN 17-FOOT SECTION OF 7 X 10 FOOT LOW SPEED WIND TUNNEL, NASA, LANGLEY RESEARCH CENTER, VA. (CONTINUED)

RUN NO.	q	α	β	RPM			δ_T		δ_N	δ_F	i_v	i_h	GROUND PLANE HEIGHT	REMARKS
				LEFT	RIGHT	NOSE	LEFT	RIGHT						
85	RNG	0°	0°	17500	17500	17500	60°	60°	90°	41°	OFF	OFF	OGE	THRUST CALIBRATION RAKES INSTALLED
86	↓	↓	↓	15000	15000	15000	↓	↓	↓	↓	↓	↓	↓	
87	↓	↓	↓	WM	WM	WM	↓	↓	↓	↓	↓	↓	↓	
88	↓	↓	↓	25000	25000	25000	↓	↓	↓	↓	↓	↓	↓	
89	10	RNG	↓	↓	↓	↓	↓	↓	↓	↓	↓	↓	↓	
90	↓	↓	↓	WM	WM	WM	↓	↓	↓	↓	↓	↓	↓	CALIB RAKES REMOVED
91	5	↓	↓	25000	25000	25000	↓	↓	↓	↓	↓	↓	↓	
92	3	↓	↓	↓	↓	↓	↓	↓	↓	↓	↓	↓	↓	
93	1	↓	↓	↓	↓	↓	↓	↓	↓	↓	↓	↓	↓	
94	10	0°	RNG	↓	↓	↓	↓	↓	↓	↓	↓	↓	↓	
95	↓	8°	↓	↓	↓	↓	↓	↓	↓	↓	↓	↓	↓	
96	↓	16°	↓	↓	↓	↓	↓	↓	↓	↓	↓	↓	↓	
97	↓	0°	↓	WM	WM	WM	↓	↓	↓	↓	↓	↓	↓	
98	↓	8°	↓	↓	↓	↓	↓	↓	↓	↓	↓	↓	↓	
99	↓	16°	↓	↓	↓	↓	↓	↓	↓	↓	↓	↓	↓	
100	5	0°	↓	25000	25000	25000	↓	↓	↓	↓	↓	↓	↓	
101	3	↓	↓	↓	↓	↓	↓	↓	↓	↓	↓	↓	↓	
102	1	↓	↓	↓	↓	↓	↓	↓	↓	↓	↓	↓	↓	
103	RNG	↓	0°	↓	↓	↓	↓	↓	↓	11°	↓	↓	↓	
104	10	RNG	↓	↓	↓	↓	↓	↓	↓	↓	↓	↓	↓	
105	3	↓	↓	↓	↓	↓	↓	↓	↓	↓	↓	↓	↓	
106	10	↓	↓	WM	WM	WM	↓	↓	↓	↓	↓	↓	↓	
107	↓	0°	RNG	25000	25000	25000	↓	↓	↓	↓	↓	↓	↓	
108	3	↓	↓	↓	↓	↓	↓	↓	↓	↓	↓	↓	↓	
109	10	↓	↓	WM	WM	WM	↓	↓	↓	↓	↓	↓	↓	
110	RNG	↓	0°	25000	25000	25000	↓	↓	↓	26°	↓	↓	↓	
111	10	RNG	↓	↓	↓	↓	↓	↓	↓	↓	↓	↓	↓	
112	↓	↓	↓	WM	WM	WM	↓	↓	↓	↓	↓	↓	↓	
113	↓	↓	↓	25000	25000	25000	↓	↓	↓	61°	↓	↓	↓	
114	↓	↓	↓	↓	↓	↓	↓	↓	↓	71°	↓	↓	↓	
115	↓	0°	RNG	↓	↓	↓	↓	↓	↓	26°	↓	↓	↓	
116	↓	↓	↓	WM	WM	WM	↓	↓	↓	↓	↓	↓	↓	
117	↓	RNG	0°	25000	25000	25000	↓	↓	↓	↓	0°	−10°	↓	
118	↓	↓	↓	↓	↓	↓	↓	↓	↓	↓	↓	+10°	↓	
119	↓	↓	↓	WM	WM	WM	↓	↓	↓	↓	↓	+20°	↓	
120	↓	↓	↓	↓	↓	↓	↓	↓	↓	↓	↓	+10°	↓	
121	↓	0°	RNG	↓	↓	↓	↓	↓	↓	↓	↓	↓	↓	
122	↓	8°	↓	↓	↓	↓	↓	↓	↓	↓	↓	↓	↓	
123	↓	16°	↓	↓	↓	↓	↓	↓	↓	↓	↓	↓	↓	
124	↓	RNG	0°	↓	↓	↓	↓	↓	↓	↓	↓	−10°	↓	
125	↓	↓	↓	↓	↓	↓	↓	↓	↓	↓	↓	0°	↓	
126	↓	↓	↓	25000	25000	25000	↓	↓	↓	↓	↓	↓	↓	
127	↓	↓	↓	↓	↓	↓	↓	↓	↓	↓	↓	↓	↓	

82 is blank

APPENDIX I

RUN SCHEDULE FOR TEST NO. 175

IN 17–FOOT SECTION OF 7 X 10 FOOT LOW SPEED WIND TUNNEL, NASA, LANGLEY RESEARCH CENTER, VA. (CONTINUED)

RUN NO.	q	α	β	RPM			δ_T		δ_N	δ_F	i_v	i_h	GROUND PLANE HEIGHT	REMARKS
				LEFT	RIGHT	NOSE	LEFT	RIGHT						
128	RNG	0°	0°	25000	25000	25000	60°	60°	90°	41°	0°	+10°	OGE	
129	10	↓	RNG	↓	↓	↓	↓	↓	↓	↓	↓	↓	↓	RERUN OF RUN 129
130	↓	↓	↓	↓	↓	↓	↓	↓	↓	↓	↓	↓	↓	↓
131	↓	8°	↓	↓	↓	↓	↓	↓	↓	↓	↓	↓	↓	↓
132	↓	16°	↓	↓	↓	↓	↓	↓	↓	↓	↓	↓	↓	↓
133	3	0°	↓	↓	↓	↓	↓	↓	↓	↓	↓	↓	↓	↓
134	↓	RNG	0°	↓	↓	↓	↓	↓	↓	↓	↓	↓	↓	↓
135	10	↓	↓	↓	↓	↓	↓	↓	↓	↓	↓	↓	↓	RERUN OF RUN 118
136	↓	↓	↓	↓	↓	↓	↓	↓	↓	↓	↓	+20°	↓	↓
137	3	↓	↓	↓	↓	↓	↓	↓	↓	↓	↓	↓	↓	↓
138	↓	↓	↓	↓	↓	↓	↓	↓	↓	↓	↓	−10°	↓	↓
139	10	↓	↓	21000	21000	21000	↓	↓	↓	↓	OFF	OFF	↓	↓
140	3	↓	↓	↓	↓	↓	↓	↓	↓	↓	↓	↓	↓	↓
141	10	↓	↓	25000	25000	25000	70°	50°	↓	↓	↓	↓	↓	↓
142	↓	0°	RNG	↓	↓	↓	↓	↓	↓	↓	↓	↓	↓	↓
143	↓	RNG	0°	↓	↓	OFF	60°	60°	PLUG	↓	↓	↓	↓	↓
144	↓	0°	RNG	↓	↓	↓	↓	↓	↓	↓	↓	↓	↓	↓
145	↓	↓	↓	↓	↓	↓	↓	↓	↓	↓	0°	+10°	↓	↓
146	↓	RNG	0°	↓	↓	↓	↓	↓	↓	↓	↓	↓	↓	↓
147	RNG	0°	↓	↓	↓	25000	↓	↓	90°	11°	↓	↓	↓	↓
148	10	RNG	↓	↓	↓	↓	↓	↓	↓	↓	↓	↓	↓	RERUN OF RUN 148
149	↓	↓	↓	↓	↓	↓	↓	↓	↓	↓	↓	↓	↓	↓
150	3	↓	↓	↓	↓	↓	↓	↓	↓	↓	↓	↓	↓	↓
151	10	↓	↓	WM	WM	WM	↓	↓	↓	↓	↓	↓	↓	↓
152	↓	0°	RNG	↓	↓	↓	↓	↓	↓	↓	↓	↓	↓	↓
153	↓	↓	↓	25000	25000	25000	↓	↓	↓	↓	↓	↓	↓	↓
154	3	↓	↓	↓	↓	↓	↓	↓	↓	↓	↓	↓	↓	↓
155	10	↓	↓	WM	WM	WM	↓	↓	↓	26°	↓	↓	↓	↓
156	↓	RNG	0°	↓	↓	↓	↓	↓	↓	↓	↓	↓	↓	↓
157	RNG	0°	↓	25000	25000	25000	↓	↓	↓	↓	↓	↓	↓	↓
158	10	RNG	↓	↓	↓	↓	↓	↓	↓	↓	↓	↓	↓	↓
159	↓	0°	↓	↓	↓	↓	↓	↓	↓	41°	↓	↓	RNG	↓
160	3	↓	↓	↓	↓	↓	↓	↓	↓	↓	↓	↓	↓	↓
161	10	RNG	↓	↓	↓	↓	↓	↓	↓	↓	↓	↓	15 7 IN	↓
162	↓	0°	RNG	↓	↓	↓	↓	↓	↓	↓	↓	↓	↓	↓
163	3	↓	0°	↓	↓	↓	↓	↓	↓	↓	OFF	OFF	RNG	↓
164	10	↓	↓	↓	↓	↓	↓	↓	↓	↓	↓	↓	↓	↓
165	↓	↓	RNG	↓	↓	↓	↓	↓	↓	↓	↓	↓	15 7 IN	↓
166	↓	RNG	0°	↓	↓	↓	↓	↓	↓	↓	↓	↓	↓	↓
167	↓	0°	↓	20000	20000	20000	↓	↓	↓	↓	↓	↓	RNG	↓
168	3	↓	↓	↓	↓	↓	↓	↓	↓	↓	↓	↓	↓	↓
169	10	RNG	↓	25000	25000	25000	70°	50°	↓	↓	↓	↓	15 7 IN	↓

84 is blank

APPENDIX I

RUN SCHEDULE FOR TEST NO. 175
IN 17--FOOT SECTION OF 7 X 10 FOOT LOW SPEED WIND TUNNEL, NASA, LANGLEY RESEARCH CENTER, VA. (CONTINUED)

RUN NO.	q	α	β	RPM			δ_T		δ_N	δ_F	i_v	i_h	GROUND PLANE HEIGHT	REMARKS
				LEFT	RIGHT	NOSE	LEFT	RIGHT						
170	10	0°	RNG	25000	25000	25000	71°	50°	90°	41°	OFF	OFF	15.7 IN	
171	↓	↓	↓	↓	↓	↓	↓	↓	↓	↓	0°	+10°	↓	
172		RNG	0°	↓	↓	↓	↓	↓	↓	↓	↓	↓	↓	
173		0°	↓	28000	28000	28000	60°	60°	↓	↓	OFF	OFF	RNG	
174	3	↓	↓	↓	↓	↓	↓	↓	↓	↓	↓	↓	↓	
175	10	↓	↓	21000	↓	25000	↓	↓	↓	↓	↓	↓	↓	
176	↓	↓	↓	25000	25000	↓	30°	30°	↓	11°	↓	↓	↓	
177	3	↓	↓	↓	↓	↓	↓	↓	↓	↓	↓	↓	↓	
178	10	↓	↓	↓	↓	↓	↓	↓	↓	↓	0°	0°	↓	
179	3	↓	↓	↓	↓	↓	↓	↓	↓	↓	↓	↓	↓	
180	10	RNG	↓	↓	↓	↓	↓	↓	↓	↓	↓	↓	15.7 IN	
181	↓	↓	↓	↓	↓	↓	↓	↓	↓	↓	↓	↓	42 IN	
182	↓	↓	↓	↓	↓	↓	↓	↓	↓	↓	OFF	OFF	↓	GROUND PLANE OFF
183	↓	↓	↓	↓	↓	↓	↓	↓	↓	↓	↓	↓	↓	GROUND PLANE ON
184	↓	↓	↓	↓	↓	↓	↓	↓	↓	↓	↓	↓	15.7 IN	
185	↓	0°	↓	↓	↓	↓	↓	↓	0°	↓	↓	↓	RNG	
186	3	↓	↓	↓	↓	↓	↓	↓	↓	↓	↓	↓	↓	
187	RNG	↓	↓	↓	↓	↓	↓	↓	↓	↓	↓	↓	OGE	
188	10	RNG	↓	↓	↓	↓	↓	↓	↓	↓	↓	↓	↓	
189	3	↓	↓	↓	↓	↓	↓	↓	↓	↓	↓	↓	↓	
190	10	↓	↓	WM	WM	WM	↓	↓	↓	↓	↓	↓	↓	
191	↓	0°	RNG	↓	↓	↓	↓	↓	↓	↓	↓	↓	↓	
192	↓	↓	↓	25000	25000	25000	↓	↓	↓	↓	↓	↓	↓	
193	3	↓	↓	↓	↓	↓	↓	↓	↓	↓	↓	↓	↓	
194	10	↓	↓	↓	↓	OFF	↓	↓	↓	↓	↓	↓	↓	
195	↓	RNG	0°	↓	↓	↓	↓	↓	↓	↓	↓	↓	↓	
196	↓	↓	↓	↓	↓	↓	↓	↓	↓	↓	0°	0°	↓	RERUN OF RUN 195
197	↓	↓	↓	↓	↓	↓	↓	↓	↓	↓	↓	↓	↓	
198	↓	0°	RNG	↓	↓	↓	↓	↓	↓	↓	↓	↓	↓	
199	↓	RNG	0°	WM	WM	WM	↓	↓	↓	↓	↓	↓	↓	
200	↓	↓	↓	↓	↓	↓	↓	↓	↓	↓	↓	−10°	↓	
201	↓	↓	↓	25000	25000	25000	↓	↓	↓	↓	↓	↓	↓	
202	↓	↓	↓	↓	↓	↓	↓	↓	↓	↓	↓	0°	↓	
203	3	↓	↓	↓	↓	↓	↓	↓	↓	↓	↓	↓	↓	
204	↓	0°	RNG	↓	↓	↓	↓	↓	↓	↓	↓	↓	↓	
205	10	↓	↓	WM	WM	WM	↓	↓	↓	↓	↓	↓	↓	
206	↓	RNG	0°	↓	↓	↓	↓	↓	↓	↓	↓	+10°	↓	
207	↓	↓	↓	↓	↓	↓	↓	↓	↓	↓	↓	−20°	↓	
208	↓	↓	↓	25000	25000	25000	↓	↓	↓	↓	↓	↓	↓	
209	RNG	0°	↓	↓	↓	↓	↓	↓	↓	↓	↓	0°	↓	
210	10	0°	RNG	↓	↓	↓	↓	↓	↓	↓	↓	↓	↓	
211	↓	RNG	0°	↓	↓	↓	↓	↓	↓	↓	↓	+10°	↓	
212	↓	↓	↓	↓	↓	↓	↓	↓	↓	↓	↓	0°	↓	CENTERLINE VERTICAL TAIL INSTALLED

86 is blank

RUN SCHEDULE FOR TEST NO. 175

IN 17-FOOT SECTION OF 7 X 10 FOOT LOW SPEED WIND TUNNEL, NASA, LANGLEY RESEARCH CENTER, VA. (CONCLUDED)

RUN NO.	q	α	β	RPM			δ_T		δ_N	δ_F	i_V	i_h	GROUND PLANE HEIGHT	REMARKS
				LEFT	RIGHT	NOSE	LEFT	RIGHT						
213	10	0°	RNG	25000	25000	25000	30°	30°	0°	11°	0°	0°	OGE	CENTERLINE VERTICAL TAIL INSTALLED
214		RNG	0°								OFF			
215		0°	RNG											
216		RNG	0°									OFF		
217		0°	RNG											
218		RNG	0°								0°			VERT TAIL REMOVED
219		0°	RNG											
220		RNG	0°	WM	WM	WM								
221		0°	RNG											
222		RNG	0°	25000	25000	25000				41°	OFF			
223										26°				

88 is blank

APPENDIX II

ANALYSIS OF C_{m_o} AND C_{D_o} SHIFTS

A comparison of the intersection point of the tails off and tails on curves of Figure 5 with that of Figure 37 shows a significant difference. This difference is not believed to be due to an effect of the plugged nose on the boom-mounted tails, but a result of shifts in balance output between run batches and days of different temperature and humidity. It is noted that certain runs have unreasonably high drag values and at the same time have an apparent C_{m_o} shift of -0.06 to -0.08. Runs 195 and 196 of Figure 5, which are repeat runs, intersect the tails on Run 197 at about $\alpha = 0°$, or about $\alpha = 6°$ using the dotted line which is compatible with unplugged nose characteristics. At the same time reference to the drag data of Figure 38 shows about equal drag for these runs as expected. However, comparable runs in Figure 37 (runs 188 and 202) intersect at $\alpha = 16°$ on the tails off curve, and the drag data of run 188 presented in Figure 39 is obviously too high. The same situation holds for run 206 in Figure 6, where C_{m_o} is obviously shifted negatively and the drag data in Figure 40 is about three times the value of the rest of the runs. Run 220 presented in Figures 2 and 6 is also doubtful because of its apparent C_{m_o} and C_{D_o} shifts. Therefore, using Figure 5 as a guide for the intersection point, runs 188 and 218 of Figure 37 have been arbitrarily shifted by $\Delta C_{m_o} = .067$ and a new set of comparison data is shown in Figure 3. Run 218 was shifted with Run 188 because it is believed that below $\alpha = -3°$, removal of the outboard vertical tails should have negligible effect on C_{m_o}, as is the case for runs 202 and 214.

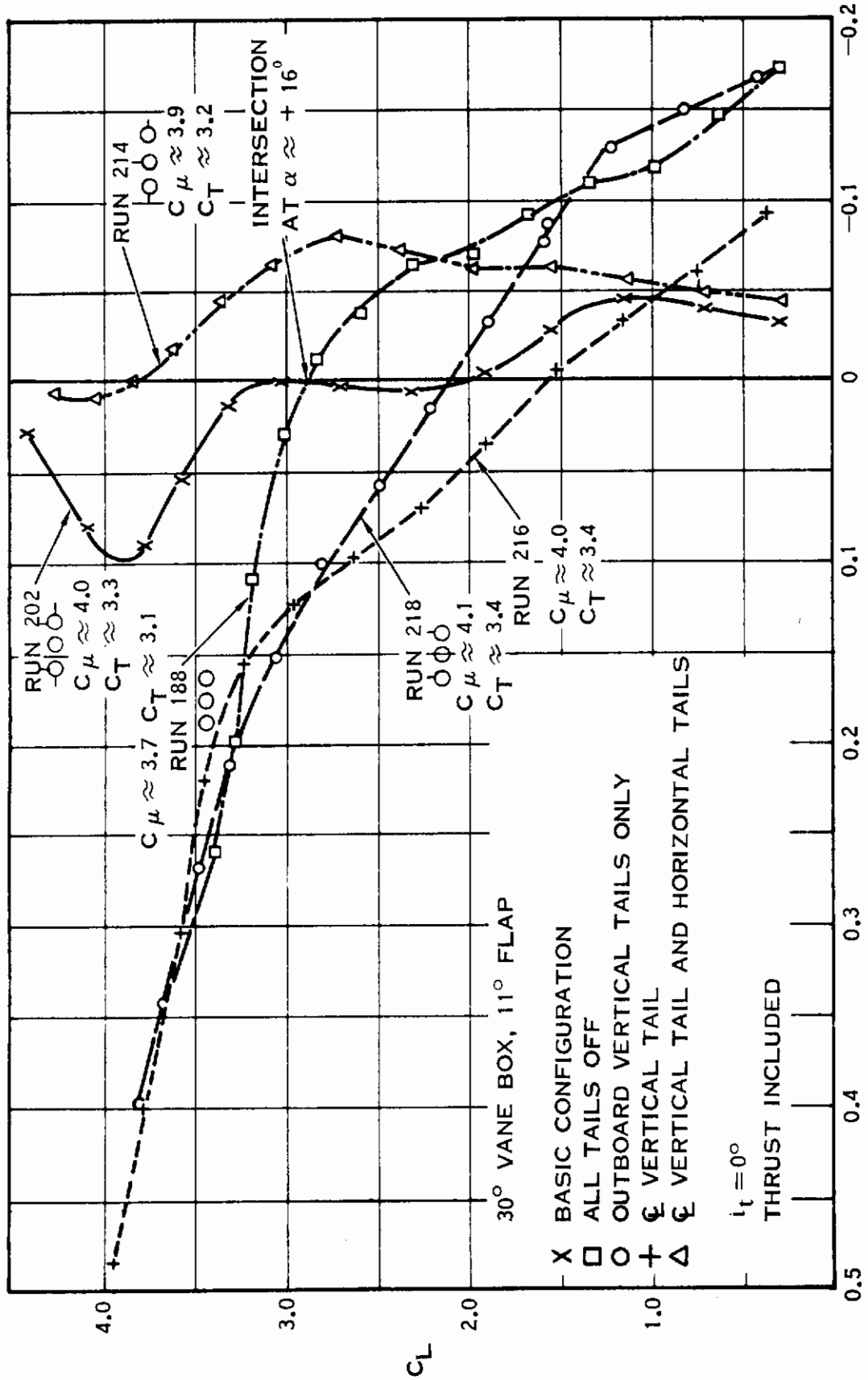

Figure 37. Effect of Tail Buildup on Longitudinal Characteristics

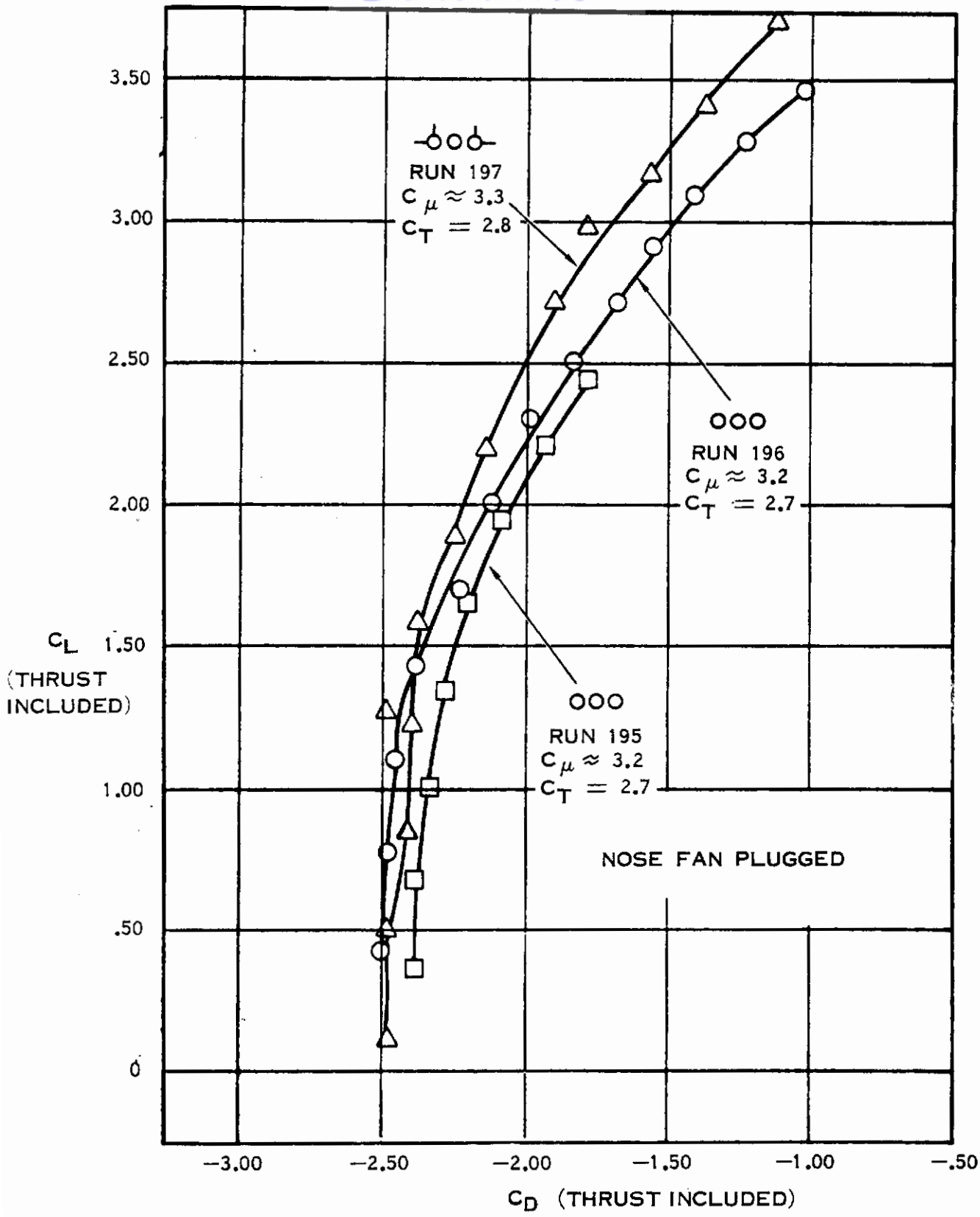

Figure 38. Plugged Nose Drag Characteristics, 30° Vane Box

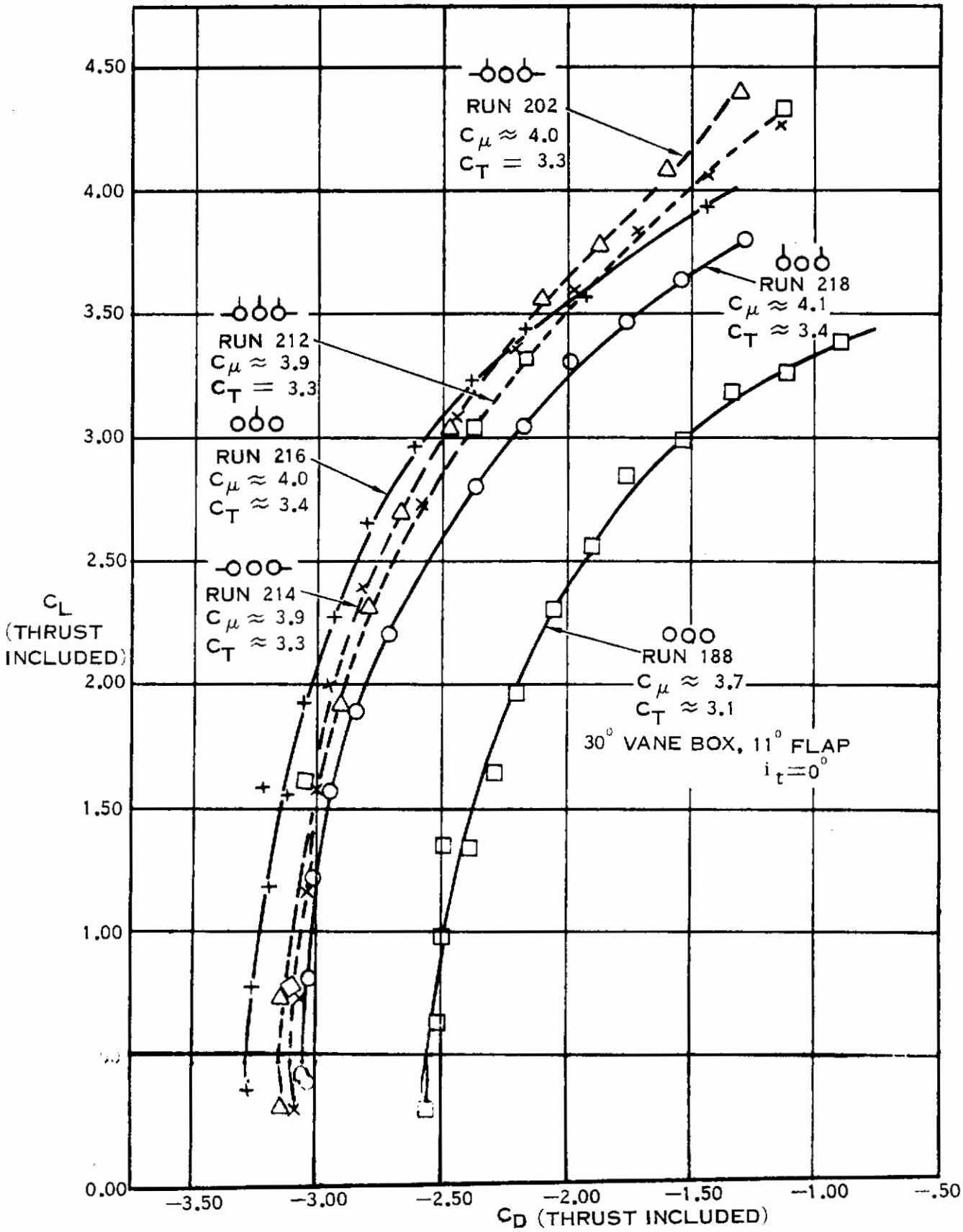

Figure 39. Drag Characteristics with Tail Buildup, 30° Vane Box

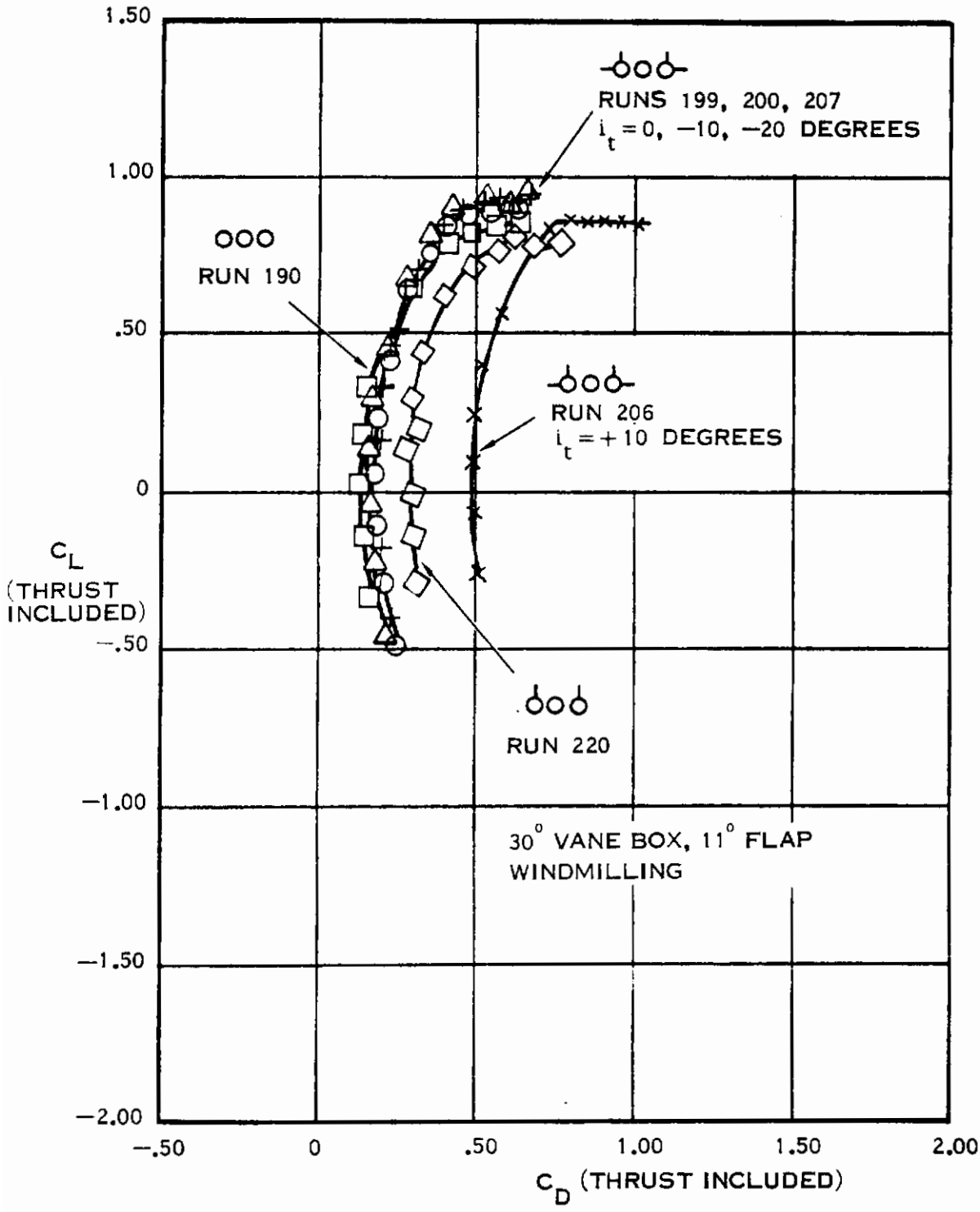

Figure 40. Windmilling Drag Characteristics, 30° Vane Box

94 is blank

DISTRIBUTION LIST

Addressee	No. of Copies
Air Force Systems Command Wright-Patterson Air Force Base, Ohio 45433	
ATTN: FDP (STINFO)	1
ATTN: FDE (Library)	1
ATTN: FDMM	10
ATTN: ASNPD-30	1
ATTN: SEPDE	1
ATTN: ASB	1
ATTN: APT	1
ATTN: ARD-1	1
ATTN: AFIT (Library)	1
DDC-TIASS Cameron Station Alexandria, Virginia 22314	20
Secretary of the Air Force (SAFRD) Washington, D.C. 20330	1
Headquarters U. S. Air Force (AFRSTF) Washington, D.C. 20330	1
AFCSAI Study Information Group Assistant Chief of Staff Studies and Analysis Headquarters U. S. Air Force Washington, D.C. 20330	1
AEDC ATTN: Technical Library Arnold Air Force Station, Tennessee 37389	2
Air Force Missile Development Center Holloman Air Force Base, New Mexico 88330	1
Air University Library Maxwell Air Force Base, Alabama 36112	1
DFSLB U. S. Air Force Academy, Colorado 80840	1

DISTRIBUTION LIST (continued)

Addressee	No. of Copies
Air Force Office of Scientific Research Washington, D.C. 20325	1
Air Force Systems Command Reference 1366 CA ATTN: SCS-41 Andrews Air Force Base Washington, D.C. 20331	3
AFSC ATTN: SCTSM Andrews Air Force Base Washington, D.C. 20331	1
Office of Aerospace Research ATTN: Technical Library United States Air Force Washington, D.C. 20333	1
DOL ATTN: Technical Library Bolling Air Force Base Washington, D.C. 20332	1
AFSC STLO Langley Research Center (NASA) Langley Air Force Base, Virginia 23365	6
AFSC STLO Ames Research Center (NASA) Moffett Field, California 94035	3
Headquarters U. S. Army Material Command ATTN: AMCRD-RP-A AMCRD-DF Washington, D.C. 20315	 1 1
Chief of Research and Development Department of the Army ATTN: Physical Science Division 3045 Columbia Pike Arlington, Virginia 22204	1
Chief of Research and Development Department of the Army ATTN: Air Mobility Division Mr. John Beebe Washington, D.C. 20310	1

DISTRIBUTION LIST (continued)

Addressee	No. of Copies
Commanding Officer U. S. Army Aviation Material Laboratories ATTN: SAVFE-PP Fort Eustis, Virginia 23604	6
Headquarters U. S. Army Research Office-Durham ATTN: Technical Library Box CM Duke Station Durham, North Carolina 27706	1
Commanding General U. S. Army Aviation Material Command Administration Services Office ATTN: AMSAV-ADR P. O. Box 209, Main Office St. Louis, Missouri 63166	3
U. S. Army Aeronautical Research Laboratory ATTN: P. F. Yaggy Moffett Field, California 94035	2
Chief of Naval Material (0314) Navy Department Washington, D.C. 20360	1
Chief of Naval Material (0331) Navy Department ATTN: Mr. H. P. Santiago Washington, D.C. 20360	1
Commander Naval Air Systems Command (320) ATTN: Mr. G. L. Desmond Washington, D.C. 20360	1
Commander Naval Air Systems Command (3032) ATTN: Mr. F. W. S. Locke Washington, D.C. 20360	1
Commander Naval Air Systems Command (5301) ATTN: Mr. William Kovin Washington, D.C. 20360	1

DISTRIBUTION LIST (continued)

Addressee	No. of Copies
Commandant U. S. Marine Corps (AX) Headquarters U. S. Marine Corps Washington, D.C. 20025	1
Commandant U. S. Marine Corps (AX-5) Headquarters U. S. Marine Corps ATTN: Col. J. F. Paul Washington, D.C. 20025	1
U. S. Marine Corps Marine Corps Schools (CMCLFDA) Quantico, Virginia 22134	1
Chief of Naval Research Navy Department Air Programs Branch ATTN: Mr. Dean Lauver Washington, D.C. 20325	1
Commanding Officer and Director Naval Ship Research and Development Center Aerodynamics Laboratory (046) Washington, D.C. 20007	1
Director Aeronautical Research National Aeronautics and Space Administration Washington, D.C. 20325	1
National Aeronautics and Space Administration Ames Aeronautical Laboratory Moffett Field, California 94035	1
National Aeronautics and Space Administration Langley Aeronautical Laboratory Langley Field, Virginia 23365	1
National Aeronautics and Space Administration Lewis Flight Propulsion Laboratory Cleveland, Ohio 44118	1
Bell Aerospace Corporation ATTN: Technical Library P. O. Box 1 Buffalo, New York 14200	1

DISTRIBUTION LIST (continued)

Addressee	No. of Copies
The Boeing Company ATTN: Technical Library 7755 East Marginal Way Seattle, Washington 98108	1
Cornell Aeronautical Laboratory, Inc. ATTN: Library 4455 Genessee Street Buffalo, New York 14221	1
Douglas Aircraft Company ATTN: Max Klotzsche C1-23 3855 North Lakewood Boulevard Long Beach, California 90808	1
Douglas Aircraft Company ATTN: Technical Library 3000 Ocean Park Boulevard Santa Monica, California 90405	1
Grumman Aircraft Engineering Corporation ATTN: Library South Oyster Bay Road Bethpage, Long Island, New York 11714	1
Lockheed Aircraft Corporation California Division 2555 North Hollywood Way Burbank, California 91502	1
McDonnell Aircraft Corporation ATTN: Library P. O. Box 516 St. Louis, Missouri 63100	1
North American Aviation, Inc. ATTN: Library International Airport Los Angeles, California 90009	1
Northrop Corporation Norair Division ATTN: Library 1001 East Broadway Hawthorne, California 90250	1

DISTRIBUTION LIST (concluded)

Addressee	No. of Copies
Republic Aviation Corporation ATTN: Library Farmingdale, Long Island, New York 11735	1
United Aircraft Corporation Research Laboratories ATTN: Library 400 Main Street East Hartford, Connecticut 06118	1

UNCLASSIFIED
Security Classification

DOCUMENT CONTROL DATA - R&D

(Security classification of title, body of abstract and indexing annotation must be entered when the overall report is classified)

1. ORIGINATING ACTIVITY (Corporate author)
LTV Aerospace Corporation

2a. REPORT SECURITY CLASSIFICATION
Unclassified

2b. GROUP

3. REPORT TITLE
Design, Fabrication, Testing, and Data Analysis of ADAM II Concept - Part III

4. DESCRIPTIVE NOTES (Type of report and inclusive dates)
Final Report 2 December 1966 - 7 July 1967

5. AUTHOR(S) (Last name, first name, initial)
Part III - William E. Brownrigg, Jr.; Robert D. Meyer; Robert B. English; et al

6. REPORT DATE	7a. TOTAL NO. OF PAGES	7b. NO. OF REFS
May 1968		

8a. CONTRACT OR GRANT NO.	9a. ORIGINATOR'S REPORT NUMBER(S)
AF33(615)-3293	
b. PROJECT NO. 1366	
c. Task No. 136617	9b. OTHER REPORT NO(S) (Any other numbers that may be assigned this report)
d.	AFFDL-TR-68-31, Part III

10. AVAILABILITY/LIMITATION NOTICES This document is subject to special export controls, and each transmittal to foreign governments or foreign nationals may be made only with prior approval of Air Force Flight Dynamics Laboratory (FDMM), Wright-Patterson Air Force Base, Ohio, 45433

11. SUPPLEMENTARY NOTES	12. SPONSORING MILITARY ACTIVITY
All parts are required for a complete understanding of subject	U.S. Air Force Flight Dynamics Lab., Air Force Systems Command, WPAFB, Ohio, U.S. Army Aviation Materials Lab. Ft. Eustis, Va.

13. ABSTRACT

This report contains in four parts, the details of design, fabrication, low and transonic speed wind tunnel testing of a powered propulsive wing model of the LTV ADAM II, V/STOL Aircraft Concept. Part I of this report contains the details of the design and fabrication of the model and includes a description of a new type of "flow-thru" internal strain-gage balance that was developed specifically for testing the model at transonic speeds. Parts II, III, and IV contain analyses of the results from three separate wind tunnel tests. Results presented in these volumes concern the hover, transition, and cruise flight modes. Adequate low speed pitch control power is demonstrated with the use of a vectored thrust nose fan. Cruise mode tests indicate that satisfactory flying qualities can be achieved. A high drag rise Mach number is verified. Requirements for further wind tunnel testing are indicated.

DD FORM 1 JAN 64 1473

UNCLASSIFIED
Security Classification

14. KEY WORDS	LINK A		LINK B		LINK C	
	ROLE	WT	ROLE	WT	ROLE	WT
a. ADAM II, V/STOL Propulsive Wing Aircraft						
b. Powered Model Testing						
c. "Flow-Thru" Balance						
d. High Bypass Ratio Fans						
e. Vectored Thrust						
f. Propulsive Interactions						
g. Sting Interference						
h. Jet Flap						
i. Jet Augmented Flap						
j. Outboard Tails						
k. Delayed Drag Rise						
l. Pitch Control Nose Fan						
m. Ground Effects						
n. Integrated Aerodynamic, Propulsive and Structural Systems						

INSTRUCTIONS

1. ORIGINATING ACTIVITY: Enter the name and address of the contractor, subcontractor, grantee, Department of Defense activity or other organization *(corporate author)* issuing the report.

2a. REPORT SECURITY CLASSIFICATION: Enter the overall security classification of the report. Indicate whether "Restricted Data" is included. Marking is to be in accordance with appropriate security regulations.

2b. GROUP: Automatic downgrading is specified in DoD Directive 5200.10 and Armed Forces Industrial Manual. Enter the group number. Also, when applicable, show that optional markings have been used for Group 3 and Group 4 as authorized.

3. REPORT TITLE: Enter the complete report title in all capital letters. Titles in all cases should be unclassified. If a meaningful title cannot be selected without classification, show title classification in all capitals in parenthesis immediately following the title.

4. DESCRIPTIVE NOTES: If appropriate, enter the type of report, e.g., interim, progress, summary, annual, or final. Give the inclusive dates when a specific reporting period is covered.

5. AUTHOR(S): Enter the name(s) of author(s) as shown on or in the report. Enter last name, first name, middle initial. If military, show rank and branch of service. The name of the principal author is an absolute minimum requirement.

6. REPORT DATE: Enter the date of the report as day, month, year; or month, year. If more than one date appears on the report, use date of publication.

7a. TOTAL NUMBER OF PAGES: The total page count should follow normal pagination procedures, i.e., enter the number of pages containing information.

7b. NUMBER OF REFERENCES: Enter the total number of references cited in the report.

8a. CONTRACT OR GRANT NUMBER: If appropriate, enter the applicable number of the contract or grant under which the report was written.

8b, 8c, & 8d. PROJECT NUMBER: Enter the appropriate military department identification, such as project number, subproject number, system numbers, task number, etc.

9a. ORIGINATOR'S REPORT NUMBER(S): Enter the official report number by which the document will be identified and controlled by the originating activity. This number must be unique to this report.

9b. OTHER REPORT NUMBER(S): If the report has been assigned any other report numbers *(either by the originator or by the sponsor)*, also enter this number(s).

10. AVAILABILITY/LIMITATION NOTICES: Enter any limitations on further dissemination of the report, other than those imposed by security classification, using standard statements such as:

(1) "Qualified requesters may obtain copies of this report from DDC."

(2) "Foreign announcement and dissemination of this report by DDC is not authorized."

(3) "U. S. Government agencies may obtain copies of this report directly from DDC. Other qualified DDC users shall request through _____."

(4) "U. S. military agencies may obtain copies of this report directly from DDC. Other qualified users shall request through _____."

(5) "All distribution of this report is controlled. Qualified DDC users shall request through _____."

If the report has been furnished to the Office of Technical Services, Department of Commerce, for sale to the public, indicate this fact and enter the price, if known.

11. SUPPLEMENTARY NOTES: Use for additional explanatory notes.

12. SPONSORING MILITARY ACTIVITY: Enter the name of the departmental project office or laboratory sponsoring *(paying for)* the research and development. Include address.

13. ABSTRACT: Enter an abstract giving a brief and factual summary of the document indicative of the report, even though it may also appear elsewhere in the body of the technical report. If additional space is required, a continuation sheet shall be attached.

It is highly desirable that the abstract of classified reports be unclassified. Each paragraph of the abstract shall end with an indication of the military security classification of the information in the paragraph, represented as *(TS)*, *(S)*, *(C)*, or *(U)*.

There is no limitation on the length of the abstract. However, the suggested length is from 150 to 225 words.

14. KEY WORDS: Key words are technically meaningful terms or short phrases that characterize a report and may be used as index entries for cataloging the report. Key words must be selected so that no security classification is required. Identifiers, such as equipment model designation, trade name, military project code name, geographic location, may be used as key words but will be followed by an indication of technical context. The assignment of links, roles, and weights is optional.